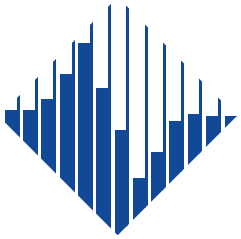

PACIFIC EARTHQUAKE ENGINEERING
RESEARCH CENTER

Ground-Motion Directivity Modeling for Seismic Hazard Applications

Jennifer L. Donahue, Ph.D., P.E.
JL Donahue Engineering Inc., Kentfield, California

Jonathan P. Stewart, Ph.D., P.E.

Department of Civil and Environmental Engineering
University of California, Los Angeles

Nicolas Gregor, Ph.D.
Consultant, Oakland, California

Yousef Bozorgnia, Ph.D., P.E.
Department of Civil and Environmental Engineering
University of California, Los Angeles

Project Review Panel

Jonathan D. Bray, Ph.D., P.E., and Stephen A. Mahin, Ph.D.,
University of California, Berkeley

I. M. Idriss, Ph.D., P.E.
University of California, Davis

Robert W. Graves, Ph.D. and Nicolas Luco, Ph.D.
U.S. Geological Survey

Tom Shantz, P.E.
California Department of Transportation

PEER Report No. 2019/03
Pacific Earthquake Engineering Research Center
Headquarters at the University of California, Berkeley

May 2019

PEER 2019/03
May 2019

Disclaimer

The opinions, findings, and conclusions or recommendations expressed in this publication are those of the author(s) and do not necessarily reflect the views of the study sponsor(s), the Pacific Earthquake Engineering Research Center, or the Regents of the University of California.

Ground-Motion Directivity Modeling for Seismic Hazard Applications

Jennifer L. Donahue, Ph.D., P.E.
JL Donahue Engineering Inc., Kentfield, California

Jonathan P. Stewart, Ph.D., P.E.
Department of Civil and Environmental Engineering
University of California, Los Angeles

Nicolas Gregor, Ph.D.
Consultant, Oakland, California

Yousef Bozorgnia, Ph.D., P.E.
Department of Civil and Environmental Engineering
University of California, Los Angeles

Project Review Panel

Jonathan D. Bray, Ph.D., P.E., and **Stephen A. Mahin, Ph.D.**,
University of California, Berkeley

I. M. Idriss, Ph.D., P.E.
University of California, Davis

Robert W. Graves, Ph.D. and **Nicolas Luco, Ph.D.**
U.S. Geological Survey

Tom Shantz, P.E.
California Department of Transportation

PEER Report 2019/03
Pacific Earthquake Engineering Research Center
Headquarters at the University of California, Berkeley

May 2019

Executive Summary

We reviewed five models for modifying the natural log mean and within-event standard deviation of ground-motion models (GMMs) to account for directivity effects in the near-fault environment. We found broad consistency for strike–slip ruptures, with positive and negative directivity effects for cases of rupture towards and away from a site of interest, respectively. We found substantial divergence among directivity models for reverse slip, with some providing maximum directivity for sites positioned to experience the peak alignment of rupture direction with the fault-slip direction (this occurs in the up–dip direction), while others optimize directivity based on the amount of fault rupture towards the site (even if the azimuth of rupture propagation does not align with the fault-slip direction).

We found four of five NGA-West2 GMMs to be centered on a condition of null directivity. Therefore, we consider those GMMs suitable for use in combination with similarly centered directivity models.

We present two deterministic methods for adjusting ground-motion hazard results for the effects of directivity: one modifies ground motions for a specified hazard level based on location-specific (relative to fault) changes in mean and standard deviation; and the second produces a directivity-compatible conditional mean spectra. We also provide recommendations for incorporating directivity effects into calculations within the hazard integral by either (1) modifying the mean and standard deviation of ground motion to approximately account for the effect of variable hypocenter location; (2) integrating over a location-specific distribution of the directivity parameter, which also indirectly accounts for variable hypocenter location; or (3) integrating directly over alternate hypocenter locations.

Keywords: conditional mean spectra, directivity, ground-motion prediction, near-fault ground motions, probabilistic seismic hazard analysis

Acknowledgments

This work benefited from feedback and coordination with directivity model developers, including Jack Baker, Jeff Bayless, Brian Chiou, Badie Rowshandel, and Paul Spudich. Our work was overseen by an expert panel consisting of Jonathan D. Bray, I. M. Idriss, Robert W. Graves, Nicolas Luco, Stephen A. Mahin, and Tom Shantz. Their input was impactful and is very much appreciated. Professor Stephen Mahin unfortunately passed away before the conclusion of this project. His advice and input were always illuminating and constructive, and are truly missed. Claire Johnson provided valuable editorial corrections to the document.

Partial financial support was provided by the California Department of Transportation and the Pacific Gas & Electric Company. Any opinions, findings, and conclusions or recommendations expressed in this material are those of the authors and do not necessarily reflect those of the sponsors.

Any opinions, findings, and conclusions or recommendations expressed in this material are those of the authors and do not necessarily reflect those of the Pacific Earthquake Engineering Research Center or the Regents of the University of California.

1 Introduction

Ground-motion models (GMMs) estimate the log mean and standard deviation (μ_{ln} and σ_{ln} if natural log is used) of earthquake ground-motion intensity measures (IMs) conditional on independent variables such as earthquake magnitude (**M**), site-to-source distance, and various site parameters. For horizontal-component ground motions, the μ_{ln} and σ_{ln} provided by modern GMMs are for the median-component IM, which is denoted the RotD50 component [Boore 2010]. Similar definitions, such as geometric mean, have also been used.

Ground-motion models are updated periodically to reflect new knowledge from study of recorded and simulated ground motions. The NGA-West2 project [Bozorgnia et al. 2014] is such a research effort, which focused on active shallow crustal regions. While NGA-West2 GMMs can be used to predict ground motions at short rupture distances from large **M** earthquakes, those GMMs are generally not formulated to capture near-fault effects, which include:

1. *Rupture directivity effect on RotD50-component ground motions.* In general, directivity produces larger long-period ground motions when rupture occurs towards the site of interest and smaller motions when rupture propagates away from the site.
2. *Orientation of maximum component*. Whereas the orientation of maximum-component ground shaking is generally random and variable across oscillator periods, for some near-fault sites, acceleration response spectral ordinates for long periods are likely to be stronger than RotD50 in the fault-normal (FN) direction. This is sometimes referred to as polarization of ground motion in the FN (or nearly FN) direction.
3. *Pulses*. Ground motions for sites subject to forward rupture directivity or "fling" step have an increased likelihood of containing pulse-like characteristics in their velocity-time series.

As seismic hazard analyses are typically performed for the RotD50 component of horizontal ground motion, Consideration (1) creates a potential for biased estimates of hazard when GMMs are used as-published for near-fault sites. Strategies for removing this bias are the subject of this manuscript. Considerations (2) and (3) affect ground-motion selection and application of the motions to structural models; guidelines for addressing these effects can be found in Chapter 16 of ASCE 7-16 [ASCE 2016] and in Chapter 3 of the Tall Buildings Initiative report [PEER 2017].

While this document emphasizes the topic of rupture directivity, it should be recognized that fling step effects also have the potential to affect near-fault ground motions. Currently available models consider its effects as modifications to ground-motion time series [Kamai et al. 2014; Burks and Baker 2016]. Hence, our recommendation is to perform hazard analysis in consideration of directivity effects and, as appropriate, modify selected time series for fling step effects.

To address the potential for bias in the RotD50-component (or similar definitions, such as geometric mean) ground motions, engineering practice has applied modifications to the moments from GMMs to account for directivity effects. Some models that apply these modifications include: Somerville et al. [1997] and Abrahamson [2000] (pre-NGA-West1); Spudich and Chiou [2008] (NGA-West1); and a series of models summarized in Spudich et al. [2014] from NGA-West2.

Table 1 lists five models for directivity developed in NGA-West2 along with their key attributes (model explanations provided in Chapter 3). As described by Spudich et al. [2014], these model developers sought to address the principle problems with pre-NGA-West2 directivity models as follows:

1. Sampling bias: The near-fault sampling of data in NGA-West1 was biased towards sites with forward directivity. Therefore, GMM medians at close distance reflected a degree of forward-directivity effect. We refer to this subsequently as a problem of *centering*, i.e., the GMM median is not centered on a null directivity effect. The term can also be applied to the directivity models: do they produce on average (i.e., for the central value of their directivity parameter) a null change in μ_{ln}?

4. Source dimension normalization: Some pre-NGA-West2 directivity models normalized the along–fault distance over which rupture propagates towards a site by the full fault

dimension. As shown in Figure 1, this causes a larger directivity effect to be predicted for the **M**7.5 rupture than the **M**7.8 rupture, when the actual length of rupture towards the site is identical in both instances. This undesirable result was addressed using actual (not normalized) distances in the NGA-West2 directivity models.

While in the NGA-West2 directivity project these objectives were met, a number of additional problems have impeded the use of the models from Table 1, including lack of clarity on whether NGA-West2 GMMs are centered for near-fault conditions and in some cases significant divergences between models. With this in mind, in 2015 the Pacific Earthquake Engineering Research center (PEER) formed an expert panel identified in the Acknowledgments and chaired by the several of this report's authors, which sought to (1) document and illustrate the issues identified above; (2) develop guidelines for current practice regarding the modeling of directivity effects on RotD50-component intensity measures (IMs) in hazard calculations; and (3) provide recommendations for targeted research to improve capabilities for directivity modeling in future GMMs. We present here the outcome of the committee's work, which benefitted extensively from the input of the Panel.

Subsequent sections of this document include: (1) description of current practice regarding directivity modeling; (2) a review of key attributes of the models in Table 1, including a discussion of conditions for which alternate model predictions are broadly consistent and divergent, (3) recommendations regarding directivity model selection in practice; (4) an assessment of the degree to which the NGA-West2 GMMs are centered; (5) description of alternative means by which directivity effects can be modeled in seismic hazard calculations; and, lastly, (6) recommendations for research needs to improve directivity modeling in the future.

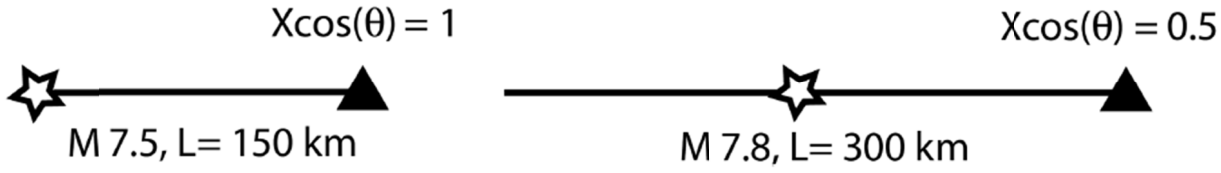

Figure 1 **Schematic depiction of two earthquake scenarios in which identical lengths of fault rupture occur towards a site, but the products *X*cos(θ) are different. *X* is the fraction of the fault length that ruptures towards the site, and θ is the angle between the fault strike and a line drawn from**

Table 1 Attributes of NGA-West2 directivity models.

Model	Bayless and Somerville (2013): bay13	Chiou and Spudich /Chiou and Youngs (2013): cscy	Rowshandel (2013): row13	Shahi and Baker (2013): sb13	Spudich and Chiou (2013): sc13
Directivity term	f_{geom}	ΔDPP	ξ	s, θ, d, Φ	Δ*IDP*
Data used for development	NGA-West2 flatfile, no sims	NGA-West2 flatfile, FF sims	NGA-West2 flatfile, FF sims	NGA-West2 flatfile, records 1-8163	NGA-West2 flatfile
Period range	0.5–10 sec	0.4–10 sec	0.3–10 sec	0.6–10 sec	0.5–10 sec
Bandwidth1	Broadband	0.5545	0.6	0.61	0.6132
M range	5.0–8.0	5.5–7.9	5.5–8.0	5–7.9	5.75–7.9
M taper	5.0–6.5	5.5–6.3	None	n/a2	None
Distance range	R_{rup} 0–200 km	R_{rup} 0–70 km	R_{rup} 0–40 km (1 sec) 0–86 km (10 sec)	R_{rup} 0–-70 km2	R_{rup} 0–70 km
Distance taper	(L or W)/2 to (L or W)	40–70 km	Taper applies to last half of R_{rup} range	n/a2	40–70 km
Distance qualifier	Closest point	Direct point	Integration over rupture surface	Closest point	Closest point
Centered	No	Yes	Yes	Yes	Yes
Components of motion	RotD50, FN, FP	RotD50	RotD50	RotD50, FN3	RotD50
Physical basis	Intuitive model	Isochrone	Intuitive model	Intuitive model	Isochrone
Discontinuous fault segments allowed?	No	Yes	Yes	No	Yes
Reverse/ normal fault distinction	No	No	Yes	No	No

[1] For narrow-band models, bandwidth taken as log standard deviation of pulse period, T_p. For broadband models, bandwidth is undefined.

[2] sb13 model does not have linear tapers to zero adjustment at a specific magnitude and distance. Magnitude and distances ranges are provided here based on the range of values associated with identified pulse-like motions, to approximately represent the ranges over which the model may predict an adjustment.

[3] Model for FN/RotD50 in Shahi and Baker [2014].

2 Current Practice

The traditional understanding of rupture directivity is as follows: the propagation of rupture toward a site at a velocity that is almost as large as the shear-wave velocity and with a slip direction that coincides with the direction of rupture causes most of the seismic energy from the rupture to arrive in a single large pulse of motion at the beginning of the record [Benioff 1955; Boore and Joyner, 1978; Singh 1985; and Somerville et al., 1997]. An early model for this process by Somerville et al. [1997] is illustrated in Figure 2. Two key aspects of this model are: (1) directivity parameters ($X\cos\theta$ and $Y\cos\phi$) represent the degree to which the component of fault rupture aligned with the slip direction is towards a site of interest (X and Y for strike– and dip–slip faults, respectively) and the effect of the along–fault radiation pattern (cosine terms); and (2) it modifies response spectral ordinates using functions conditional on directivity parameters. Abrahamson [2000] modified the model to saturate the directivity effect for $X\cos\theta >$ 0.4 and to reduce directivity effects through the use of tapers for distances > 30 km and **M** < 6.5; see also Bozorgnia and Campbell [2004].

Despite the presence of more recent models developed with far larger datasets (e.g., NGA-West1 and NGA-West2), our experience has been that in practice the Somerville et al. [1997] model in conjunction with the Abrahamson [2000] modification continues to be applied to analyze directivity effects on response spectral ordinates. It is most often applied *a posteriori* to modify the uniform hazard spectra in a subjective manner (specifically, analyst judgment is required on hypocenter locations that control directivity parameters). Listed below are three reasons why, in our opinion, the use of these models should be discontinued:

- The models are developed from residuals of late-1990s era GMMs, which are not properly centered for near-fault conditions.

- As with all other GMMs from that era, the vast increase in the size and quality of data developed since that time render the current models obsolete.
- The parameterization using dimensionless (normalized) fault lengths is now recognized as non-physical, which has been corrected in the NGA-West2 directivity models.

In the state of California, design spectra for Caltrans bridges are modified for directivity effects by increasing spectral ordinates at periods of 1.0 sec and beyond by 20%, as shown in Figure 3 [Caltrans 2013]. This modification applies for closest distances R_{rup} < 15 km with no magnitude tapers or modification for style-of-faulting. A linear distance taper is applied to remove the 20% increase for distances > 25 km.

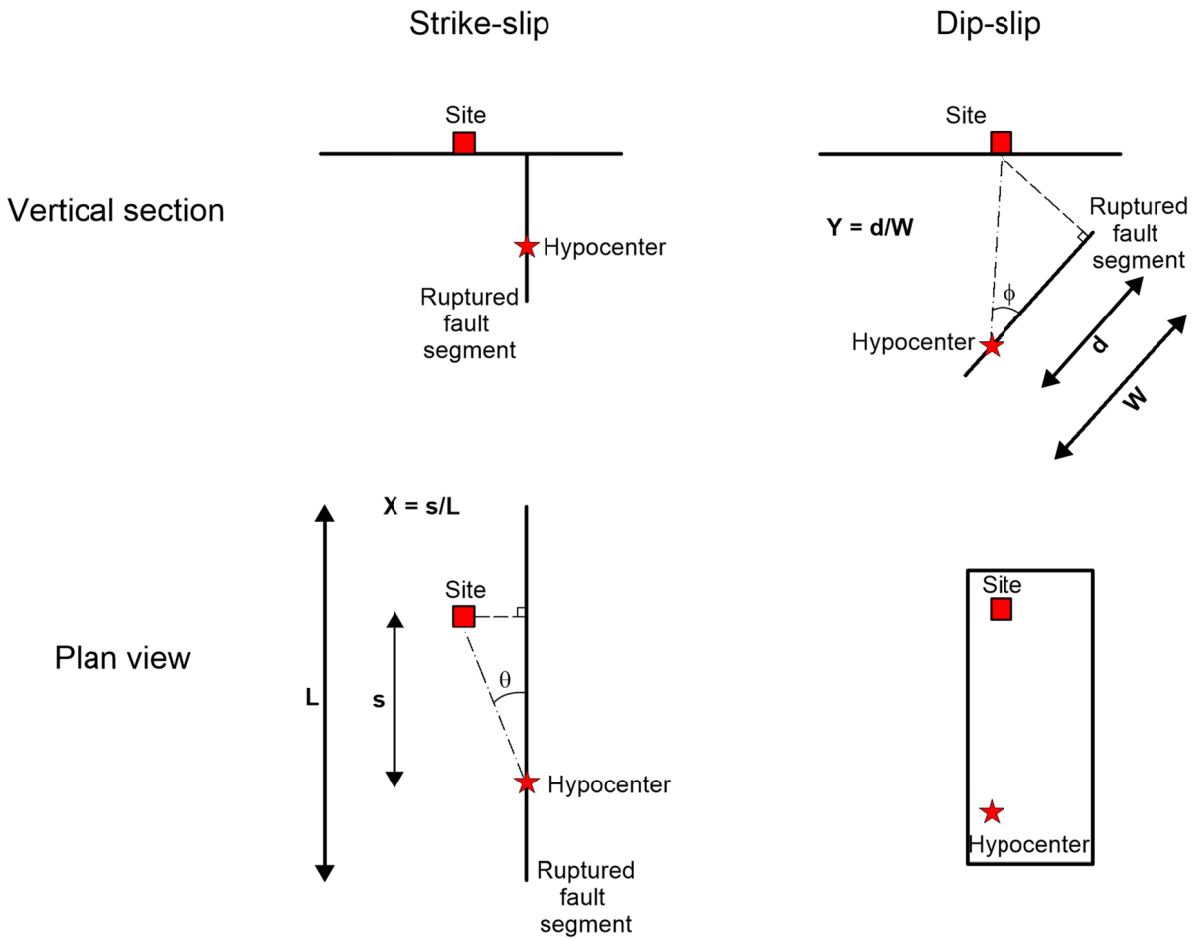

Figure 2 **Definition of directivity parameters for strike–slip and reverse-slip faults as given by Somerville et al. [1997].**

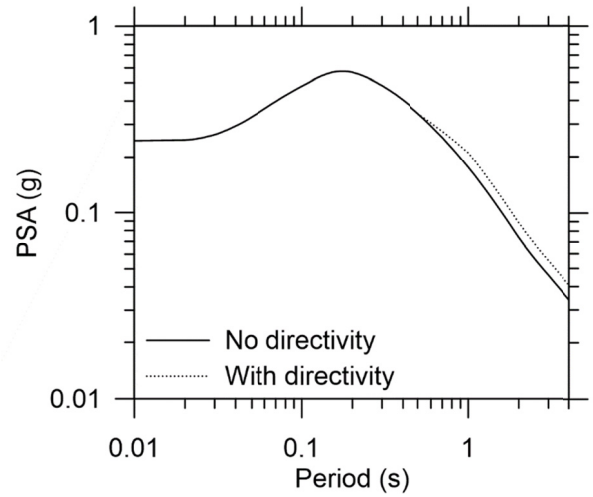

Figure 3 **Modification of pseudo acceleration response spectra (PSA) for near-fault directivity effects as given by Caltrans [2013].**

Building code procedures recently developed for structure-specific response history analysis suggest consideration of near-fault effects as part of ground-motion hazard characterization in the *NEHRP Recommended Seismic Provisions for New Buildings and Other Structures* [BSSC 2015]. Provisions in Chapter 16 of that document [BSSC 2015] and ASCE 7-16 [2016] provide guidance on ground-motion selection in consideration of pulse-like ground motions and orientation of the maximum component of ground motion in the FN direction. No specific guidance was provided regarding accounting for directivity effects on IMs, which is a procedural gap filled by this document.

The present work is intended to advance practice by providing guidance on the application of NGA-West2 directivity models for predicting RotD50 response spectral ordinates. While the recommendations provided in this report are most directly implemented within the hazard integral, these models can also be applied *a posteriori* to uniform hazard spectra or scenario (e.g., conditional mean) spectra, as is now commonly done with earlier models.

3 NGA-West2 Directivity Models

Five directivity models were analyzed (and in some cases developed) by the Directivity Working Group as part of the NGA-West2 project. As shown in Table 1, these models are: Bayless and Somerville [2013] (bay13), Chiou and Spudich/Chiou and Youngs [2013/2014]) (cscy), Rowshandel [2013] (row13), Shahi and Baker [2013] (sb13), and Spudich and Chiou [2013] (sc13). Most of the NGA-West2 directivity models have not been significantly changed since their release in 2013. An exception is the row13 model for which a number of revisions from 2013 through approximately 2016 were considered as part of the Panel's work; additional subsequent refinements are described by Rowshandel [2018a,b]. These models were developed to estimate the change in the RotD50 ground motion at a site given a known hypocenter location. These models were previously compared and summarized by Spudich et al. [2013; 2014]. Our objectives in this section are as follows: (1) to explain several attributes that were considered in forming recommendations for practical application; (2) demonstrate differences in model-to-model variability for various source types; and (3) provide recommendations for model selection given the current state of model development.

3.1 Model Attributes

The directivity models in Table 1 predict changes in 5%-damped pseudo-spectral acceleration (PSA) as a function of oscillator period. In natural log units, the additive change to the mean PSA is denoted f_D. Most models are narrow-band such that the PSA change is concentrated around a pulse period, T_p, although the bay13 model is broadband for oscillator period $T > 0.5$ sec. In these models, PSA changes are related to the effects of geometric parameters that, in different ways, capture (1) the degree to which rupture on the fault occurs towards the site of interest; (2) slip on the fault is aligned with the rupture direction; and (3) the extent to which the

site would be expected to see a pulse given the source radiation pattern. Further details on these parameters are provided in the source reports. A brief summary for each follows:

- The bay13 model is parameterized similarly to the Somerville et al. [1997] model (Figure 2), except that the dimension of the fault rupturing towards the site is used without normalization. Effects (1–3) above are considered.
- The cscy model is rooted in isochrone theory [Bernard and Madariaga 1984; Spudich and Frazer 1984, 1987], with the fault represented as a line source between the hypocenter and the *direct point* (P_D), which is defined in consideration of the site location as shown in Figure 4. In that figure, P_P indicates the projection of the site to the plane containing the fault on a line perpendicular to that plane. The direct point is defined by the intersection of a line connecting the hypocenter (P_H) and P_P with the edge of the ruptured fault. Fault slip along the line source occurs at the rake angle. The effects of slip direction are accounted for by a radiation pattern term computed as the average over the source length. Directivity is associated with the component of slip that aligns with the line source.
- The row13 model uses a geometric parameter computed as the weighted sum of two dot products for a given section of the fault. The first dot product is computed from the fault-to-site vector and a vector representing direction of rupture. The second dot product uses the fault-to-site vector and slip vector. When these weighted sums for a given section of the fault are summed over the fault surface (for a given site), directivity parameter ξ is obtained. The directivity parameter ξ is scaled to attain a maximum value of +1 when the directions of rupture and slip are both toward the site. As long as the fault-to-site vector and slip vector both have a component toward the site, however small, ξ has a non-zero value in the range (+0, +1) and directivity effects exists. If either component does not exist, no directivity effect is predicted.
- The sb13 model, which is similar to Shahi and Baker [2011], describes the effects of pulses on PSA; for forward application, the PSA change is scaled by a model for pulse probability. Pulse probability, in turn, is related to geometric parameters similar to those in Figure 2, although like bay13, the fault dimension rupturing towards the site is not normalized.

- The sc13 model is similar to cscy in that it is based in isochrone theory. While the E-path in Figure 4 is not used, the directivity parameter is computed from along–fault distance D between points P_H (hypocenter) and the *closest point* (P_C). A radiation pattern is taken from point P_H and directivity results from the component of slip that aligns with the P_H-to-P_C path.

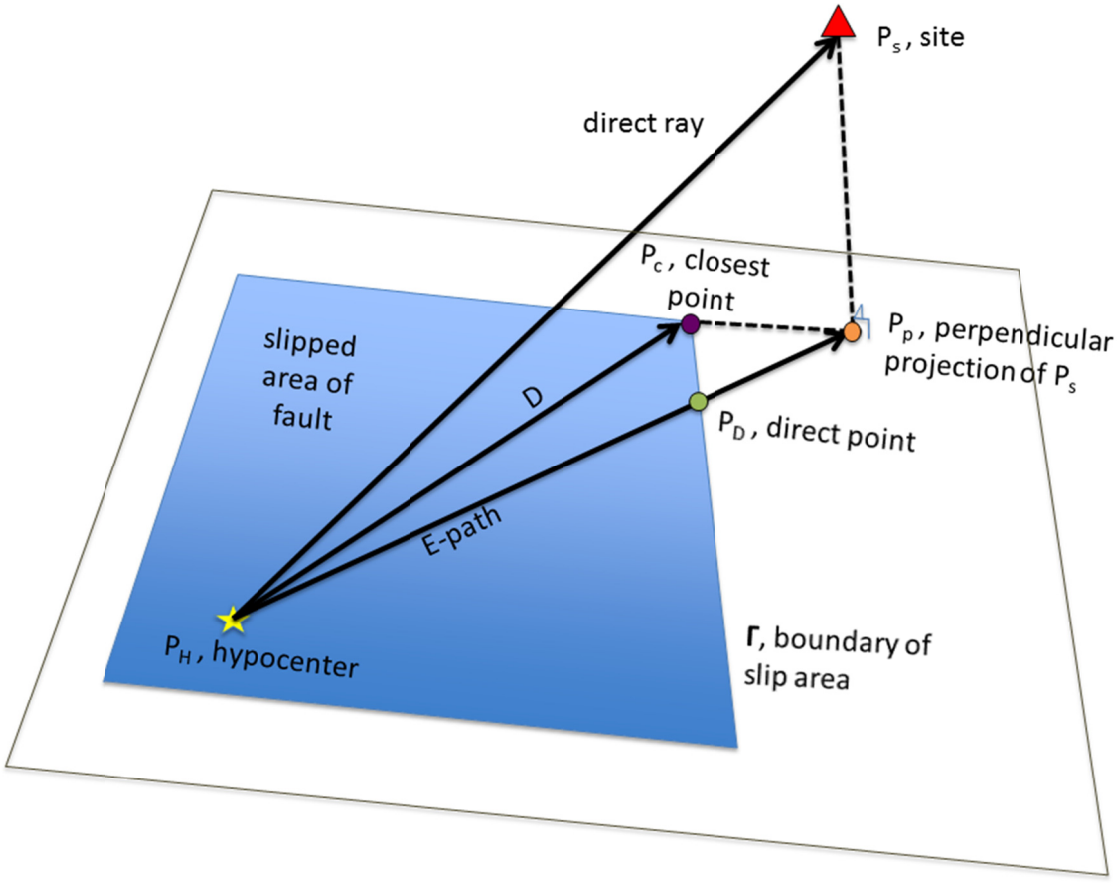

Figure 4 **Schematic representation of ruptured fault indicating locations of direct point (P_D) and closest point (P_C) given site location (P_S) and hypocenter (P_H). The cscy model directivity parameter is based on path P_H-to-P_D (E-path) and its alignment with fault slip, as represented by the average radiation pattern over that length. The sc13 model directivity parameter is similarly computed from the P_H-to-P_C path and its alignment with fault slip as represented by radiation pattern at the hypocenter.**

An important model attribute listed in Table 1 is that of centering. As noted in Chapter 1, directivity model centering refers to whether a model produces on average (i.e., for the central value of their directivity parameter) a null change in ground motion. Directivity model developers have used two general approaches to achieve centering. One approach is to ensure that if the directivity term calculated for a rupture is averaged over potential hypocenters and "racetracks" having constant rupture distance, the resulting average should be zero. This is typically accomplished by simply taking the directivity parameter as the difference between its value for a point and the racetrack average, e.g., for cscy, we have:

$$\Delta DPP = DPP - \overline{DPP} \tag{1}$$

where DPP is the point value, and $\overline{DPP}$ is the racetrack average. The cscy and sc13 models are centered in this manner.

A second approach to achieve centering is empirical. Models developed with this approach are regressed against ground-motion data and are centered with respect to the directivity effects implied by that data. Such models are best viewed as being conditionally centered in the sense that their centering depends on the degree to which the data itself is centered. The centering of the NGA-West2 GMMs at close distance—and by extension the data those models are based on—is investigated in Chapter 4. The sb13 and row13 models are centered in this manner. Our summary of model centering in Table 1 records a model as "centered" according to either approach. Only the bay13 model is not centered according to one of these approaches. The use of centered directivity models with GMMs is discussed subsequently.

All of the directivity models in Table 1 apply tapers that reduce the directivity effect at large distances and/or small magnitudes. As shown in Table 1, only bay13 and cscy apply magnitude tapers; all the other models with the exception of sb13 apply distance tapers. Bay13 based their tapers on residuals analysis, while cscy based their magnitude taper on interpretation of simulated ground motions. In other cases, tapers either are not applied or are assumed from prior models.

A commonly encountered problem with application of prior directivity models (e.g., Somerville et al. [1997] and Spudich and Chiou [2008]) is fault complexity. Whereas the model development was conceptualized using relatively simple fault geometries (e.g., Figure 2),

applications may involve changes in strike and/or dip along their length as well as discontinuous segments. The NGA-West2 directivity models (Table 1) were developed with this in mind: all models allow changes in strike (generally < 90º) for contiguous segments along the fault length, and cscy and row13 allow offset fault segments (Table 1). Bay13 calculate the weighted average of the directivity adjustment terms f_D for each segment using the seismic moments of the individual segments as the weights; hence, the weighting is based on slip distribution. A similar approach can be used for sb13 because this model uses the same directivity parameters as bay13. The cscy, row13, and sc13 models are based on geometric parameters that can readily span across fault segments. Figure 5 shows three examples of directivity parameters computed for the complex fault model of the 1999 Chi Chi, Taiwan, earthquake mainshock [Zeng and Chen 2001]: ΔIDP for sc13, ΔDPP for cscy, and ξ' for row13. There is a relatively smooth variation of the ΔDPP and ξ directivity parameters around the fault, which is an improvement over the stronger spatial variations of ΔIDP (these features of ΔIDP partially motivated development of the alternate ΔDPP parameter).

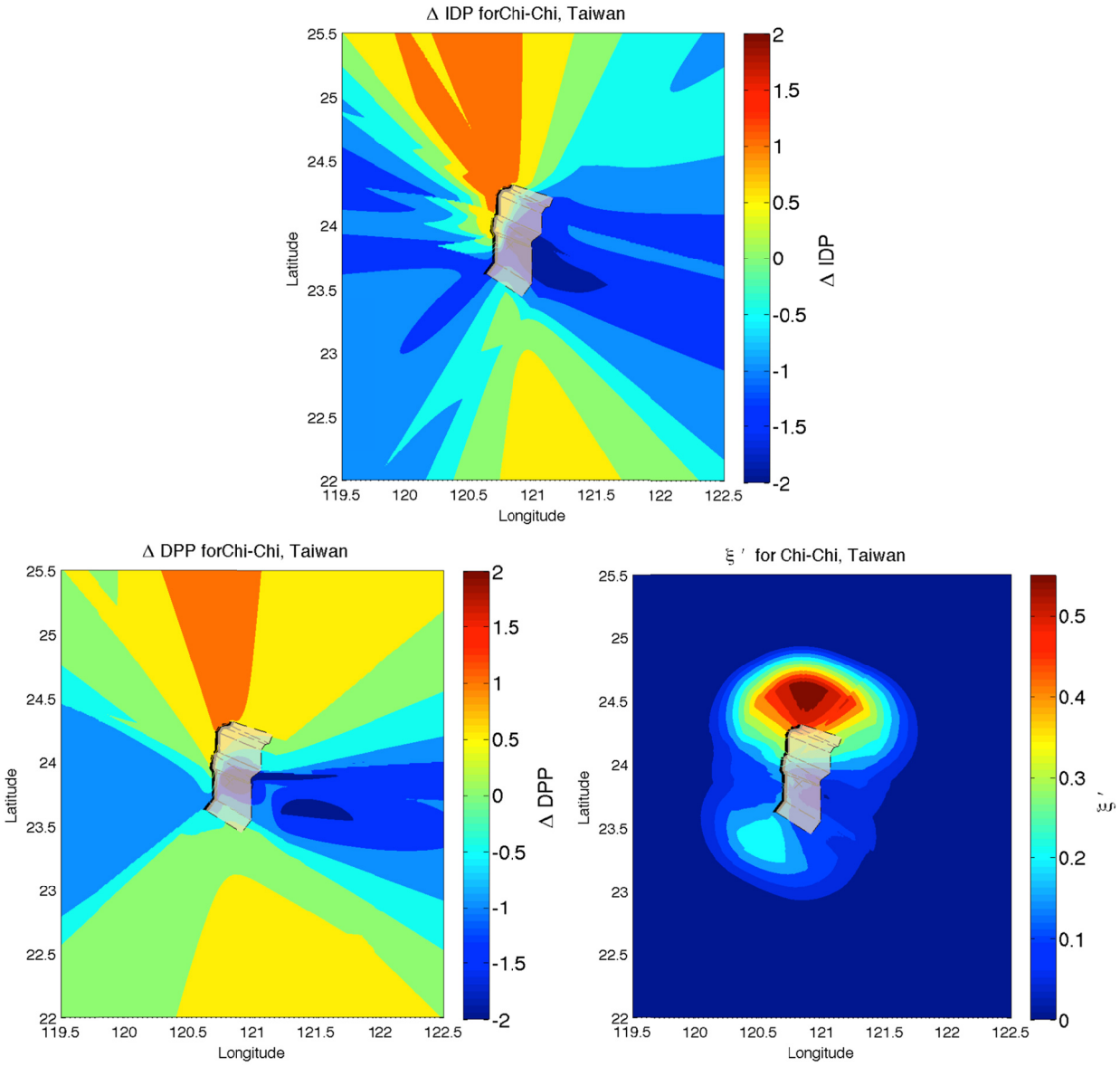

Figure 5 **Maps of three directivity parameters around the Chi-Chi, Taiwan, fault trace (black line indicates top of rupture). Top is map of Δ*IDP*, left-bottom is map of Δ*DPP*, and right-bottom is map of ξ.**

3.2 Model-to-Model Variability

Figures 6–8 show directivity model mean predictions for three rupture scenarios:

1. Vertically-dipping strike–slip fault, rake = 180º, hypocenter near south end. **M**7.8 (Figure 6).
2. 45º-dipping reverse fault, rake = 90º, hypocenter at base near south end. **M**7.0 (Figure 7)
3. 45º-dipping oblique rupture, rake = 135º, **M**7.0 (Figure 8)

All results are shown in arithmetic units $[\exp(f_D)]$. The strike–slip results (Figure 6) have broadly similar patterns, with negative directivity near the south end of the rupture and positive to the north. The amplitude of the directivity effects vary to some extent between models, in particular whereas the bay13 directivity is relatively consistent for T = 1.0–10 sec (broadband), the other models are narrow band and hence vary more strongly with period.

The reverse-slip scenarios have significant model-to-model variability, which can be understood by their parameterization of directivity. Models parameterizing directivity in a manner similar to Figure 2 (bay13, sb13), only consider fault dimension in the direction of slip, which is up–dip in this scenario. Because this dimension does not change along the fault strike, there is no variation along strike in the directivity until the ends of the fault are passed. In contrast, cscy, row13, and sc13 consider the component of slip in the direction of rupture, which allows directivity to accumulate both in the up–dip direction and the along–strike direction. This is most evident in the cscy and row13 models, which have the strongest directivity at the upper corner of the fault opposite the hypocenter. The use of the closest point in the sc13 model diminishes this effect relative to cscy and row13. All three models have strong along-strike variations in directivity.

The oblique-slip scenario (Figure 8) shows a directivity pattern that is more similar to that for the strike–slip than the reverse–slip cases. This demonstrates the stronger directivity from the along-strike component of rupture, which results from fault lengths generally exceeding fault widths for large **M** crustal events.

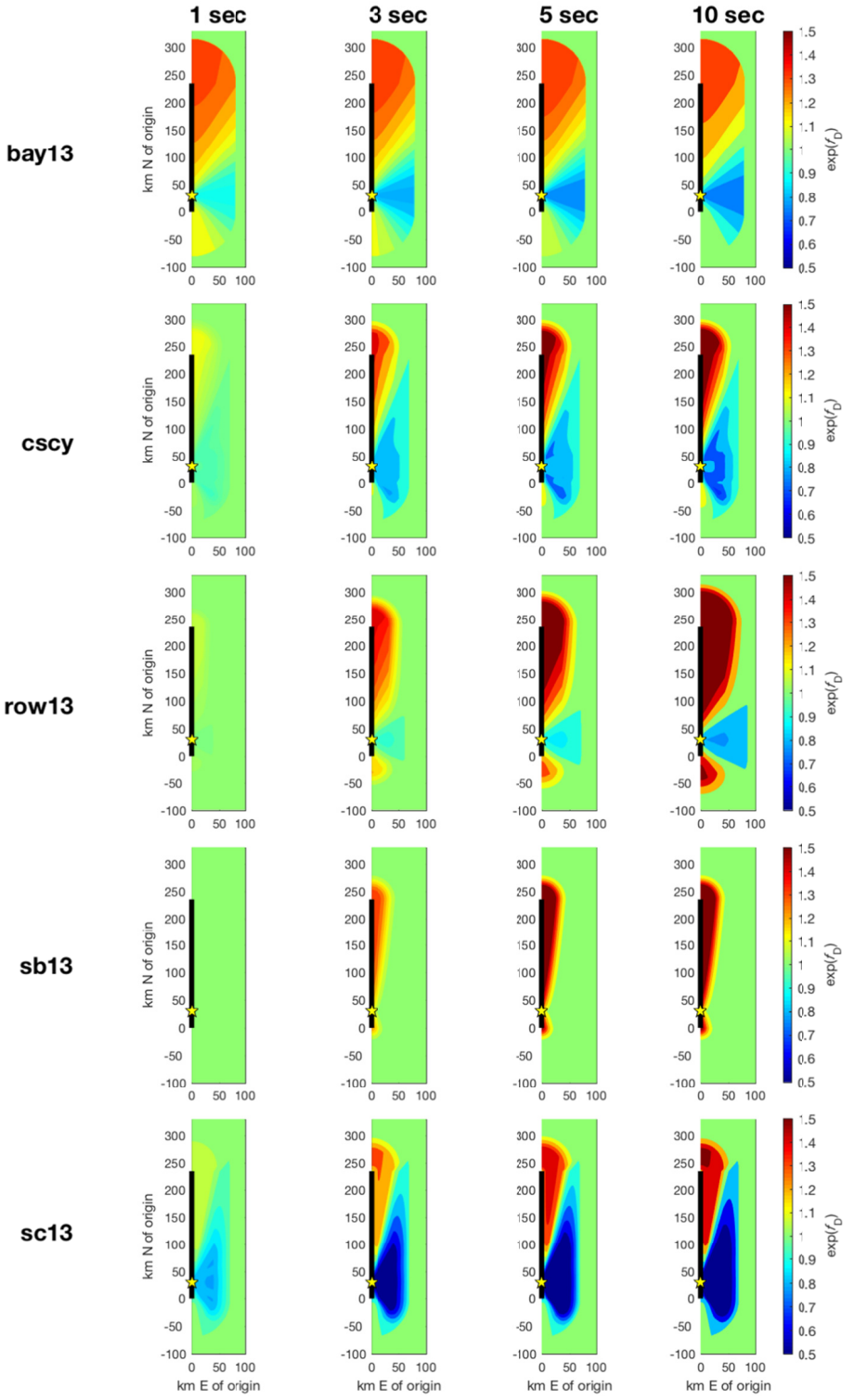

Figure 6 **Model predictions in arithmetic units $[\exp(f_D)]$ for four PSA oscillator periods (T = 1.0, 3.0, 5.0, and 10.0 sec) for five models in Table 1. M7.8 strike–slip rupture scenario. Only right side of fault is shown due to symmetry.**

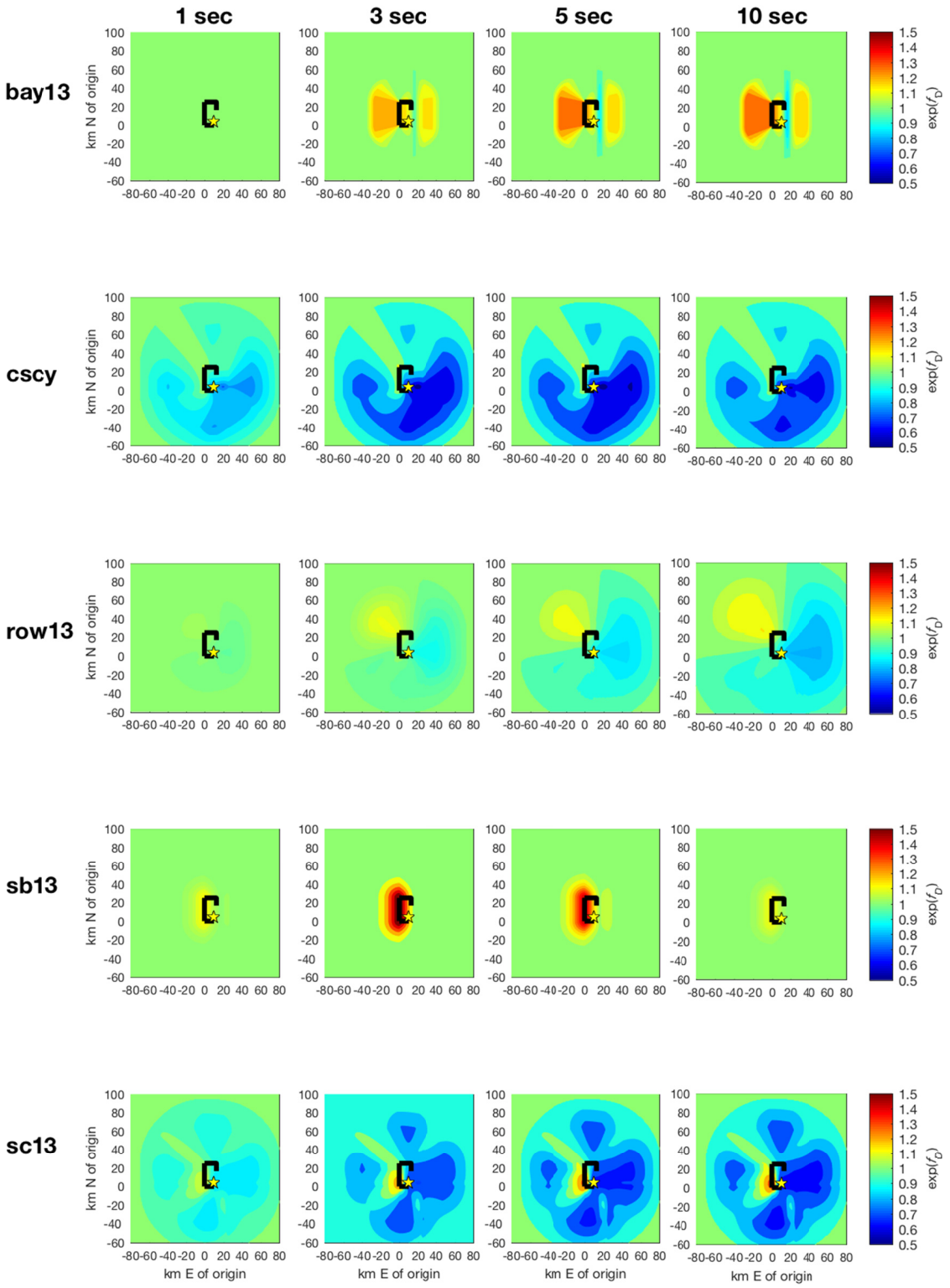

Figure 7 **Model predictions in arithmetic units $[\exp(f_D)]$ for four PSA oscillator periods (T = 1.0, 3.0, 5.0, and 10.0 sec) for five models in Table 1. M7.0 reverse–slip rupture scenario. Only right side of fault is shown due to symmetry.**

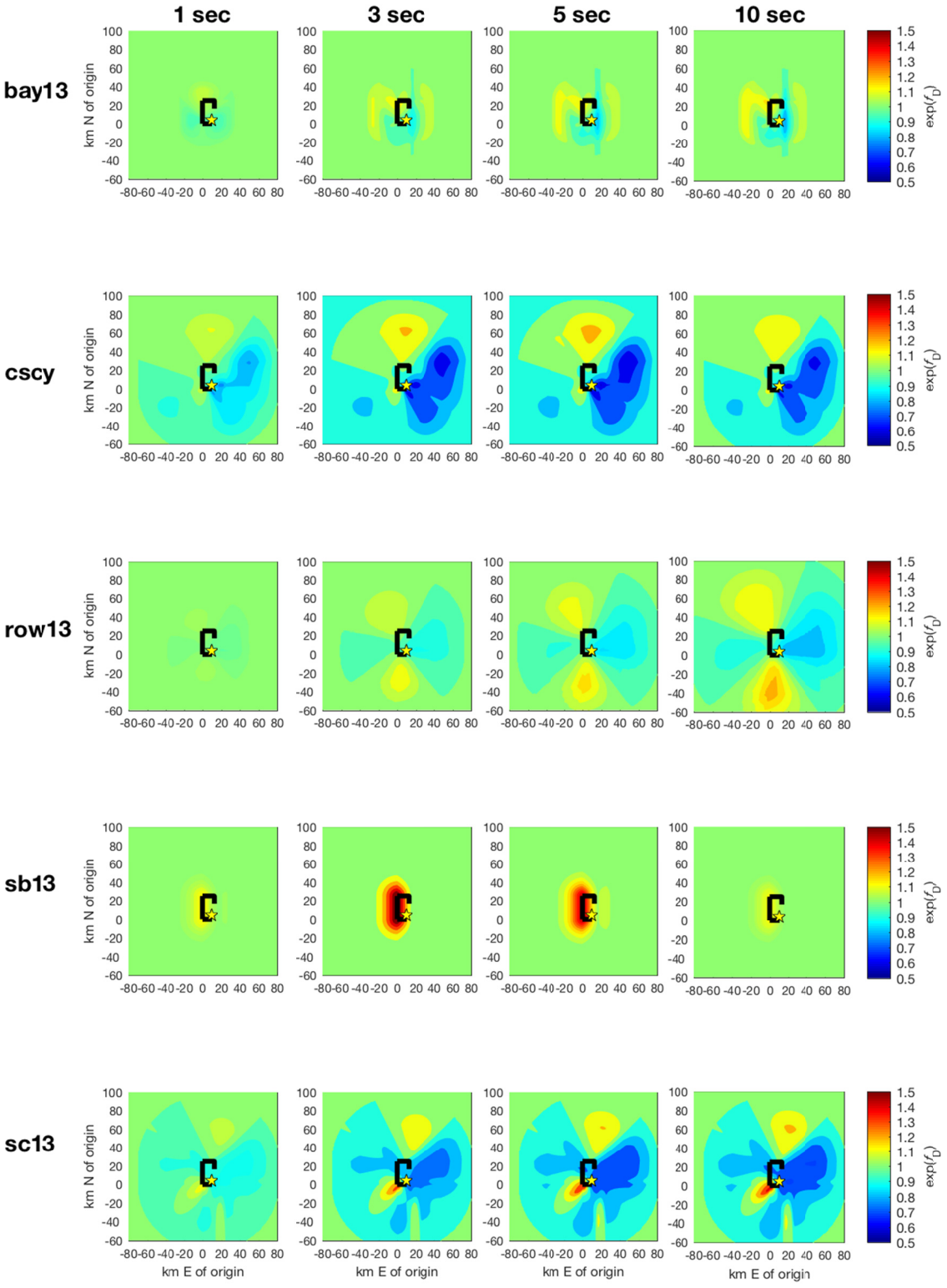

Figure 8 **Model predictions in arithmetic units $[\exp(f_D)]$ for four PSA oscillator periods (T = 1.0, 3.0, 5.0, and 10.0 sec) for five models in Table 1. M7.0 oblique–slip rupture scenario. Only right side of fault is shown due to symmetry.**

3.3 Recommendations for Directivity Model Selection

We consider each of the models listed in Table 1 to be a defensible choice for modeling of rupture directivity effects on the RotD50 component of ground motion. However, we recognize that many users will prefer to select a reduced number of models for practical application. In contemplating these selections, we considered whether the physical parameterizations, the level of model documentation, and whether the model has been widely applied previously on engineering projects. It is also important for the selected models to reasonably capture epistemic uncertainties, a major driver of which is whether directivity is parameterized primarily using fault dimension parallel to the slip direction (referred to as Group 1 models: bay13, sb13) or fault dimension in the rupture direction (Group 2: cscy) (variations of which also consider the slip direction, and are also included in Group 2; row13, sc13). These effects are especially important for application to reverse-slip earthquakes.

In consideration of these factors, we would ideally suggest that four models be used, providing two models in each group: bay13 and sb13 (Group 1), as well as cscy and row13 (Group 2). Models in the first group have been used on engineering projects, and, in general, are reasonably well documented and understood within the earthquake engineering profession. Models in the second group have seen limited application (the only application of which we are aware is the row13 model in Shakemap [Worden and Wald 2016] [*usgs.github.io/shakemap*], are not as well documented, and, in general, are not familiar to earthquake engineers. Despite these drawbacks, these models have a sound physical basis and are needed to capture epistemic uncertainties.

Given challenges with model implementation in hazard codes, we recognize that use of four models may be impractical and a reduced set of two models may often be needed. In this case, our current recommendation is to use bay13 and cscy, which stems in part from the extent to which they have been implemented in prior work and have a history of being subjected to project-level peer review.

The primary motivation for not selecting sb13 in the reduced set is the linking of directivity to pulse probability; we consider these two issues as not necessarily being fully correlated (e.g., it is possible to have a directivity effect on PSA without detectable pulse features in the time series). The motivation for not including sc13 is that the *DPP* parameterization in cscy has to some extent replaced the IDP parameterization in sc13. Although the row13 model

has many attractive features, its implementation has been limited. All of the models have attractive features and we hope to see them develop further and find utilization in practice in the future.

4 NGA-West2 Ground-Motion Model Centering

Recall from Chapter 1 that two centering issues are at play when using directivity models with GMMs. In the previous section we described centering of the directivity models. Here we address the related issue of GMM centering for the prediction of near-fault ground motions.

Four of the five NGA-West2 GMMs do not include a directivity term [Abrahamson et al. 2014; Boore et al. 2014; Campbell and Bozorgnia 2014; and Idriss 2014], whereas Chiou and Youngs [2014] incorporate the cscy directivity model. Because cscy is centered, when the Chiou and Youngs [2014] GMM is applied with $\Delta DPP = 0$, it presumably produces directivity-neutral ground motions. By comparing model predictions for other GMMs to Chiou and Youngs [2014] (with $\Delta DPP = 0$), we evaluated the extent to which these models may also estimate directivity-neutral ground motions such that they also could be considered as approximately centered.

Figure 9 illustrates ground-motion selection among the five GMMs for the approximate range of conditions relevant for near-fault ground motions: $\mathbf{M} > 6.5$ and distance $R_{rup} < 40$ km. Other than Idriss [2014] (for which most soil recordings were not selected), data selection among the remaining models was similar. This similarity of the datasets is important because it suggests that differences between Chiou and Youngs [2014] and other GMMs (with exception of Idriss [2014]) are unlikely to result from differences in the underlying data but rather from the model formulation.

Figure 10 compares GMM median predictions for reference rock ($V_{S30} = 760$ m/sec) for the ASK, BSSA, CB, CY, and Idriss models using the same three scenarios considered in Figures 6–8. These plots and many others for different scenarios generally do not support a finding of systematic bias of the CY model relative to the others at close distance. One exception is for oscillator periods of 5 and 7.5 sec, where CY plots below the others for distances > ~ 3–5 km. If this difference were a result of implicit directivity (from lack of centering) in non-CY

models, we would expect the largest difference at close distance, whereas the opposite is shown in Figure 10. Rather, this difference is caused by a factor applied to long-period ground motions by Chiou and Youngs that attempted to capture potential bias related to the limited available data [Chiou, *Personal Communication*, 2018]. This factor is not applied in other NGA-West2 models. Overall, our interpretation is that the results in Figure 10 are suggestive of centering of the ASK, BSSA, CB, and Idriss models.

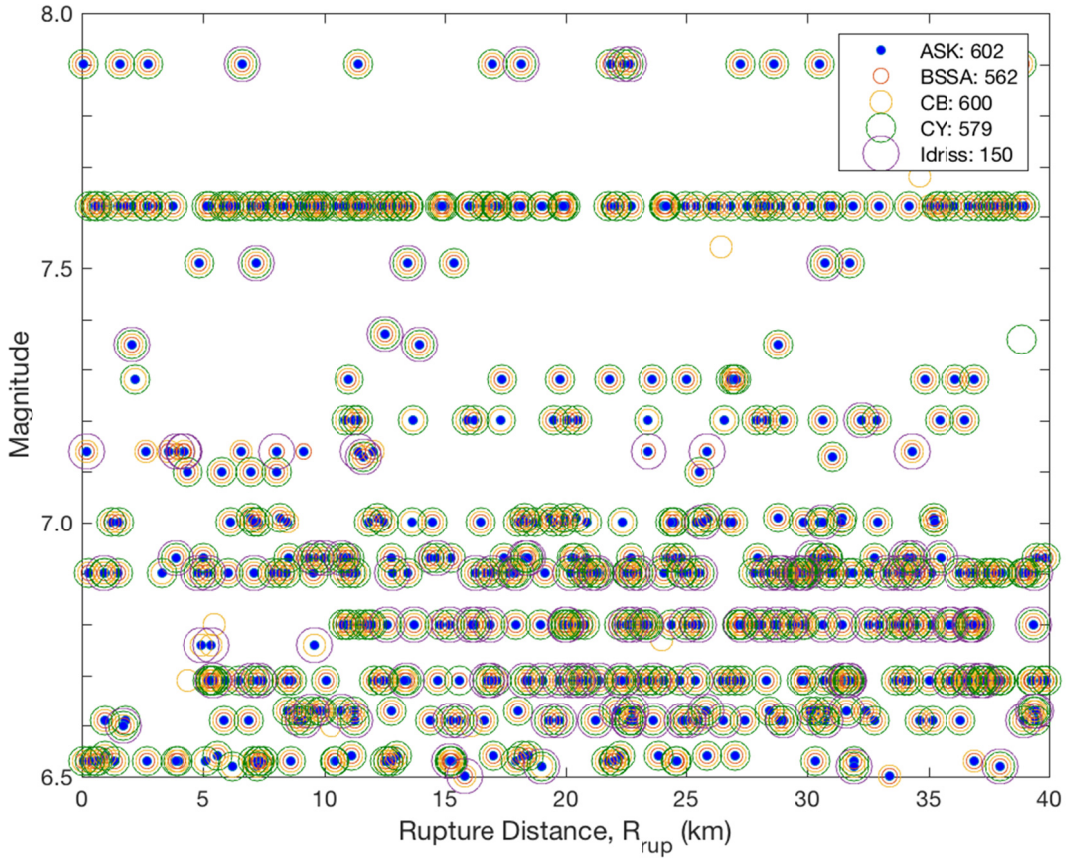

Figure 9 **Data selection for the five NGA-West2 GMMs for M > 6.5 events and R_{rup} < 40 km. The numbers of considered recordings for each GMM are marked in the legend. ASK = Abrahamson et al. [2014]; BSSA = Boore et al. [2014]; CB = Campbell and Bozorgnia [2014]; and CY = Chiou and Youngs [2014].**

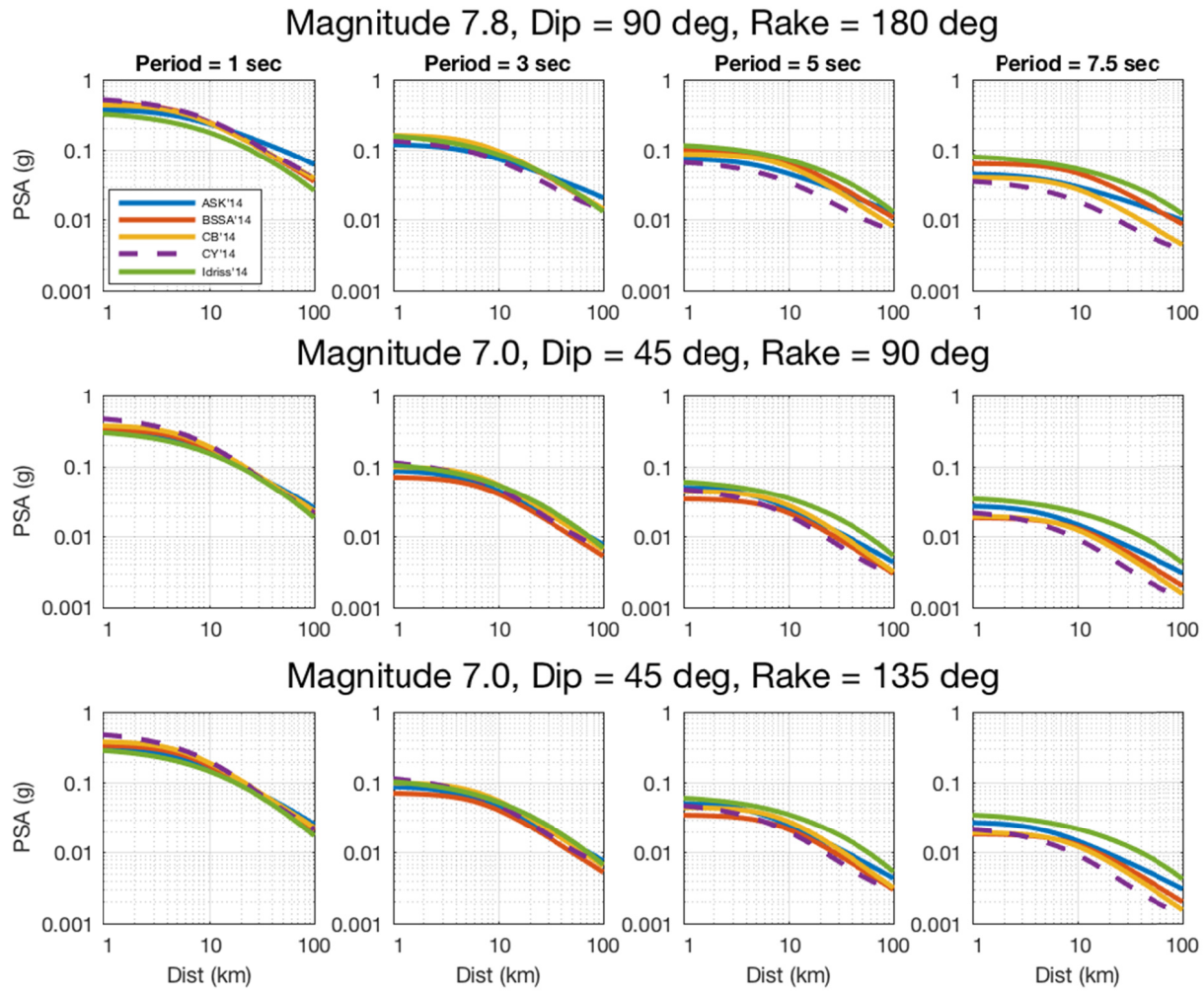

Figure 10 **Variations of median PSA with distance for three selected scenarios (as used in Figure 6–8) using the ASK, BSSA, CB, CY, and Idriss GMMs.**

As an independent check of centering, we examined the distribution of directivity parameter Δ*DPP* for events contributing data for the magnitude range depicted in Figure 9 (**M** > 6.5). We computed four mean Δ*DPP* values as follows (the standard error of the mean is also indicated):

1. Mean of all Δ*DPP* values in flatfile, regardless of distance: 0.011 ± 0.001 (75 events)
2. Mean of Δ*DPP* values for events with ≥ 10 recordings, regardless of distance: 0.033 ± 0.005 (40 events)
3. Mean of Δ*DPP* values for events with ≥ 10 recordings and R_{rup} < 40 km: 0.002 ± 0.0003 (30 events)

4. Mean of ΔDPP values for events with ≥ 10 recordings and $R_{rup} < 20$ km: 0.13 ± 0.035 (14 events)

These small values of mean ΔDPP indicate that the data sampling of near-fault records is not biased (i.e., on average, the data reflect a directivity-neutral condition). For reference, a value of $\Delta DPP = 0.1$ provides a maximum change in natural log ground motion of approximately 0.025 for 3-sec spectral acceleration. Our conclusion, based on the model comparisons and mean ΔDPP checks, is that non-directive NGA-West2 models ASK, BSSA, CB, and Idriss can be considered to reflect a directivity-neutral condition.

5 Application in Seismic Hazard Analysis

We have defined five alternative approaches by which rupture directivity effects, computed using models of the type in Table 1, can either be directly incorporated into probabilistic seismic hazard analysis (PSHA) or can be used to adjust PSHA results developed using relatively standard (without directivity) GMMs. These approaches consider alternate hypocenter locations within the finite area of a fault rupture in different ways. Those alternate hypocenters produce some degree of ground-motion variability, termed ϕ_{dir}. The symbol ϕ is used because it modifies the within-event variability in hazard calculations. Hypocenter locations and their associated ground-motion variabilities (ϕ_{dir}) are not considered in conventional PSHA. In concept, the availability of additional information on hypocenter location and its effect on ground motions may reduce within-event variability (ϕ_{ln}); because this effect is sufficiently small (and poorly developed) in the literature, it is not considered herein. The alternative methods, along with a baseline condition in which directivity is not considered, are described in the following subsections.

5.1 Baseline Directivity Neglected

Our baseline is composed of a PSHA that neglects directivity. This is typically calculated by either using: (1) GMMs that do not consider directivity; or (2) GMMs that include a directivity parameter, but with the value of the parameter set at the central value.

Figure 11 shows the location of reference sites in Hayward and Richmond, California. The Hayward site is located 0.5 km off the fault near the center of the fault. The Richmond site is located 0.5 km off the fault and 10 km south of the northern end of the fault. We performed PSHA using the ASK, BSSA, CB, and CY GMMs with the UCERF3 source model [Field et al. 2013]. The site conditions were taken as V_{S30} = 270 m/sec and default basin depths. Figure 12(a) and 12(b) show hazard curves for PSA at periods of 1, 3, and 10 sec for Hayward and Richmond,

respectively, while Figure 12(c) and 12(d) shows the uniform hazard spectra for return periods of 475 and 2475 years for each site. These baseline results are compared to subsequent results in which directivity is considered.

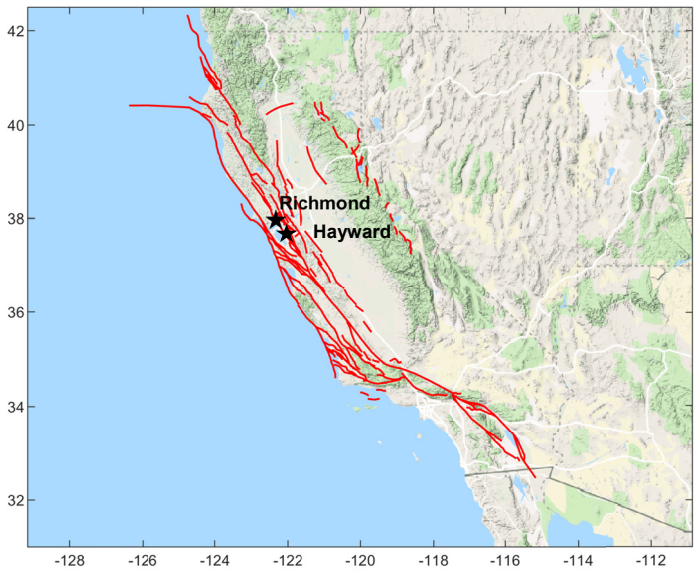

Figure 11 **Locations of reference sites in Hayward (mid-portion of Hayward fault) and Richmond (near end of Hayward fault).**

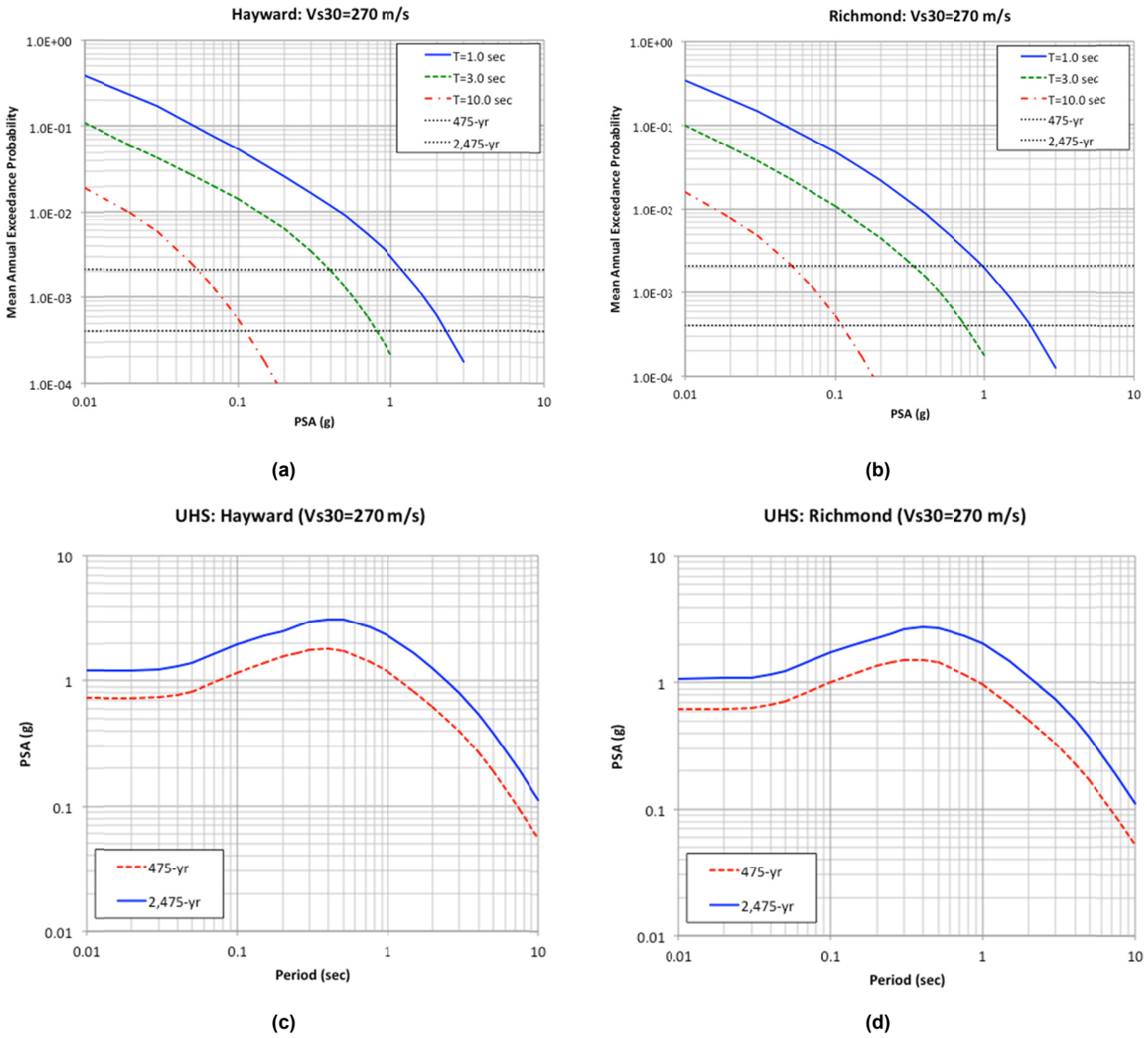

Figure 12 **Hazard curves for 1, 3, 10 sec PSA for baseline case (without directivity) for (a) Hayward and (b) Richmond sites; and uniform hazard spectra (UHS) without directivity for return periods of 475 and 2475 years for (c) Hayward and (d) Richmond sites.**

5.2 *A Posteriori* Modification

The options described in this section consist of running PSHA with directivity-neutral GMMs and then modifying the results in order to approximately account for directivity effects. The main advantage of these approaches is that by not modifying the hazard calculations, relatively familiar sources of hazard results to many engineers (e.g., USGS national maps, Petersen et al. [2015]; various commercial codes), which do not consider directivity, are used. A disadvantage

is that the resulting ground motions do not maintain the probability level (return period) determined from the PSHA.

Option 1. Composite Distribution Approach: Charts are used to provide location-specific: (1) change of mean in natural log units ($\Delta\mu$) relative to the directivity-neutral GMM for the applicable magnitude and distance; and (2) additional within-event ground-motion dispersion ϕ_{dir} associated with variations in ground motion from randomized hypocenter locations. Sets of plots for $\Delta\mu$ and ϕ_{dir} for various earthquake scenarios have been generated by Watson-Lamprey [2018] (using the cysc directivity model) and Rowshandel [*Personal Communication*, 2016] (using the row13 directivity model). Their results are based on sampling median ground motions on a grid of points at a range of constant distances around the fault (i.e., "racetracks") using multiple realizations of the hypocenter. The ground-motion computations use a non-directive GMM combined with the respective directivity models noted above. Figures 13 and 14 show example results for $\Delta\mu$ and ϕ_{dir} for the cases of **M**7 strike–slip and reverse–slip events (results for ϕ_{dir} are provided by Watson-Lamprey only). Results for additional scenarios are provided in the Appendix.

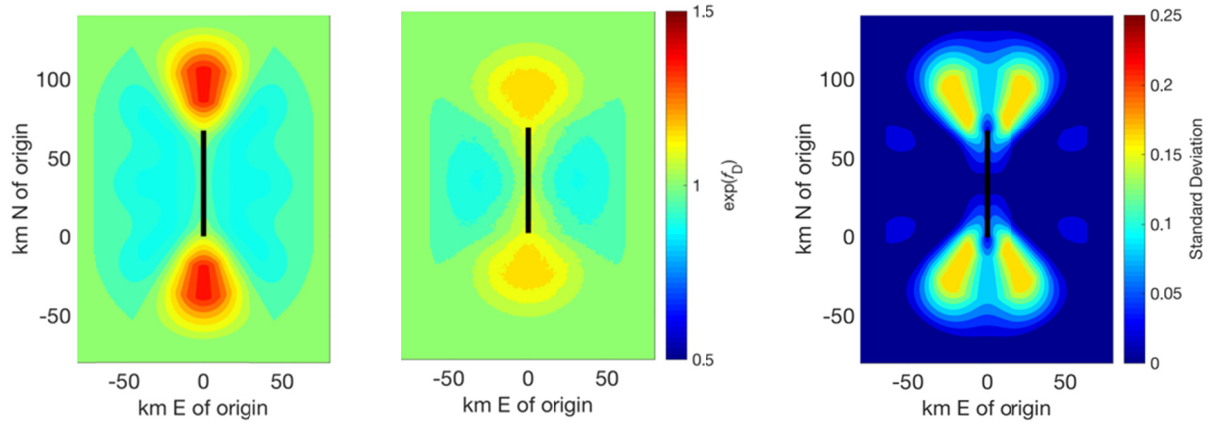

Watson-Lamprey, $\Delta\mu$ **Rowshandel, $\Delta\mu$** **Watson-Lamprey, ϕ_{dir}**

Figure 13 **For M7 strike–slip rupture, spatial pattern of change of natural log mean ($\Delta\mu$) and directivity-related aleatory variability (ϕ_{dir}) for a 3.0-sec PSA resulting from alternate hypocenter locations within rupture surface.**

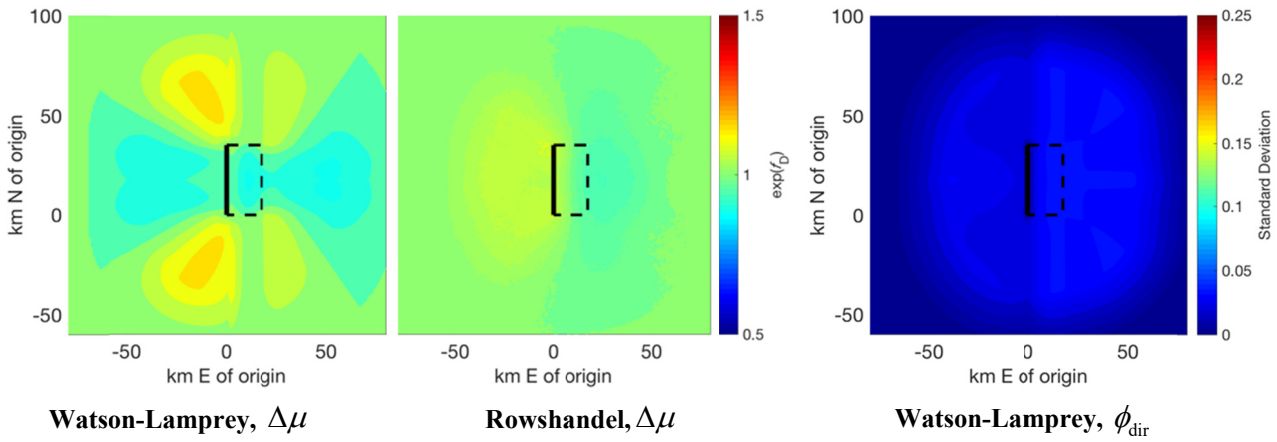

Figure 14 **For M7 reverse rupture, spatial pattern of change of natural log mean ($\Delta\mu$) and directivity-related aleatory variability (ϕ_{dir}) for a 3.0-sec PSA resulting from alternate hypocenter locations within rupture surface.**

The composite distribution approach allows for *a posteriori* changes to baseline PSHA results. This ground-motion change is computed as follows:

1. Perform ordinary hazard analysis for the location of interest;
2. Deaggregate the hazard for the hazard level and IM of interest. Find the relative contribution (*RC*) to the hazard from the proximate fault for which directivity effects are to be considered. The *RC* term could be a sum over multiple faults if more than one might contribute to the directivity effect;
3. From deaggregation, find the epsilon (ε) for the fault of interest from Step 2 (ε is defined as the fractional number of standard deviations above or below the natural log mean). Alternatively, with some approximation, ε could be taken as the mean value across all sources, which is a typical output of hazard codes; and
4. Compute the modified IM level using Equation (2)

$$\ln\left(IM_{\text{mod}}\right) = \ln\left(IM_{\text{bl}}\right) + RC\left[\Delta\mu + \varepsilon\left(\sqrt{\sigma_{\ln}^2 + \phi_{dir}^2} - \sigma_{\ln}\right)\right] \quad (2)$$

where IM_{bl} is the baseline hazard result for the point of interest, and $\sigma_{\ln}$ is the total dispersion (including within- and between-event contributions) from the GMM used in hazard analysis, which should be evaluated using the magnitude and distance from deaggregation (as applicable). The *RC* term is included on the right side of the equation under the expectation that only the fault

from Step (2) produces directivity effects at the site. As noted by Watson-Lamprey [2018], the effect of standard deviation change is often small.

For the Hayward site shown in Figure 11, deaggregation results are shown in Figure 15(a). The relative contribution of the Hayward fault to the 3.0-sec hazard at the 475 year return period is 81%. Using the composite distribution models by Watson Lamprey [2018], and the site location relative to the fault indicated in Figure 15(b), the spatial pattern maps provide $\Delta\mu = -0.048$ and $\phi_{\text{dir}} = 0.0142$. These effects largely offset each other, and the resulting change on the uniform hazard spectrum is negligible in this case, as shown in Figure 15(c). The ordinates shown in Figure 15(c) follow the procedure given above for each spectral period and both return periods. Figure 15(d) shows that this site location has a stronger mean directivity effect using the Rowshandel model. To develop the composite distribution spectra in Figure 15(e), we use ϕ_{dir} from Watson-Lamprey, although the effect of applying this uncertainty is very small. The larger mean directivity effect $(\Delta\mu = +0.060)$ from the Rowshandel model is apparent in the spectra [Figure 15(e)], which are appreciably increased relative to the non-directive spectra for periods greater than 1.0 sec.

For the Richmond site shown in Figure 11, deaggregation results are shown in Figure 16(a). The relative contribution of the Hayward fault to the 3.0-sec hazard at the 475 year return period is 74%. Using the composite distribution models by Watson Lamprey [2018], and the site location relative to the fault indicated in Figure 16(b), the spatial pattern maps provide $\Delta\mu = 0.03$ and $\phi_{\text{dir}} = 0.0471$. The resulting change on the uniform hazard spectrum is again small, as shown in Figure 16(c). This occurs because the composite distribution model only provides significant forward directivity off the end of the fault, and the Richmond site is about 5 km inward from the end of the fault. The composite distribution spectra for the Rowshandel model are developed as described above, with the mean directivity effect being $\Delta\mu = 0.068$. As with the Hayward site, the directivity effect is stronger when the Rowshandel model is used, although the differences between the two sites is modest.

The deterministic application of the change in mean and standard deviation that is proposed in this section is an approach that is suggested by the authors of this report and endorsed by the Panel. No endorsement by the developers of the underlying relations (Jennie

Watson-Lamprey and Badie Rowshandel) is implied. Their development of these procedures was intended for a different implementation approach (Option 3, Section 5.3).

Option 2. Scenario Event Incorporating Directivity: The conditional mean spectrum (CMS) [Baker 2011] is sometimes used to provide a more realistic representation of seismic demand for a particular structure than the UHS. The CMS is computed for a *scenario event* identified through disaggregation of the hazard at a matching period (T*) where the CMS ordinate matches the uniform hazard spectral ordinate. As such, the scenario applies for a specific magnitude and distance, which can usually be attributed to a particular fault. We suggest the following modification of the scenario event for the effects of directivity in the CMS computation:

$$\mu_{\ln PSA(T)|\ln PSA(T^*)} = \left[\mu_{\ln PSA(T)}\left(\mathbf{M}, R, F, site\right) + f_D\left(\mathbf{M}, R, F, \boldsymbol{h}, T\right)\right] + \rho\left(T, T^*\right)\bar{\varepsilon}\left(T^*\right)\sigma_{\ln(T)} \quad (3)$$

where $\mu_{\ln PSA(T)|\ln PSA(T^*)}$ is the CMS ordinate at period T; $\mu_{\ln PSA(T)}$ is the natural log mean ground motion from a non-directive GMM; **M** and R are the magnitude and distance for the scenario event, respectively; F represents the style of faulting for the source of that event; *site* represents suitable site parameters; $\boldsymbol{h}$ represents an assumed hypocenter location used for calculation of the directivity term; $f_D, \bar{\varepsilon}(T^*)$ is the mean epsilon value from disaggregation at matching period T^* (which causes the CMS ordinate at T^* to match the UHS); and $\rho(T, T^*)$ is the correlation coefficient between PSA ordinates at different oscillator periods; see Baker and Jarayam [2008]).

Equation (3) has been modified from the standard CMS calculation through the use of the additive f_D term, which requires the specification of a hypocenter location. Previous studies [e.g., Abrahamson [2000]) have shown that if the return period of essentially full-segment ruptures on a fault is substantially less than the return period of ground motions being considered in the hazard analysis, the hazard will be controlled at long periods by scenarios producing forward directivity. Until further research can be completed to provide more detailed guidance, we suggest to conservatively assume that the hypocenter is located relative to the site at the furthest location along–strike for strike–slip earthquakes or along–strike and down–dip for dip–slip earthquakes. Note that ϕ_{dir} does not appear in Equation (3); this is because the directive CMS applies for a single (assumed) hypocenter.

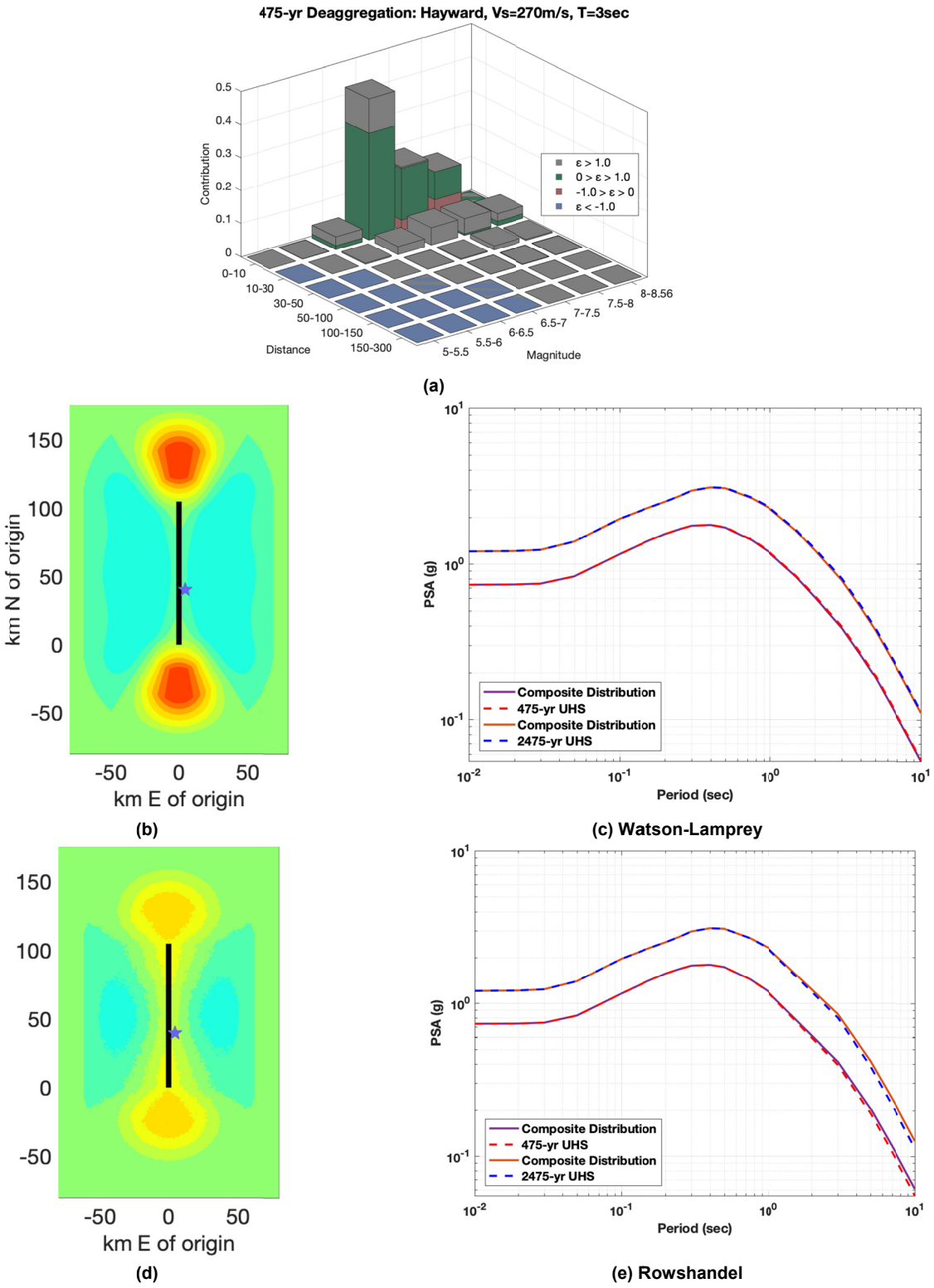

Figure 15 **(a) Deaggregation for 3.0 sec Sa at the Hayward site; (b, d) change of natural log mean ($\Delta\mu$) with approximate site location for Watson-Lamprey and Rowshandel models; (c, e) uniform hazard spectra with directivity adjustment from composite distribution approach.**

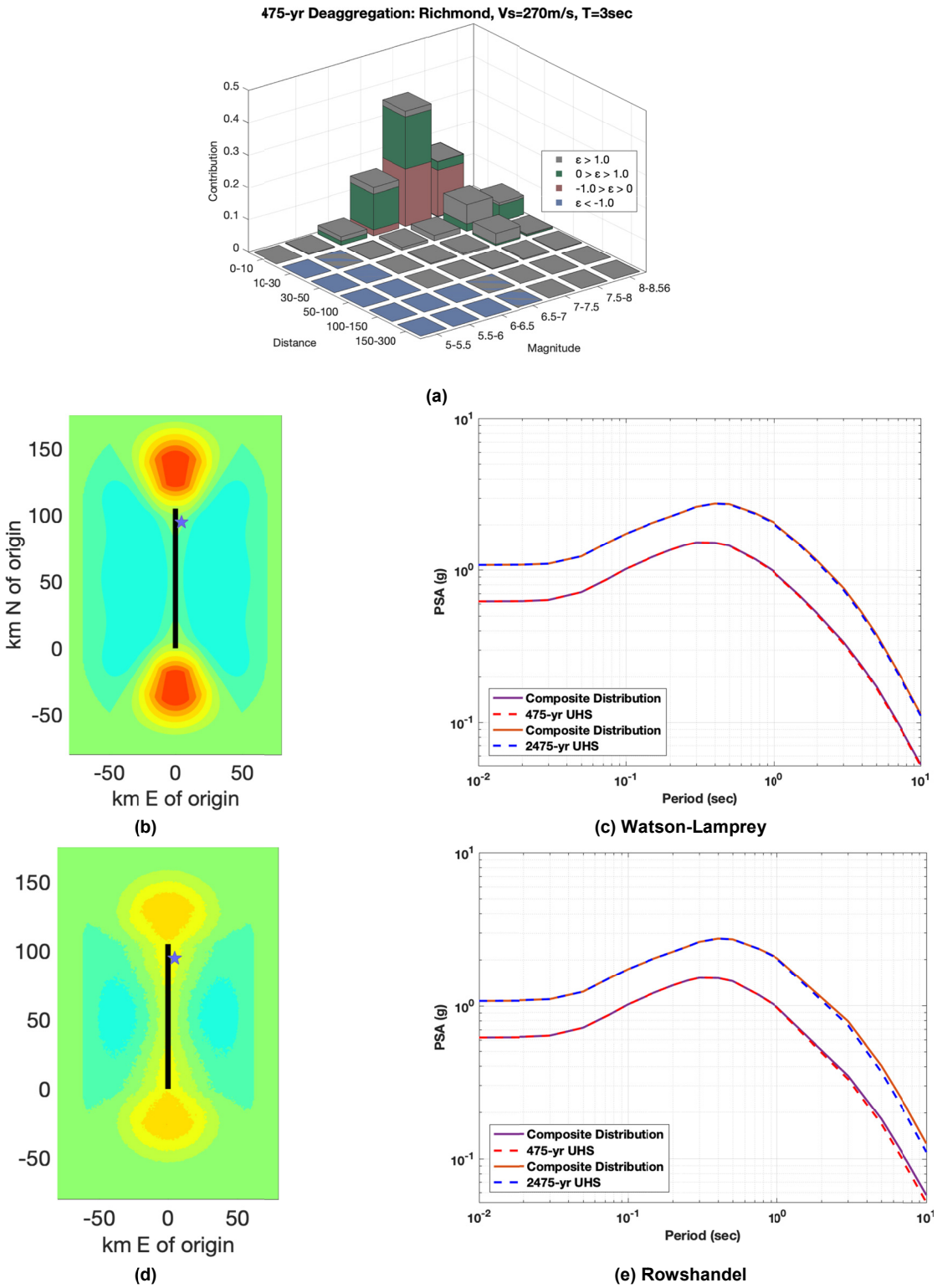

Figure 16 **(a) Deaggregation for 3.0-sec Sa at the Richmond site; (b, d) change of natural log mean $(\Delta\mu)$ with approximate site location for Watson-Lamprey and Rowshandel models; and (c, e) uniform hazard spectra with directivity adjustment from composite distribution approach.**

Returning to the examples introduced in Figure 11, the baseline (directivity-neutral) UHS, their associated (directivity neutral) CMS using a matching period of 3 sec, and CMS computed using Equation (3) in which rupture is assumed to occur from the southern-most end of the Hayward fault towards the sites are plotted in Figure 17. The bay13 directivity model was used for this calculation. As expected, the directive CMS at long periods has spectral ordinates exceeding those from the non-directive CMS. Note that the directive CMS ordinate at T^* does not match the UHS if the f_D correction at that period is non-zero. Relative to the non-directive CMS, the increase at T^* (3.0 sec) is larger than that observed with the composite distribution approach (approximately 10% for Hayward site and 20% for the Richmond site).

We recognize that some engineers prefer the use of the UHS to the CMS for use in seismic demand characterization. Other publications discuss the relative merits of each approach; see NIST [2011] and Haselton et al. [2017]. For the present application of incorporating directivity into *a posteriori* spectra, the CMS is preferred because the scenario event is defined from deaggregation of a specific IM, which is inherently compatible with the use of a conditioning period in CMS. Nonetheless, an approach similar to that described above can be adapted to UHS under some circumstances. In cases where a single fault dominates the hazard at long periods, an approximate adjustment to the mean UHS can be made by adding (in natural log units) the f_D term that is produced by the dominant fault for an assumed hypocenter location. The hypocenter would be assumed in a conservative manner, as described above. The result of this adjustment for the example sites are shown in Figure 18.

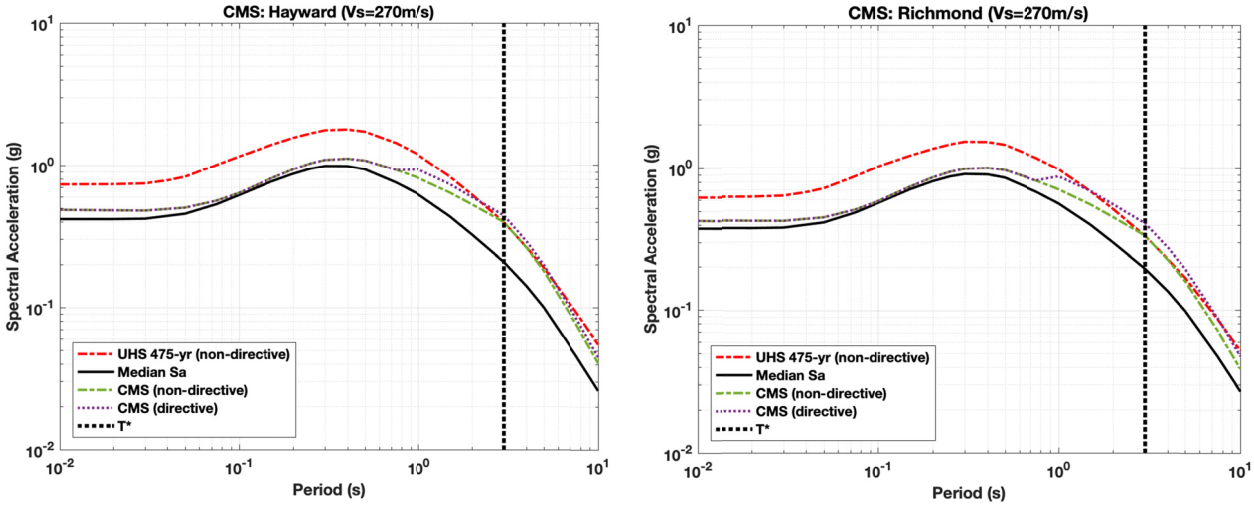

Figure 17 **(a) Example of median spectral acceleration at Hayward site given M7.1, R_{rup}=5.5 km, conditional mean spectra computed at T^* = 3 sec with $\varepsilon = 0.8$, using directive and non-directive approaches, and uniform hazard spectra (non-directive); and (b) example of median spectral acceleration at Richmond site given M7.3, R_{rup} = 7.7 km, conditional mean spectrum computed at T^* = 3 sec with $\varepsilon = 0.65$, using directive and non-directive approaches, and uniform hazard spectrum (non-directive).**

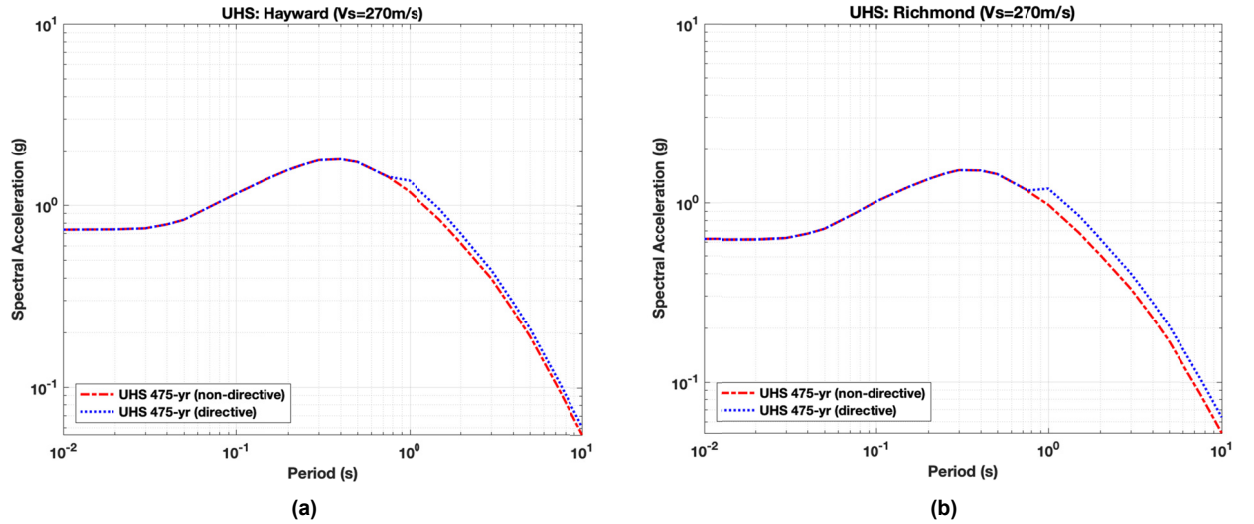

Figure 18 **Example of uniform hazard spectrum adjusted for rupture directivity using the bay13 directivity model at the (a) Hayward and (b) Richmond sites. These sites lend themselves to such an adjustment because Hayward events are dominant for the full period range of the spectrum.**

5.3 Incorporation of Directivity into Hazard Integral

The standard hazard integral that is used for conditions where directivity is not considered can be written as follows for a single fault (modified from Kramer [1996]):

$$v_{\mathrm{PSA}}(psa) = \lambda_{\mathbf{M}_0} \int_{\mathbf{M}} \int_{R} P[PSA > psa \,|\, \mathbf{m}, r] \, f_M(\mathbf{m}) \, f_R(r) d\,\mathbf{m}\, d\, r \tag{4}$$

where $v_{\mathrm{PSA}}(psa)$ is the time rate of exceedance of target spectral acceleration level (*psa*), and $\lambda_{\mathbf{M}_0}$ is the time rate of earthquakes with $\mathbf{M} > \mathbf{M}_0$. The integrations in Equation (4) are over magnitude and distance. A further integration over ε is implicit to computation of the ground-motion probability term. The standard hazard integral in Equation (4) is extended below to incorporate directivity effects by considering, directly or indirectly, variability in hypocenter location on the fault.

Option 3. Modified Moments from Randomized Hypocenter: The adjustments to the natural log mean ($\Delta\mu$) and standard deviation ϕ_{dir} produced by the composite distribution approach can be utilized within the hazard integral. These adjustments affect the mean and standard deviation of the probability density function for an IM as follows:

$$\mu'_{\ln PSA} = \mu_{\ln PSA} + \Delta\mu \tag{5}$$

$$\sigma'_{\ln} = \sqrt{\sigma^2_{\ln} + \phi^2_{dir}} \tag{6}$$

where the prime ($'$) indicates the modified GMM moment, and $\Delta\mu$ and ϕ_{dir} are evaluated for each fault considered in the hazard analysis using mapped values as in Figures 13–14 and the Appendix. Moments $\mu'_{\ln PSA}$ and $\sigma_{\ln}$ are the natural log mean and standard deviation from a non-directive GMM. This approach has not been implemented in hazard codes as of this writing. Option 3 requires only modest additional computational burden relative to a standard hazard analysis. Options 4 and 5 involve additional loops in the hazard integral and are more computationally intensive. Option 3 is the originally intended approach for implementation of the recommendations in Watson-Lamprey [2018].

Option 4. Directivity Parameter Randomization: An additional integration loop is added to the hazard integral to sample the range of the directivity parameter that is realizable given the site location relative to the fault. A suite of directivity parameters on racetracks around the fault

are computed in much the same manner used for computing changes in ground motion in the composite distribution approach. For a given location, this process leads to a distribution of the directivity parameter (*DP*), which has a probability density function $f_{DP}(dp)$. As shown in Figure 19, preliminary investigations for directivity parameter Δ*DPP* by Brian Chiou [*Personal Communication*, 2018] suggest distribution shapes that peak at or near one or both limits of the parameter range; such distributions are incompatible with the commonly used normal density function, but can be described using a beta distribution. Further work will be needed to map the distribution of the four parameters required to describe the beta distribution as a function of position around faults, magnitude, and source type. Moreover, the distribution of other types of directivity parameters has not been investigated. That being the case, Option 4 has not yet been implemented.

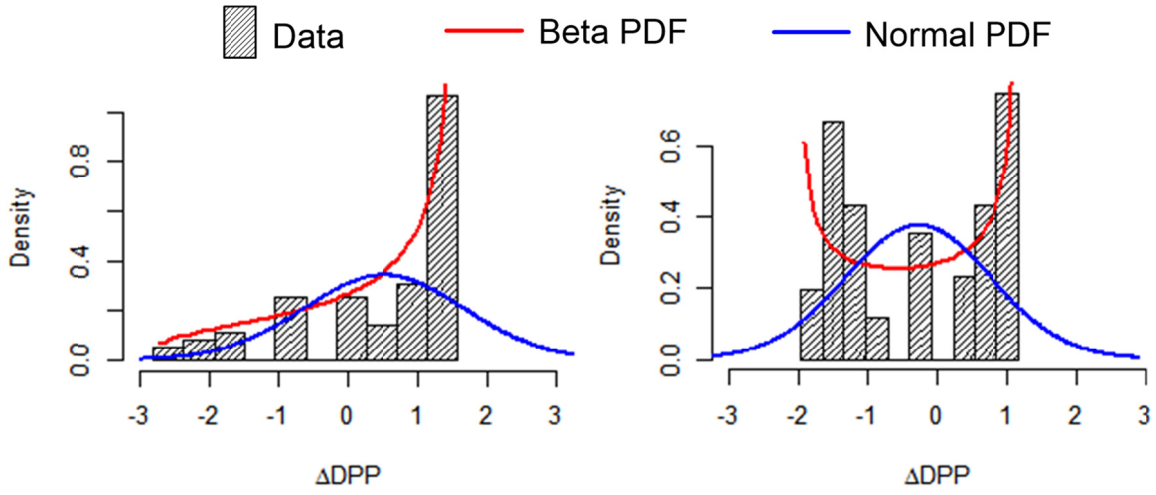

Figure 19 **Distributions of directivity parameter Δ*DPP* at different locations near a vertically dipping strike slip fault [Chiou, *Personal Communication*, 2018]. A normal distribution does not fit the data, whereas a beta distribution provides a reasonable match.**

The resulting hazard integral can be written:

$$v_{\mathrm{PSA}}(psa) = \lambda_{\mathbf{M}_0} \int_{\mathbf{M}} \int_{R} \int_{DP} P[PSA > psa \,|\, \mathbf{m}, r, dp] \, f_M(\mathbf{m}) f_R(r) f_{DP}(dp) d\,\mathbf{m}\, d\, r\, d(dp) \qquad (7)$$

Note that the ground-motion probability computation in Equation (7) includes conditioning on *dp*; the underlying model includes a non-directive GMM modified with a directivity model f_{DP}. The use of location-specific probability density function $f_{DP}(dp)$ accounts for variability in hypocenter location.

Option 5. Hypocenter Randomization: Relative to Equation (4), an additional loop in the hazard integral is provided based directly on hypocenter location, as follows:

$$v_{PSA}(psa) = \lambda_{\mathbf{M}_0} \int_{\mathbf{M}} \int_{R} \int_{\mathcal{H}} P[PSA > psa \,|\, \mathbf{m}, r, hyp] \, f_M(\mathbf{m}) f_R(r) f_{HYP}(\boldsymbol{h}) d\,\mathbf{m}\, dr d\boldsymbol{h} \qquad (8)$$

where $\boldsymbol{h}$ represents hypocenter location, which affects the calculation of directivity parameters. Variants on Equation (8) have been presented previously by Abrahamson [2000], Chioccarelli and Iervolino [2013], and Spagnuolo et al. [2016]. Equation (8) is more computationally demanding than Options 1–4 due both to the looping over hypocenter locations and the computation of directivity parameters (and their effect on ground motions) for each location.

Results of hazard calculations using Equation (8) are considered to be the most accurate, and, as such, it is useful to compare outcomes of more approximate procedures (e.g., Options 1 and 2) to those for Option 5. For this purpose, we performed PSHA using the same GMMs and source model as for the non-directive case; see Figure 12. The directivity model used in the calculation is bay13, and the hypocenter distribution was taken as uniform.

Figure 20 shows hazard curves at periods of 1, 3, and 10 sec and UHS for return periods of 475 and 2475 years for each site. Table 2 shows % changes in the 1.0-, 3.0-, and 10-sec hazard relative to the non-directive case for the two hazard levels. The results indicate an amplifying effect of directivity at long periods, which is slightly stronger for the Richmond site than the Hayward site. This occurs because ruptures producing forward directivity (i.e., originating near the ends of the fault) dominate the hazard, as found previously by Abrahamson [2000]. The effect of directivity is qualitatively similar in trend to that found in the Option 2, although without the spectral peak associated with the use of the CMS. The effect is markedly different from that found with Option 1. There are two potential causes of these differences: (1) the

approximation implicit to the composite distribution approach; and (2) the use of different directivity models in the two alternative composite distribution maps (cscy and row13). Of these, cause 1 is likely to be more significant, given the general similarity of directivity models for strike–slip faults (Figure 6). Based on these preliminary results, the use of the composite distribution approach may be unconservative for sites along (not off the ends of) strike–slip faults, like in the two example sites. Different results may be obtained for sites off the ends of faults.

Table 2 **For the Hayward and Richmond sites: percent change in spectral accelerations for two hazard levels when directivity is considered in the hazard calculation (change is computed relative to the non-directive hazard).**

Site and Return Period	Sa (1.0 sec)	Sa (3.0 sec)	Sa (10 sec)
Hayward, 475 year	10	7.7	10
Hayward, 2475 year	11	9.5	16
Richmond, 475 year	11	11	11
Richmond, 2475 year	13	12	16

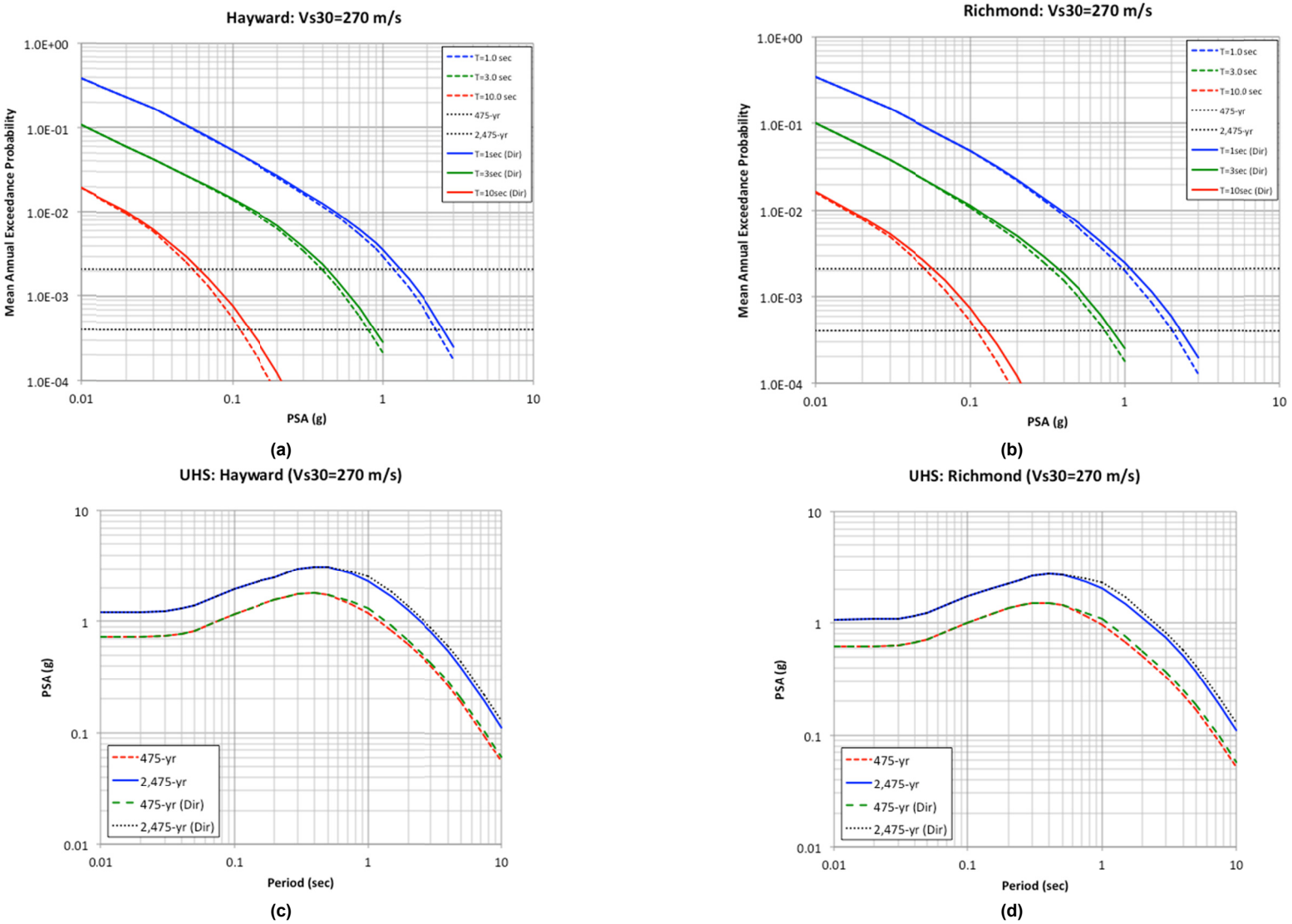

Figure 20 **Probabilistic seismic hazard analysis results in which directivity effects are incorporated into the hazard integral using the bay13 model. Hazard curves for 1-, 3-, and 10-sec spectral acceleration for (a) Hayward and (b) Richmond. Uniform hazard spectra for (c) Hayward and (d) Richmond.**

6 Conclusions

This report reviewed the available directivity models, as developed in the NGA-West2 project and summarized in Table 1. Based on this evaluation, guidance for their implementation using probabilistic and deterministic procedures was provided. There are some notable differences in the parameterization of these models, with the principal difference being that some quantify directivity based strictly on the direction of the fault rupture propagation aligning with the slip direction, while others only consider the amount of fault rupture towards the site (even if the azimuth of rupture propagation does not align with the fault-slip direction). The significance of this difference is realized most strongly for dip–slip faults, where the former approach produces directivity in the up–dip direction, while the latter tends to accumulate these effects in the direction of rupture propagation provided it is not orthogonal to the slip direction.

There is broad similarity between model predictions for strike–slip ruptures, but, consistent with previous studies, substantial differences are evident for dip–slip ruptures due to the different directivity parameterizations. We consider all of the models to be suitable for application to capture directivity effects on the RotD50 component of ground motion. We understand that a reduced set of models will typically be used for practical applications. To capture epistemic uncertainties in such a reduced set, it is important to include models with both types of directivity parameterization: (1) primarily using fault dimension parallel to the slip direction (bay13, sb13) or (2) primarily using fault dimension in the rupture direction (cscy) (variations of which also consider the slip direction, e.g., row13 or sc13). These differences are especially important for application to reverse-slip earthquakes. In consideration of these factors, we suggest that four models be used, providing two in each group: bay13 and sb13 for the first group) and cscy and row13 for the second. Models in the first group have seen widespread use by the engineering profession, and are generally reasonably well documented and understood. Models in the second group have not been widely applied within the earthquake engineering

profession and are not as well documented or understood, but they have a sound physical basis and should be represented in model selection to capture epistemic uncertainties. For cases where a reduced set of two models is needed, our current recommendation is to use bay13 and cscy, which stems in part from the extent to which they have been implemented in prior work and subject to project-level peer review. Further discussion of these recommendations is provided in Section 3.3.

We present five alternative means by which directivity effects may be considered in ground-motion hazard analysis. Two of these are deterministic methods that modify PSHA results derived using traditional (non-directive) GMMs. The composite distribution approach considers the effect of variable hypocenter locations in location-specific (relative to fault) changes to the ground-motion mean and standard deviation, which in turn are used with disaggregation results to make approximate *a posteriori* ground-motion adjustments. The second deterministic method modifies the properties of scenario (conditional mean) spectra to account for rupture directivity. The three probabilistic methods consider the effects of variable hypocenter location within the hazard integral in different ways. Only one of these, in which hypocenter location is directly considered (at some computational cost), is implemented in hazard codes as of this writing.

Implementation of the two deterministic methods and the fully probabilistic method for example sites along the Hayward fault show variable effects of directivity. Some caveats need to be considered when comparing these results, the most important of which is the fully probabilistic implementation uses a different directivity model from those used in the composite distribution approach. Nevertheless, given the qualitative similarity between models of directivity results for strike–slip earthquakes (Section 3.2), probabilistic versus deterministic method comparisons, while imperfect, are not without merit.

The composite distribution approach as implemented using the Watson-Lamprey model substantially under-predicts the directivity effect relative to that from the fully probabilistic analysis for the two considered sites. This result occurs for sites located along strike–slip faults; different results would be expected for sites off the end of the fault (not considered in the examples presented here). The Rowshandel model, as implemented in the composite distribution approach, estimates directivity effects for along–fault sites in much better agreement with fully probabilistic analysis. The changes in spectral ordinates at 3.0 sec relative to non-directive

analysis are about 6–7% (similar to the $\Delta\mu$ values given in Section 5.2), which under-predicts to a less significant extent the directivity effects given in Table 2.

The conditional mean spectra approach (Option 2), implemented with the hypocenter in an unfavorable position to produce a strong forward directivity effect, produces stronger directivity effects than either the composite distribution approach (Option 1) or the fully probabilistic analysis (Option 5). The increases at 3.0 sec of approximately 10% for the Hayward site and 20% for the Richmond site can be compared to those in Table 2 (8 to 10% for Hayward, 11 to 12% for Richmond). Such differences are expected given the conservative assumption of hypocenter location made in Option 2.

References

Abrahamson N.A (2000). Effects of rupture directivity on probabilistic seismic hazard analysis, *Proceedings, 6th International Conference on Seismic Zonation*, Earthquake Engineering Research Institute, Oakland, CA.

Abrahamson N.A., Silva W.J., Kamai R. (2014). Summary of the ASK14 ground motion relation for active crustal regions, *Earthq. Spectra*, 30: 1025–1055.

ASCE (2016). *Minimum Design Loads for Buildings and Other Structures*, American Society of Civil Engineers ASCE/SEI 7-16, Reston, VA.

Baker J.W. (2011). Conditional mean spectrum: Tool for ground motion selection, ASCE, *J. Struct. Eng.*, 137: 322–331.

Baker J.W., Jayaram N. (2008). Correlation of spectral acceleration values from NGA ground motion models, *Earthq. Spectra*, 24: 299–317.

Bayless J.R., Somerville P.G. (2013). *Final Report of the NGA-West2 Directivity Working Group*, Chapter 2, *PEER Report No. 2013/09*, Pacific Earthquake Engineering Research Center, University of California, Berkeley, CA.

Benioff H. (1955). Mechanism and strain characteristics of the White Wolf fault as indicated by the aftershock sequence, in *Earthquakes in Kern County, California During 1955*, California Division of Mines, Bulletin 171, B.B. Oakeshoot (ed.), pp. 199–202.

Bernard P. Madariaga R. (1984). A new asymptotic method for the modelling of near field accelerograms, *Bull. Seismol. Soc. Am.*, 74: 539–558.

Boore D.M. (2010). Orientation-independent, nongeometric-mean measures of seismic intensity from two horizontal components of motion, *Bull. Seism. Soc. Am.*, 100: 1830–1835.

Boore D.M., Joyner W.B. (1978). The influence of rupture incoherence on seismic directivity, *Bull. Seism. Soc. Am.*, 68: 283–300.

Boore D.M., Stewart J.P., Seyhan E., Atkinson G.M. (2014). NGA-West2 equations for predicting PGA, PGV, and 5% damped PSA for shallow crustal earthquakes, *Earthq. Spectra*, 30: 1057–1085.

Bozorgnia, Y., Abrahamson N.A., Atik L.A., Ancheta T.D., Atkinson G.M., Baker J.W., Baltay A., Boore D.M., Campbel K.W.l, Chiou B.S.-J., Darragh R., Day, S., Donahue J.L., Graves R.W., Gregor N., Hanks T., Idriss I.M., Kamai R., Kishida R., Kottke A., Mahin S.A., Rezaeian S., Rowshandel B., Seyhan E., Shahi S., Shantz T., Silva W.P., Spudich P., Stewart J.P., Watson-Lamprey J.A., Wooddell K., Youngs R. (2014). NGA-West2 research project, *Earthq. Spectra*, 30: 973–987.

Bozorgnia Y., Campbell K.W. (2004). Engineering characterization of ground motion, in *Earthquake Engineering: From Engineering Seismology to Performance-Based Engineering*, Y. Bozorgnia and V.V. Bertero (eds.), CRC Press, Boca Raton, FL.

BSSC (2015). *NEHRP Recommended Seismic Provisions for New Buildings and Other Structures,* Building Seismic Safety Council*,* Federal Emergency Management Agency, Washington D.C.

Burks L.S., Baker J.W. (2016). A predictive model for fling-step in near-fault ground motions based on recordings and simulations, *Soil Dyn. Earthq. Eng.*, 80: 119–126.

Caltrans (2013). *Seismic Design Criteria –Appendix B Design Spectrum Development*, Version 1.7, California Department of Transportation, Sacramento, CA.

Campbell K.W., Bozorgnia Y. (2014). NGA-West2 ground motion model for the average horizontal components of PGA, PGV, and 5% damped linear acceleration response spectra, *Earthq. Spectra*, 30: 1087–1115.

Chioccarelli E., Iervolino I. (2013). Near source seismic hazard and design scenarios, *Earthq. Eng. Struct. Dyn.*, 42: 603–622.

Chiou B.S.-J (2018). P*ersonal Communication*.

Chiou B.S.-J., Spudich P. (2013). *Final Report of the NGA-West2 Directivity Working Group*, Chapter 6, *PEER Report No. 2013/09*, Pacific Earthquake Engineering Research Center, University of California, Berkeley, CA.

Chiou B.S.-J., Youngs R.R. (2014). Update of the Chiou and Youngs NGA model for the average horizontal component of peak ground motion and response spectra, *Earthq. Spectra*, 30, 1117–1153.

Field E.H., Biasi G.P., Bird P., Dawson T.E., Felzer K.R., Jackson D.D., Johnson K.M., Jordan T.H., Madden C., Michael A.J., Milner K.R., Page M.T., Parsons T., Powers P.M., Shaw B.E., Thatcher W.R., Weldon R.J., II, Zeng Y. (2013). Uniform California earthquake rupture forecast, Version 3 (UCERF3) – The time-independent model, *USGS Open-File Report 2013–1165*, *CGS Special Report 228*, and *Southern California Earthquake Center Publication 1792*, *http://pubs.usgs.gov/of/2013/1165/.*

Haselton C.B., Baker J.W., Stewart J.P., Whittaker A.S., Luco N., Fry A., Hamburger R.O., Zimmerman R.B., Hooper J.D., Charney F.A., Pekelnicky R.G. (2017). Response history analysis for the design of new buildings in the NEHRP Provisions and ASCE/SEI 7 Standard: Part I – Overview and specification of ground motions, *Earthq. Spectra*, 33: 373–395.

Idriss I.M. (2014). An NGA-West2 empirical model for estimating the horizontal spectral values generated by shallow crustal earthquakes, *Earthq. Spectra*, 30: 1155–1177.

Kamai R., Abrahamson N.A., Graves R.W. (2014). Adding fling effects to processed ground-motion time histories, *Bull. Seismol. Soc. Am.*, 104: 1914–1929.

Kramer S.L. (1996). *Geotechnical Earthquake Engineering*. Prentice-Hall, New Jersey.

NIST (2011). Selecting and scaling earthquake ground motions for performing response history analysis, National Institute of Standards and Technology*, NIST/GCR 11-917-15*, prepared by the NEHRP Consultants Joint Venture for the National Institute of Standards and Technology, Gaithersburg, MD.

PEER (2017). Guidelines for performance-based seismic design of tall buildings, Version 2, *Report No. 2017/06*, Pacific Earthquake Engineering Research Center, University of California, Berkeley, CA.

Petersen M.D., Moschetti M.P., Powers P.M., Mueller C.S., Haller K.M., Frankel A.D., Zeng Y., Rezaeian S., Harmsen S.C., Boyd O.S., Field N., Chen R., Rukstales K.S., Luco N., Wheeler R.L., Williams R.A., Olsen A.H. (2015). The 2014 United States national seismic hazard model, *Earthq. Spectra*, 31: S1–S30.

Rowshandel B. (2013). *Final Report of the NGA-West2 Directivity Working Group*, Chapter 3, *PEER Report No. 2013/09*, Pacific Earthquake Engineering Research Center, University of California, Berkeley, CA.

Rowshandel B. (2018). *Personal Communication*.

Rowshandel B. (2018a). Capturing and PSHA implementation of spatial variability of near-source ground motion hazard, *Proceedings, Geotechnical Engineering and Soil Dynamics V: Seismic Hazard Analysis, Earthquake Ground Motions, and Regional-Scale Assessment, Austin, TX, ASCE Geotechnical Special Publication No. 291*, S.J. Brandenberg and M.T. Manzari (eds.), pp. 56–63.

Rowshandel B. (2018b). Centering of GMPEs and of directivity models, *Proceedings, 11th National Conf. on Earthquake Engineering,* Los Angeles, CA.

Shahi S.K., Baker J.W. (2011). An empirically calibrated framework for including the effects of near-fault directivity in probabilistic seismic hazard analysis, *Bull. Seismol. Soc. Am.*, 101: 742–755.

Shahi S.K., Baker J.W. (2013). *Final Report of the NGA-West2 Directivity Working Group*, Chapter 4, *PEER Report No. 2013/09*, Pacific Earthquake Engineering Research Center, University of California, Berkeley, CA.

Shahi S.K., Baker J.W. (2014). NGA-West2 models for ground-motion directionality, *Earthq. Spectra*, 30: 1285–1300.

Singh J.P. (1985). Earthquake ground motions: Implications for designing structures and reconciling structural damage, *Earthq. Spectra*, 1: 239–270.

Somerville P.G., Smith N.F., Graves R.W., Abrahamson N.A. (1997). Modification of empirical strong ground motion attenuation relations to include the amplitude and duration effects of rupture directivity, *Seismol. Res. Lett.*, 68: 199–222.

Spagnuolo E., Akinci A., Herrero A., Pucci S. (2016). Implementing the effect of the rupture directivity on PSHA for the City of Istanbul, Turkey, *Bull. Seismol. Soc. Am.*, 106: 2599–2613.

Spudich P., Chiou B.S.-J. (2008). Directivity in NGA earthquake ground motions: Analysis using isochrone theory, *Earthq. Spectra*, 24: 279–298.

Spudich P., Chiou B.S.-J. (2013). *Final Report of the NGA-West2 Directivity Working Group*, Chapter 5, *PEER Report No. 2013/09*, Pacific Earthquake Engineering Research Center, University of California, Berkeley, CA.

Spudich P., Frazer L.N. (1984). Use of ray theory to calculate high frequency radiation from earthquake sources having spatially variable rupture velocity and stress drop, *Bull. Seismol. Soc. Am.*, 74: 2061–2082.

—— (1987). Errata, *Bull. Seismol. Soc. Am.*, 77: 2245–2246.

Spudich P. (ed.) (2013). *Final Report of the NGA-West2 Directivity Working Group*, *PEER Report No. 2013/09*, Pacific Earthquake Engineering Research Center, University of California, Berkeley, CA.

Spudich P., Rowshandel B., Shahi S.K., Baker J.W., Chiou B.S.-J. (2014). Comparison of NGA-West2 directivity models, *Earthq. Spectra*, 30: 1199–1221.

Watson-Lamprey J.A. (2018). Capturing directivity effects in the mean and aleatory variability of the NGA-West 2 ground motion prediction equations, *PEER Report No. 2018/04*, Pacific Earthquake Engineering Research Center, University of California, Berkeley, CA.

Worden C.B., Wald D.J. (2016). *ShakeMap Manual Online: Technical Manual, User's Guide, and Software Guide*, U. S. Geological Survey, *usgs.github.io/shakemap*. DOI: 10.5066/F7D21VPQ.

Zeng Y, C-H Chen C.-H. (2001). Fault rupture process of the 20 September 1999 Chi-Chi, Taiwan, earthquake, *Bull. Seismol. Soc. Am.*, 91: 1088–1098.

Appendix Additional Scenarios for Change of Mean Ground Motion and Increase of Within-Event Dispersion for Use with Composite Distribution Approach

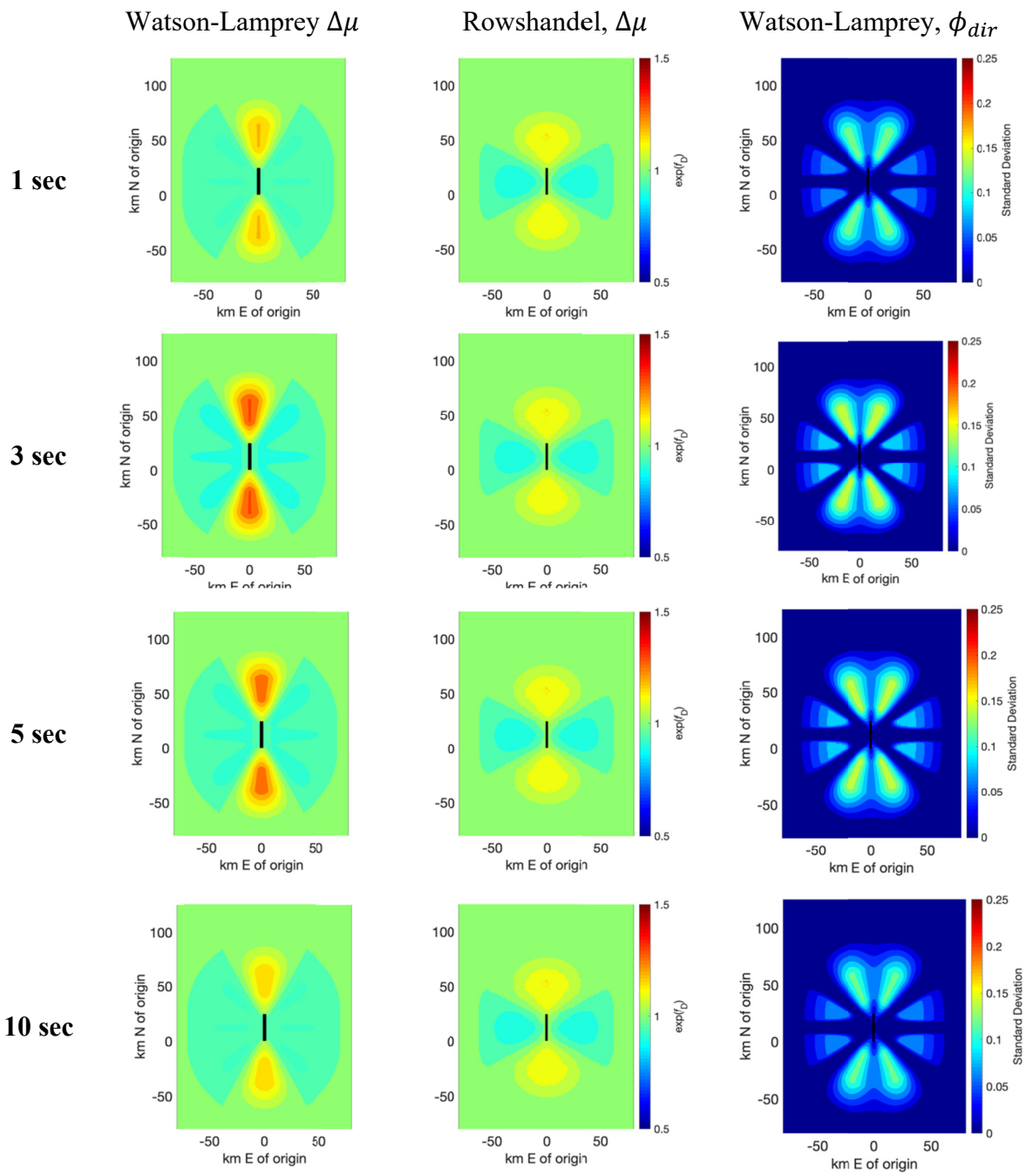

Figure A.1 **Spatial pattern of change of natural log mean $(\Delta\mu)$ and directivity-related aleatory variability (ϕ_{dir}) for four PSA oscillator periods (T = 1.0, 3.0, 5.0, and 10.0 sec). M6.5 strike–slip rupture scenario.**

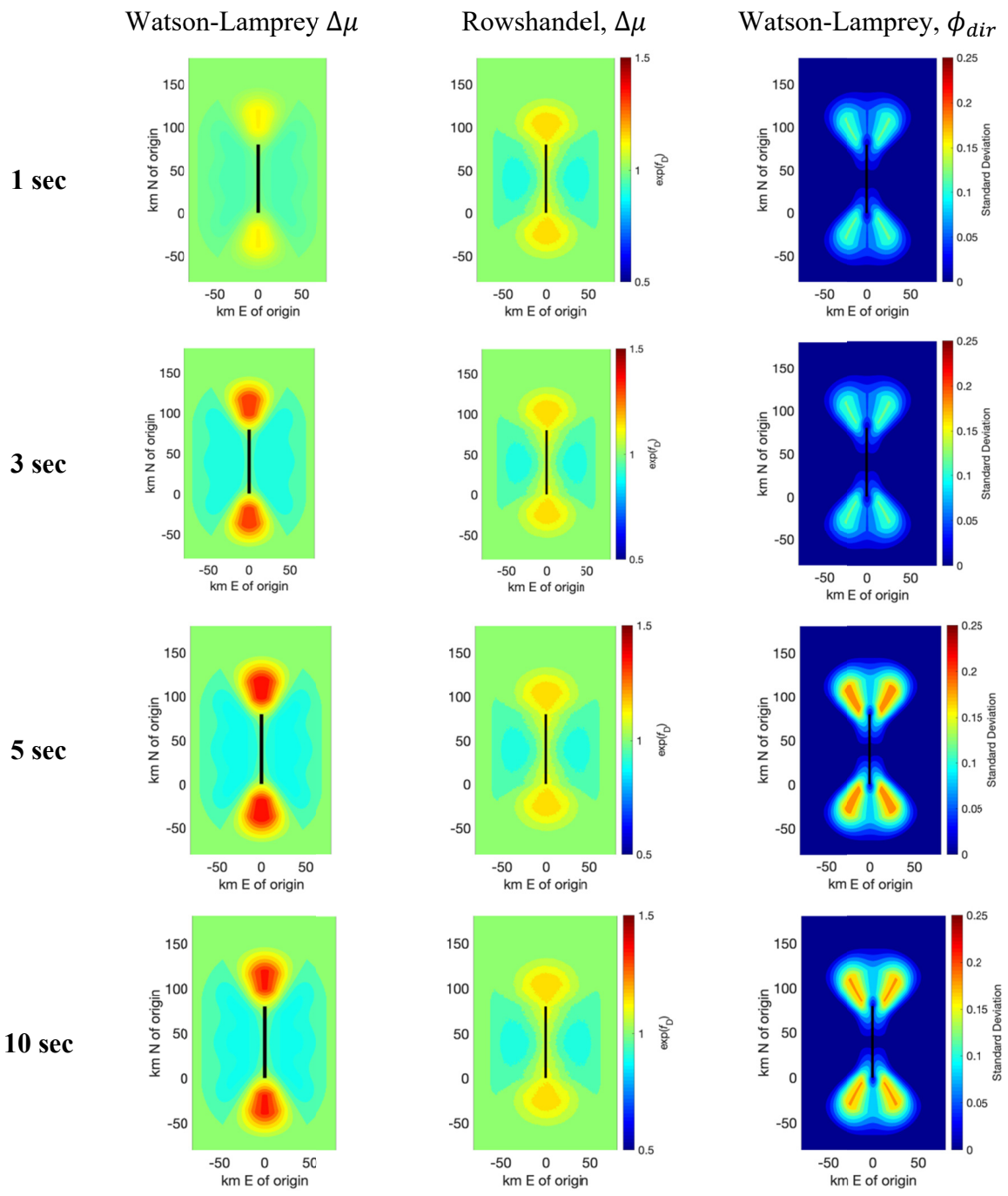

Figure A.2 **Spatial pattern of change of natural log mean $(\Delta\mu)$ and directivity-related aleatory variability (ϕ_{dir}) for four PSA oscillator periods (T = 1.0, 3.0, 5.0 and 10.0 sec). M7.2 strike–slip rupture scenario. Spatial pattern of change of natural log mean $(\Delta\mu)$ and directivity-related aleatory variability (ϕ_{dir}) for four PSA oscillator periods**

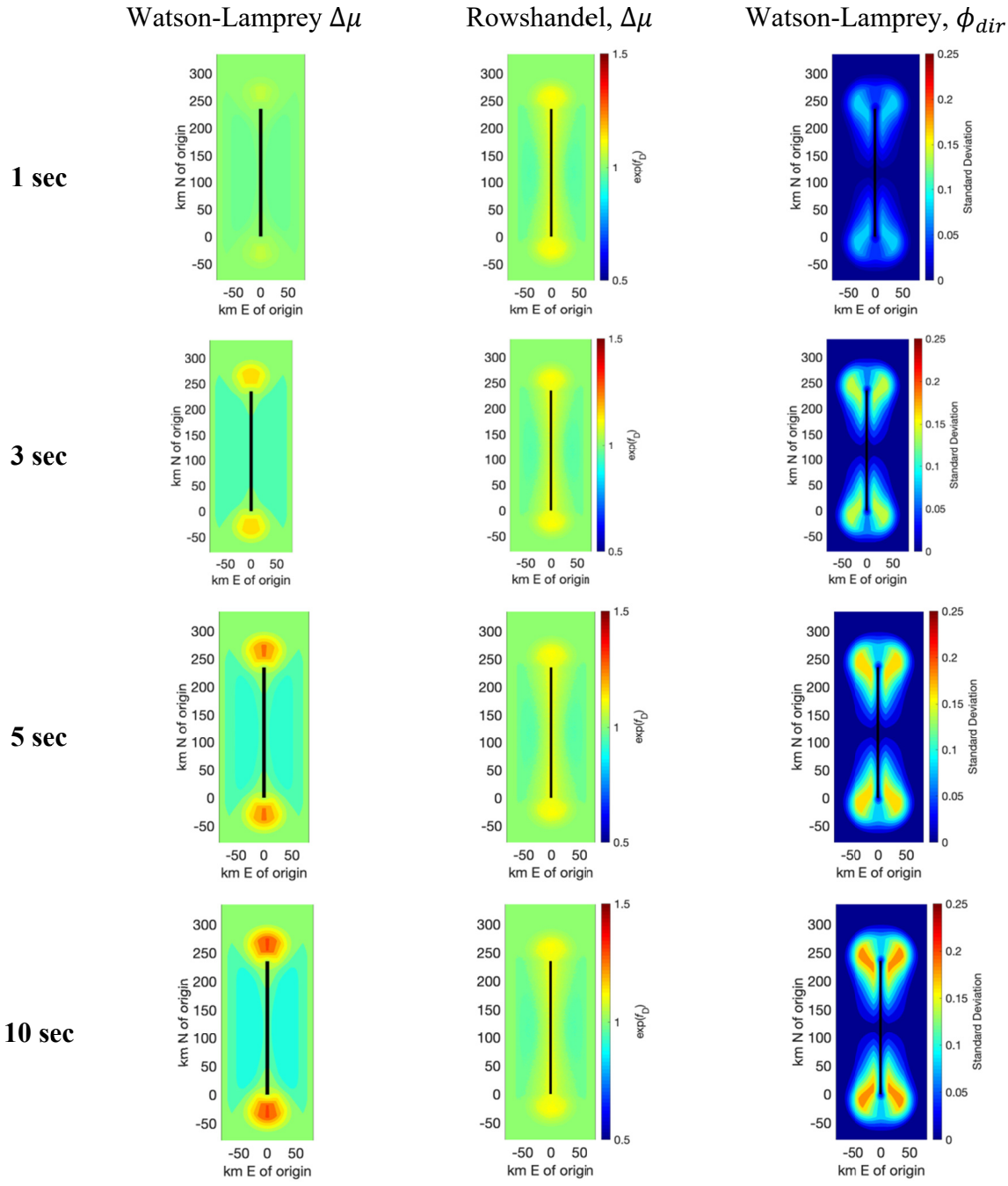

Figure A.3 **Spatial pattern of change of natural log mean ($\Delta\mu$) and directivity-related aleatory variability (ϕ_{dir}) for four PSA oscillator periods (T = 1.0, 3.0, 5.0, and 10.0 sec). M7.2 strike–slip rupture scenario.**

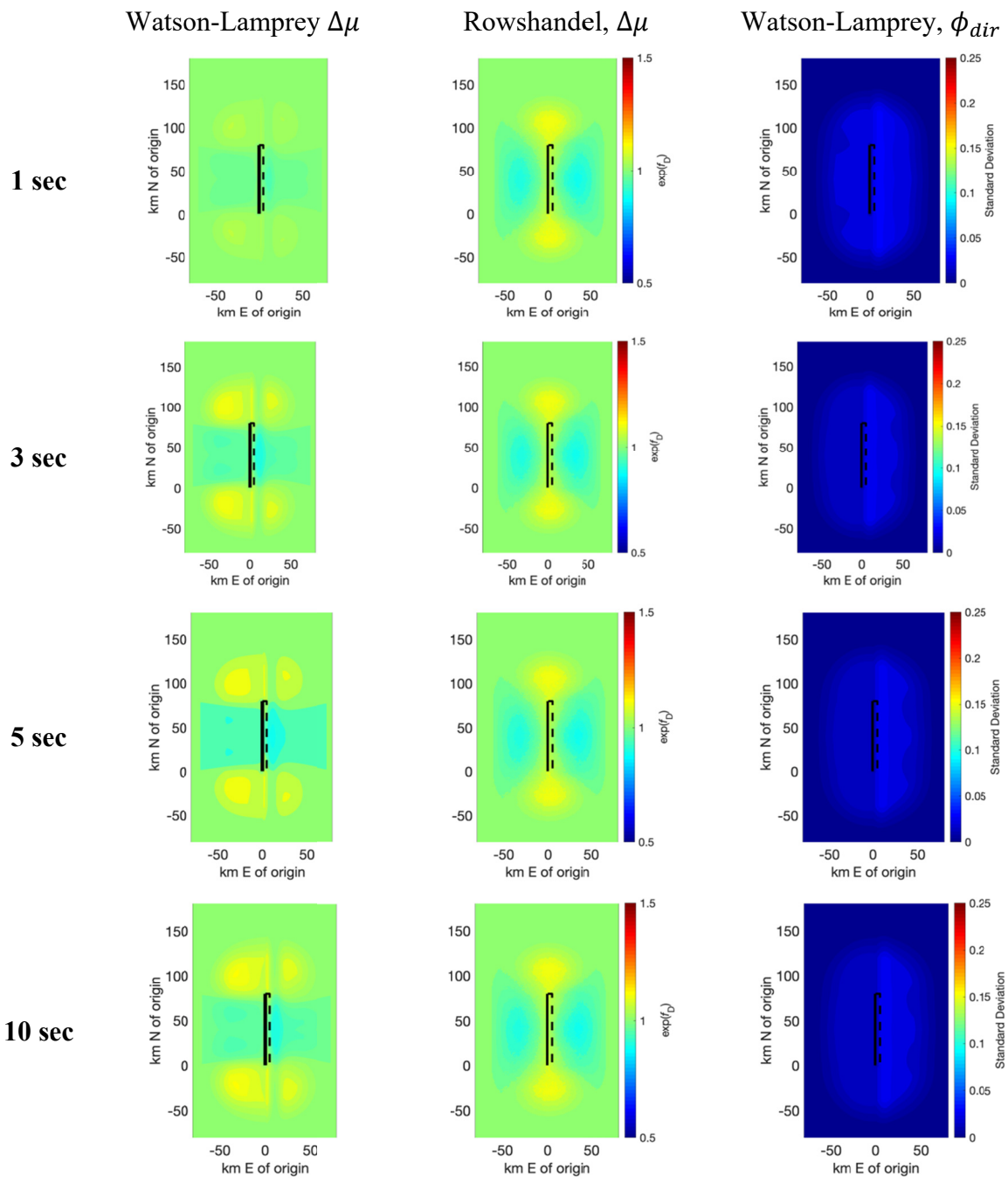

Figure A.4 **Spatial pattern of change of natural log mean ($\Delta\mu$) and directivity-related aleatory variability (ϕ_{dir}) for four PSA oscillator periods (T = 1.0, 3.0, 5.0, and 10.0 sec). M7.2 strike–slip-oblique rupture scenario.**

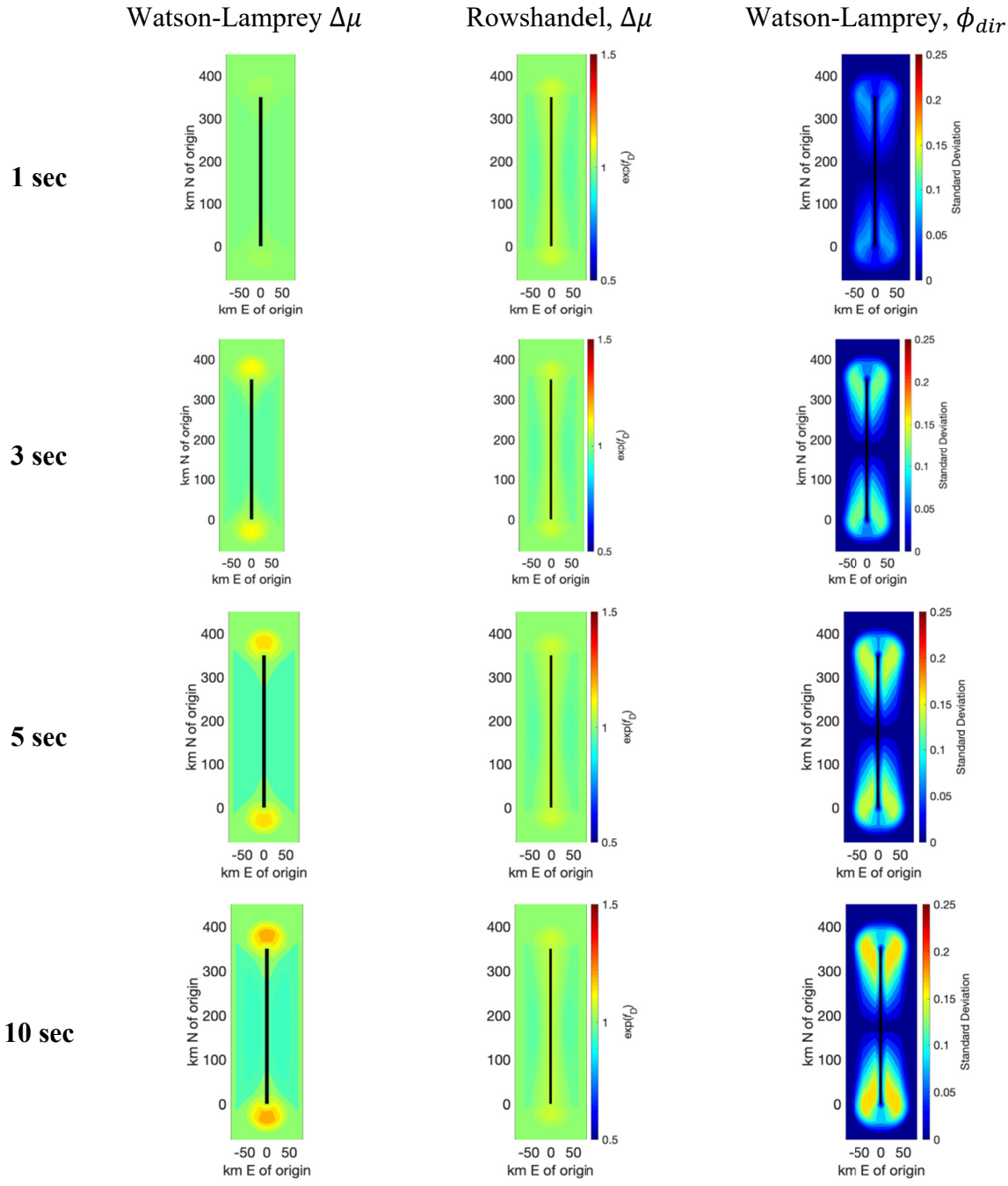

Figure A.5 **Spatial pattern of change of natural log mean ($\Delta\mu$) and directivity-related aleatory variability (ϕ_{dir}) for four PSA oscillator periods (*T* = 1.0, 3.0, 5.0, and 10.0 sec). M8.0 strike–slip rupture scenario.**

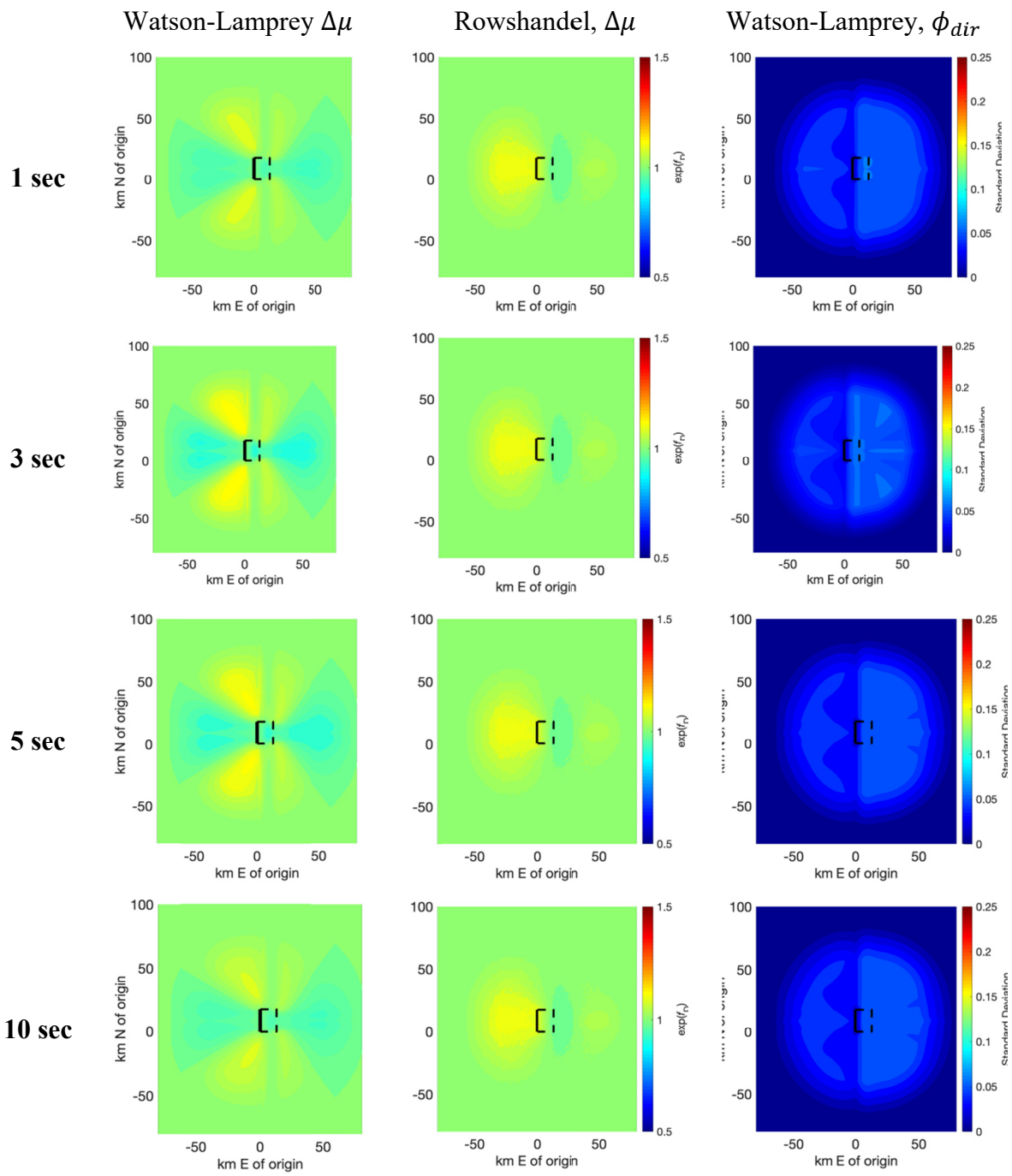

Figure A-6 **Spatial pattern of change of natural log mean ($\Delta\mu$) and directivity-related aleatory variability (ϕ_{dir}) for four PSA oscillator periods (T = 1.0, 3.0, 5.0, and 10.0 sec). M6.5, dip = 45°, top of rupture = 5.0 km, reverse rupture scenario.**

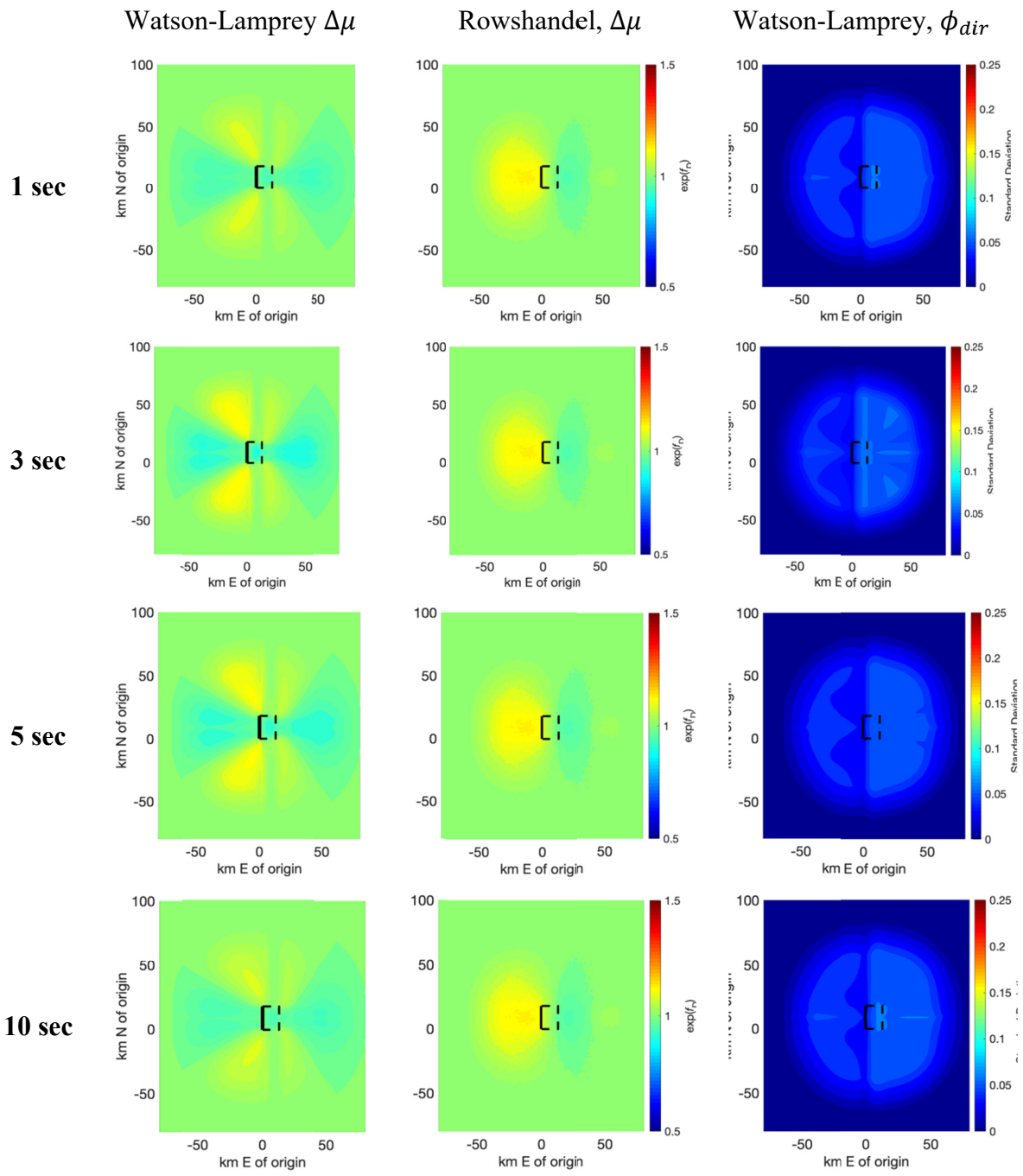

Figure A.7 **Spatial pattern of change of natural log mean ($\Delta\mu$) and directivity-related aleatory variability (ϕ_{dir}) for four PSA oscillator periods (*T* = 1.0, 3.0, 5.0, and 10.0 sec). M6.5, dip = 45°, top of rupture = 0 km, reverse rupture scenario.**

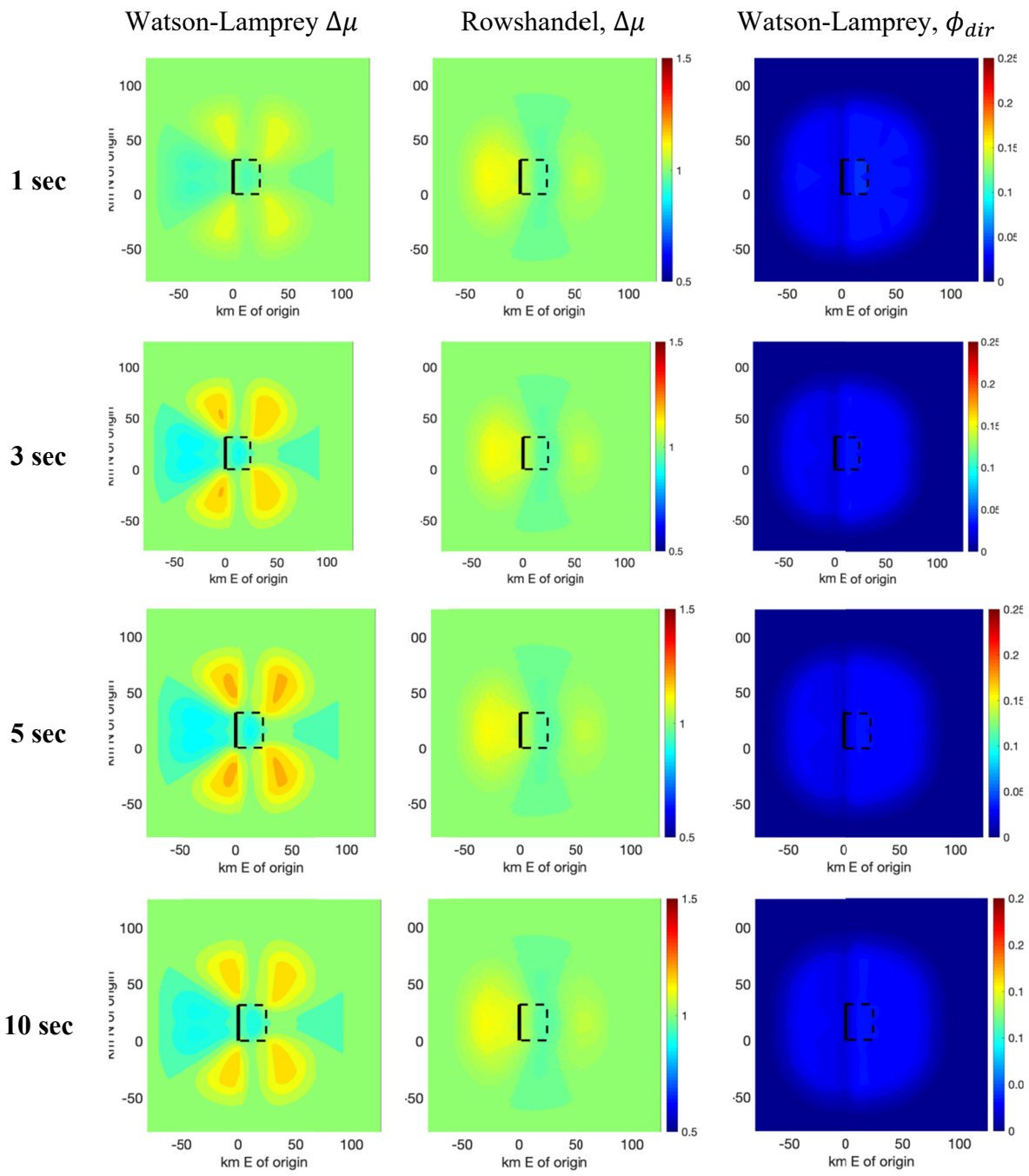

Figure A.8 **Spatial pattern of change of natural log mean $(\Delta\mu)$ and directivity-related aleatory variability (ϕ_{dir}) for four PSA oscillator periods (T = 1.0, 3.0, 5.0, and 10.0 sec). M7.0, dip = 30°, top of rupture = 0 km, reverse rupture scenario.**

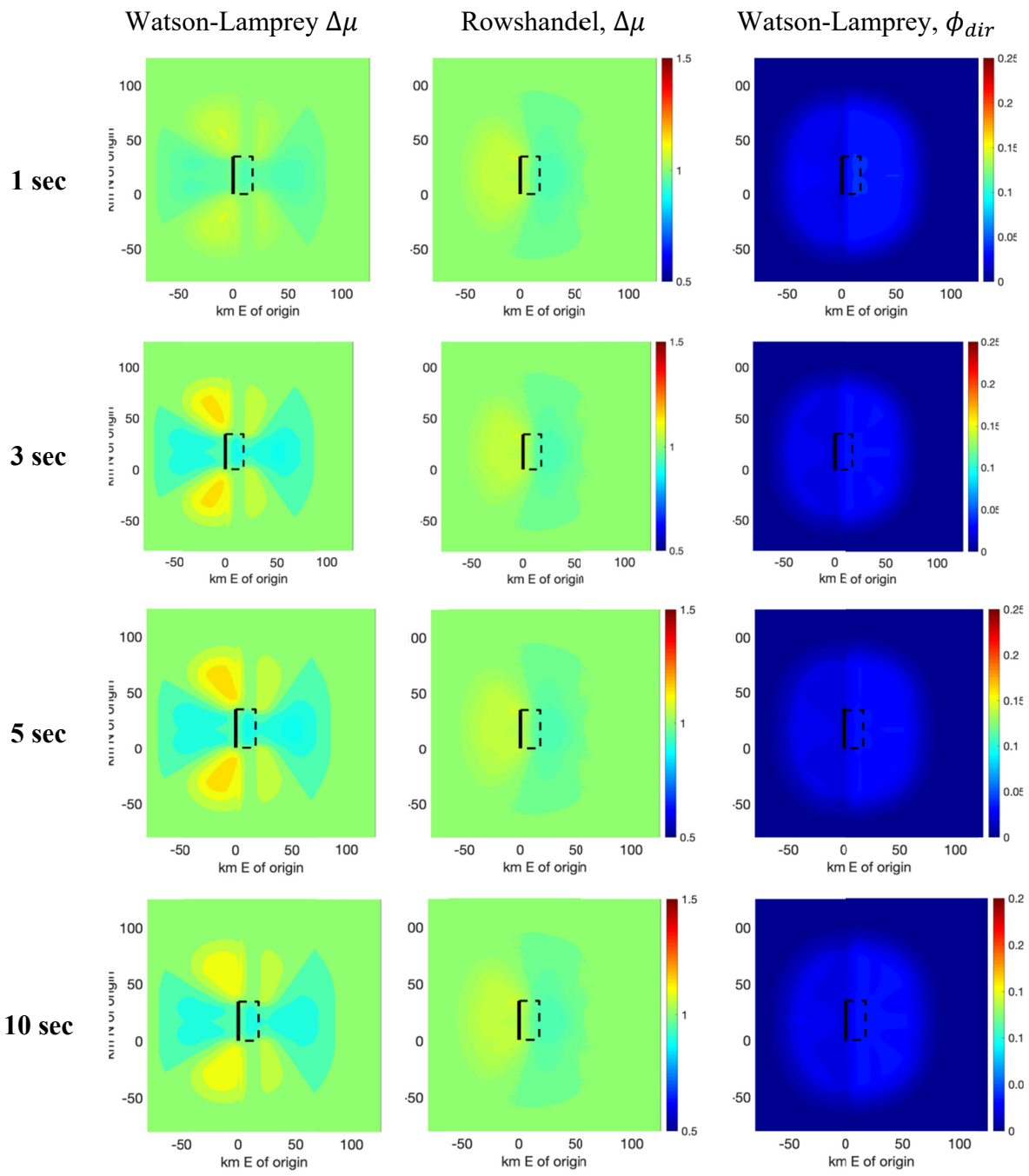

Figure A.9 **Spatial pattern of change of natural log mean $(\Delta\mu)$ and directivity-related aleatory variability (ϕ_{dir}) for four PSA oscillator periods (T = 1.0, 3.0, 5.0, and 10.0 sec). M7.0, dip = 45°, top of rupture = 0 km, reverse rupture scenario.**

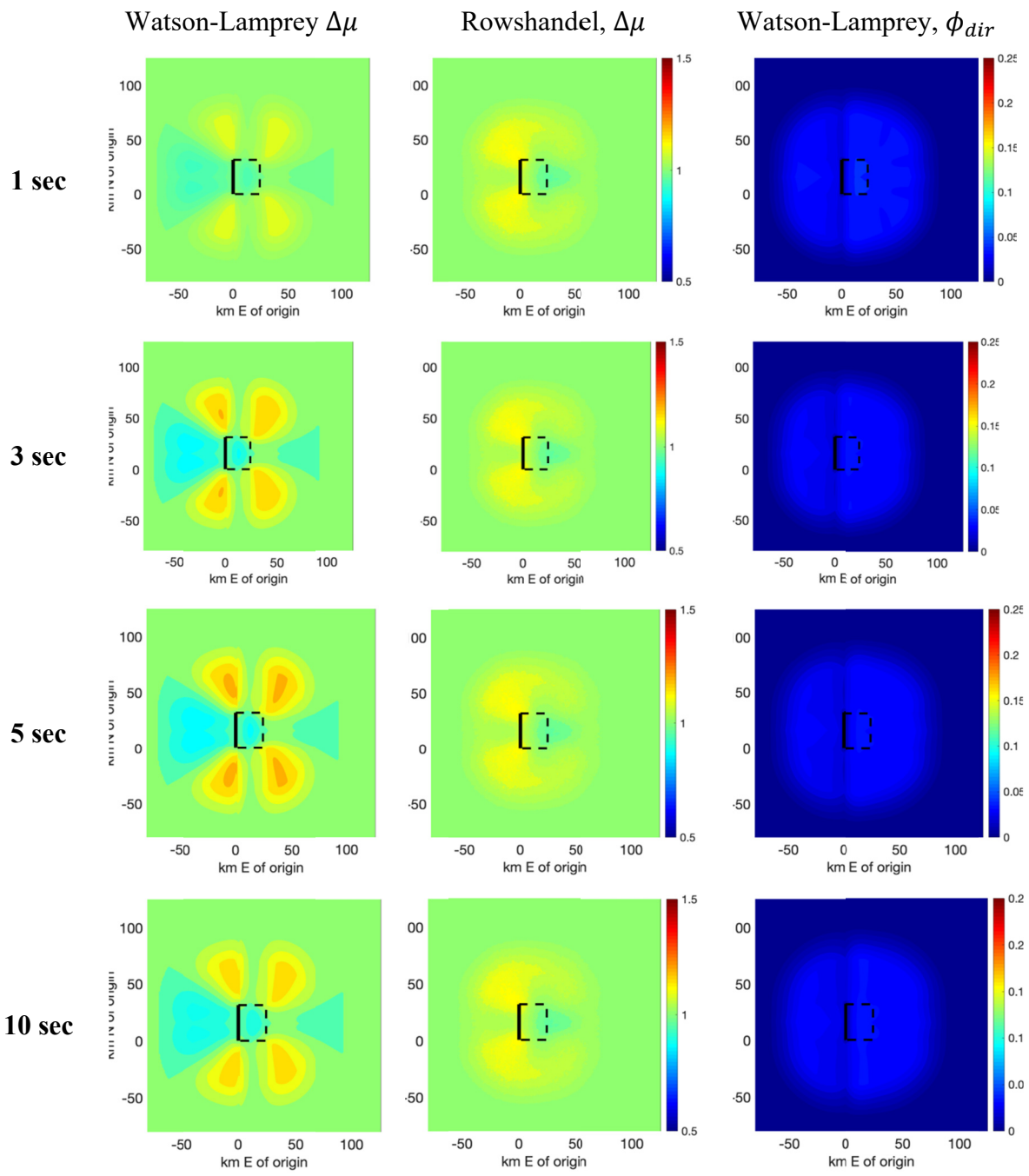

Figure A.10 **Spatial pattern of change of natural log mean $(\Delta\mu)$ and directivity-related aleatory variability (ϕ_{dir}) for four PSA oscillator periods (T = 1.0, 3.0, 5.0, and 10.0 sec). M7.0, dip = 30°, top of rupture = 0 km, reverse–oblique rupture scenario.**

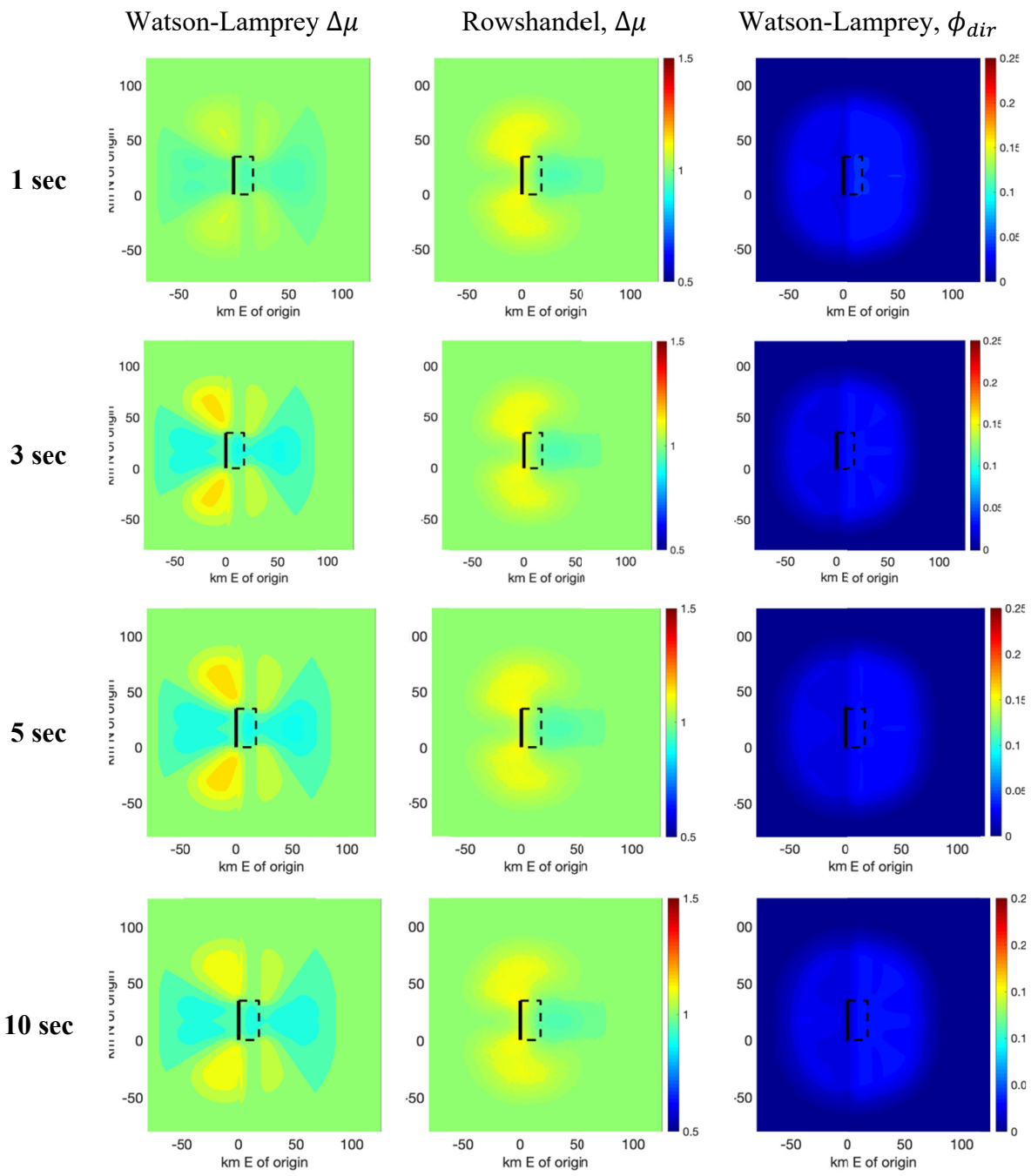

Figure A.11 **Spatial pattern of change of natural log mean $(\Delta\mu)$ and directivity-related aleatory variability (ϕ_{dir}) for four PSA oscillator periods (T = 1.0, 3.0, 5.0, and 10.0 sec). M7.0, dip = 45°, top of rupture = 0 km, reverse–oblique rupture scenario.**

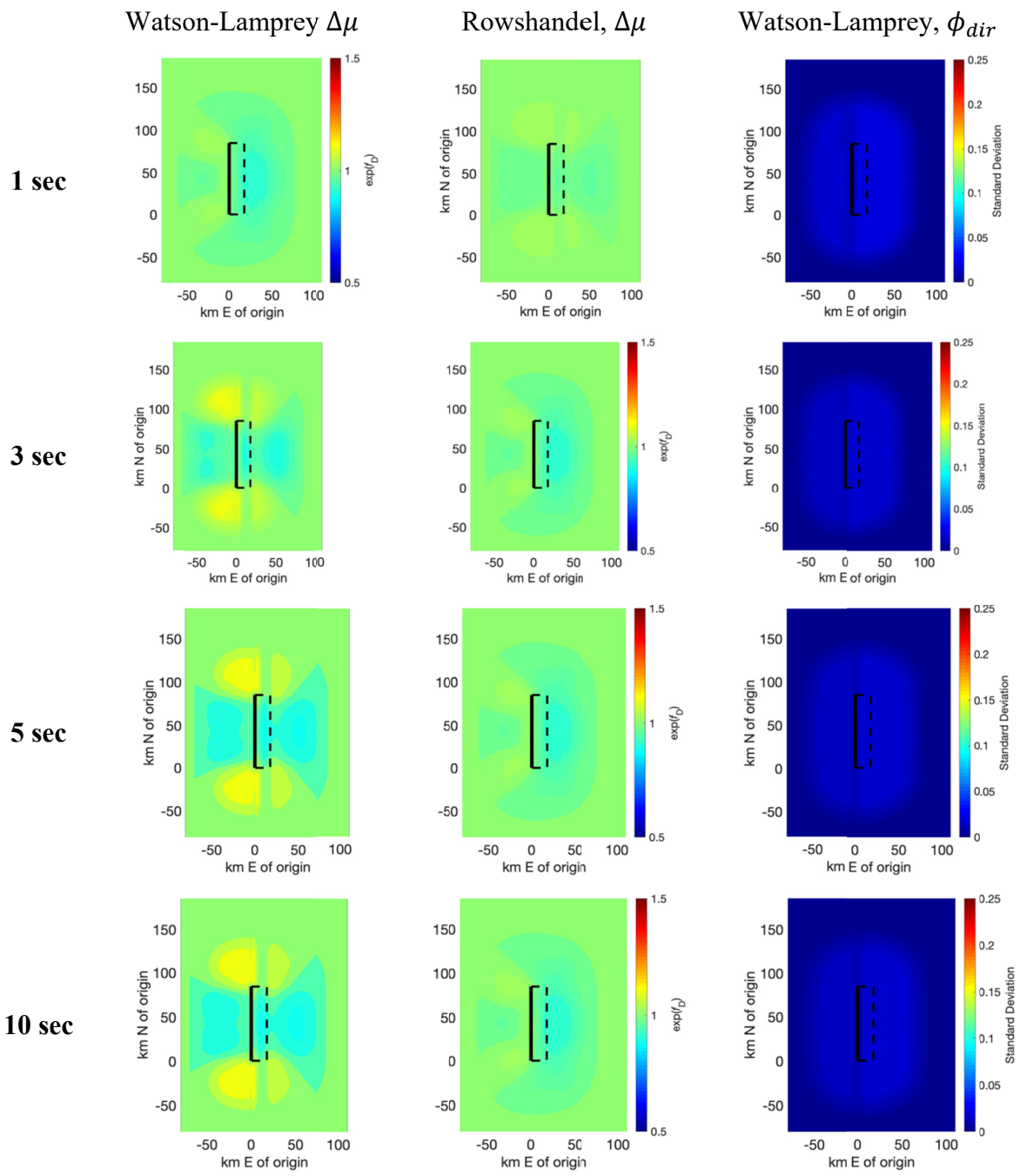

Figure A.12 **Spatial pattern of change of natural log mean ($\Delta\mu$) and directivity-related aleatory variability (ϕ_{dir}) for four PSA oscillator periods (T = 1.0, 3.0, 5.0, and 10.0 sec). M7.5, dip = 45°, top of rupture = 0 km, reverse rupture scenario.**

PEER REPORTS

PEER reports are available as a free PDF download from https://peer.berkeley.edu/peer-reports. In addition, printed hard copies of PEER reports can be ordered directly from our printer by following the instructions at https://peer.berkeley.edu/peer-reports. For other related questions about the PEER Report Series, contact the Pacific Earthquake Engineering Research Center, 325 Davis Hall, Mail Code 1792, Berkeley, CA 94720. Tel.: (510) 642-3437; and Email: peer_center@berkeley.edu.

PEER 2019/02 *Direct-Finite-Element Method for Nonlinear Earthquake Analysis of Concrete Dams Including Dam–Water–Foundation Rock Interaction.* Arnkjell Løkke and Anil K. Chopra. March 2019.

PEER 2019/01 *Flow-Failure Case History of the Las Palmas, Chile, Tailings Dam.* R. E. S. Moss, T. R. Gebhart, D. J. Frost, and C. Ledezma. January 2019.

PEER 2018/08 *Central and Eastern North America Ground-Motion Characterization: NGA-East Final Report*. Christine Goulet, Yousef Bozorgnia, Norman Abrahamson, Nicolas Kuehn, Linda Al Atik, Robert Youngs, Robert Graves, and Gail Atkinson. December 2018.

PEER 2018/07 *An Empirical Model for Fourier Amplitude Spectra using the NGA-West2 Database*. Jeff Bayless, and Norman A. Abrahamson. December 2018.

PEER 2018/06 *Estimation of Shear Demands on Rock-Socketed Drilled Shafts subjected to Lateral Loading*. Pedro Arduino, Long Chen, and Christopher R. McGann. December 2018.

PEER 2018/05 *Selection of Random Vibration Procedures for the NGA-East Project*. Albert Kottke, Norman A. Abrahamson, David M. Boore, Yousef Bozorgnia, Christine Goulet, Justin Hollenback, Tadahiro Kishida, Armen Der Kiureghian, Olga-Joan Ktenidou, Nicolas Kuehn, Ellen M. Rathje, Walter J. Silva, Eric Thompson, and Xiaoyue Wang. December 2018.

PEER 2018/04 *Capturing Directivity Effects in the Mean and Aleatory Variability of the NGA-West 2 Ground Motion Prediction Equations.* Jennie A. Watson-Lamprey. November 2018.

PEER 2018/03 *Probabilistic Seismic Hazard Analysis Code Verification*. Christie Hale, Norman Abrahamson, and Yousef Bozorgnia. July 2018.

PEER 2018/02 *Update of the BCHydro Subduction Ground-Motion Model using the NGA-Subduction Dataset.* Norman Abrahamson, Nicolas Kuehn, Zeynep Gulerce, Nicholas Gregor, Yousef Bozorgnia, Grace Parker, Jonathan Stewart, Brian Chiou, I. M. Idriss, Kenneth Campbell, and Robert Youngs. June 2018.

PEER 2018/01 *PEER Annual Report 2017–2018*. Khalid Mosalam, Amarnath Kasalanati, and Selim Günay. June 2018.

PEER 2017/12 *Experimental Investigation of the Behavior of Vintage and Retrofit Concentrically Braced Steel Frames under Cyclic Loading*. Barbara G. Simpson, Stephen A. Mahin, and Jiun-Wei Lai, December 2017.

PEER 2017/11 *Preliminary Studies on the Dynamic Response of a Seismically Isolated Prototype Gen-IV Sodium-Cooled Fast Reactor* (*PGSFR*). Benshun Shao, Andreas H. Schellenberg, Matthew J. Schoettler, and Stephen A. Mahin. December 2017.

PEER 2017/10 *Development of Time Histories for IEEE693 Testing and Analysis (including Seismically Isolated Equipment).* Shakhzod M. Takhirov, Eric Fujisaki, Leon Kempner, Michael Riley, and Brian Low. December 2017.

PEER 2017/09 *""R" Package for Computation of Earthquake Ground-Motion Response Spectra.* Pengfei Wang, Jonathan P. Stewart, Yousef Bozorgnia, David M. Boore, and Tadahiro Kishida. December 2017.

PEER 2017/08 *Influence of Kinematic SSI on Foundation Input Motions for Bridges on Deep Foundations*. Benjamin J. Turner, Scott J. Brandenberg, and Jonathan P. Stewart. November 2017.

PEER 2017/07 *A Nonlinear Kinetic Model for Multi-Stage Friction Pendulum Systems*. Paul L. Drazin and Sanjay Govindjee. September 2017.

PEER 2017/06 *Guidelines for Performance-Based Seismic Design of Tall Buildings, Version 2.02*. TBI Working Group led by co-chairs Ron Hamburger and Jack Moehle: Jack Baker, Jonathan Bray, C.B. Crouse, Greg Deierlein, John Hooper, Marshall Lew, Joe Maffei, Stephen Mahin, James Malley, Farzad Naeim, Jonathan Stewart, and John Wallace. May 2017.

PEER 2017/05 *Recommendations for Ergodic Nonlinear Site Amplification in Central and Eastern North America*. Youssef M.A. Hashash, Joseph A. Harmon, Okan Ilhan, Grace A. Parker, and Jonathan P. Stewart. March 2017.

PEER 2017/04 *Expert Panel Recommendations for Ergodic Site Amplification in Central and Eastern North America*. Jonathan P. Stewart, Grace A. Parker, Joseph P. Harmon, Gail M. Atkinson, David M. Boore, Robert B. Darragh, Walter J. Silva, and Youssef M.A. Hashash. March 2017.

PEER 2017/03 *NGA-East Ground-Motion Models for the U.S. Geological Survey National Seismic Hazard Maps*. Christine A. Goulet, Yousef Bozorgnia, Nicolas Kuehn, Linda Al Atik, Robert R. Youngs, Robert W. Graves, and Gail M. Atkinson. March 2017.

PEER 2017/02 *U.S.–New Zealand–Japan Workshop: Liquefaction-Induced Ground Movements Effects, University of California, Berkeley, California, 2–4 November 2016.* Jonathan D. Bray, Ross W. Boulanger, Misko Cubrinovski, Kohji Tokimatsu, Steven L. Kramer, Thomas O'Rourke, Ellen Rathje, Russell A. Green, Peter K. Robinson, and Christine Z. Beyzaei. March 2017.

PEER 2017/01 *2016 PEER Annual Report*. Khalid M. Mosalam, Amarnath Kasalanati, and Grace Kang. March 2017.

PEER 2016/10 *Performance-Based Robust Nonlinear Seismic Analysis with Application to Reinforced Concrete Bridge Systems*. Xiao Ling and Khalid M. Mosalam. December 2016.

PEER 2017/09 *Detailing Requirements for Column Plastic Hinges subjected to Combined Flexural, Axial, and Torsional Seismic Loading.* Gabriel Hurtado and Jack P. Moehle. December 2016.

PEER 2016/08 *Resilience of Critical Structures, Infrastructure, and Communities*. Gian Paolo Cimellaro, Ali Zamani-Noori, Omar Kamouh, Vesna Terzic, and Stephen A. Mahin. December 2016.

PEER 2016/07 *Hybrid Simulation Theory for a Classical Nonlinear Dynamical System*. Paul L. Drazin and Sanjay Govindjee. September 2016.

PEER 2016/06 *California Earthquake Early Warning System Benefit Study*. Laurie A. Johnson, Sharyl Rabinovici, Grace S. Kang, and Stephen A. Mahin. July 2006.

PEER 2016/05 *Ground-Motion Prediction Equations for Arias Intensity Consistent with the NGA-West2 Ground-Motion Models.* Charlotte Abrahamson, Hao-Jun Michael Shi, and Brian Yang. July 2016.

PEER 2016/04 *The M_W 6.0 South Napa Earthquake of August 24, 2014: A Wake-Up Call for Renewed Investment in Seismic Resilience Across California.* Prepared for the California Seismic Safety Commission, Laurie A. Johnson and Stephen A. Mahin. May 2016.

PEER 2016/03 *Simulation Confidence in Tsunami-Driven Overland Flow.* Patrick Lynett. May 2016.

PEER 2016/02 *Semi-Automated Procedure for Windowing time Series and Computing Fourier Amplitude Spectra for the NGA-West2 Database.* Tadahiro Kishida, Olga-Joan Ktenidou, Robert B. Darragh, and Walter J. Silva. May 2016.

PEER 2016/01 *A Methodology for the Estimation of Kappa (κ) from Large Datasets: Example Application to Rock Sites in the NGA-East Database and Implications on Design Motions.* Olga-Joan Ktenidou, Norman A. Abrahamson, Robert B. Darragh, and Walter J. Silva. April 2016.

PEER 2015/13 *Self-Centering Precast Concrete Dual-Steel-Shell Columns for Accelerated Bridge Construction: Seismic Performance, Analysis, and Design*. Gabriele Guerrini, José I. Restrepo, Athanassios Vervelidis, and Milena Massari. December 2015.

PEER 2015/12 *Shear-Flexure Interaction Modeling for Reinforced Concrete Structural Walls and Columns under Reversed Cyclic Loading*. Kristijan Kolozvari, Kutay Orakcal, and John Wallace. December 2015.

PEER 2015/11 *Selection and Scaling of Ground Motions for Nonlinear Response History Analysis of Buildings in Performance-Based Earthquake Engineering*. N. Simon Kwong and Anil K. Chopra. December 2015.

PEER 2015/10 *Structural Behavior of Column-Bent Cap Beam-Box Girder Systems in Reinforced Concrete Bridges Subjected to Gravity and Seismic Loads. Part II: Hybrid Simulation and Post-Test Analysis*. Mohamed A. Moustafa and Khalid M. Mosalam. November 2015.

PEER 2015/09 *Structural Behavior of Column-Bent Cap Beam-Box Girder Systems in Reinforced Concrete Bridges Subjected to Gravity and Seismic Loads. Part I: Pre-Test Analysis and Quasi-Static Experiments*. Mohamed A. Moustafa and Khalid M. Mosalam. September 2015.

PEER 2015/08 *NGA-East: Adjustments to Median Ground-Motion Models for Center and Eastern North America*. August 2015.

PEER 2015/07 *NGA-East: Ground-Motion Standard-Deviation Models for Central and Eastern North America*. Linda Al Atik. June 2015.

PEER 2015/06 *Adjusting Ground-Motion Intensity Measures to a Reference Site for which V_{S30} = 3000 m/sec*. David M. Boore. May 2015.

PEER 2015/05 *Hybrid Simulation of Seismic Isolation Systems Applied to an APR-1400 Nuclear Power Plant.* Andreas H. Schellenberg, Alireza Sarebanha, Matthew J. Schoettler, Gilberto Mosqueda, Gianmario Benzoni, and Stephen A. Mahin. April 2015.

PEER 2015/04 *NGA-East: Median Ground-Motion Models for the Central and Eastern North America Region*. April 2015.

PEER 2015/03 *Single Series Solution for the Rectangular Fiber-Reinforced Elastomeric Isolator Compression Modulus*. James M. Kelly and Niel C. Van Engelen. March 2015.

PEER 2015/02 *A Full-Scale, Single-Column Bridge Bent Tested by Shake-Table Excitation.* Matthew J. Schoettler, José I. Restrepo, Gabriele Guerrini, David E. Duck, and Francesco Carrea. March 2015.

PEER 2015/01 *Concrete Column Blind Prediction Contest 2010: Outcomes and Observations.* Vesna Terzic, Matthew J. Schoettler, José I. Restrepo, and Stephen A Mahin. March 2015.

PEER 2014/20 *Stochastic Modeling and Simulation of Near-Fault Ground Motions for Performance-Based Earthquake Engineering*. Mayssa Dabaghi and Armen Der Kiureghian. December 2014.

PEER 2014/19 *Seismic Response of a Hybrid Fiber-Reinforced Concrete Bridge Column Detailed for Accelerated Bridge Construction*. Wilson Nguyen, William Trono, Marios Panagiotou, and Claudia P. Ostertag. December 2014.

PEER 2014/18 *Three-Dimensional Beam-Truss Model for Reinforced Concrete Walls and Slabs Subjected to Cyclic Static or Dynamic Loading*. Yuan Lu, Marios Panagiotou, and Ioannis Koutromanos. December 2014.

PEER 2014/17 *PEER NGA-East Database*. Christine A. Goulet, Tadahiro Kishida, Timothy D. Ancheta, Chris H. Cramer, Robert B. Darragh, Walter J. Silva, Youssef M.A. Hashash, Joseph Harmon, Jonathan P. Stewart, Katie E. Wooddell, and Robert R. Youngs. October 2014.

PEER 2014/16 *Guidelines for Performing Hazard-Consistent One-Dimensional Ground Response Analysis for Ground Motion Prediction*. Jonathan P. Stewart, Kioumars Afshari, and Youssef M.A. Hashash. October 2014.

PEER 2014/15 *NGA-East Regionalization Report: Comparison of Four Crustal Regions within Central and Eastern North America using Waveform Modeling and 5%-Damped Pseudo-Spectral Acceleration Response*. Jennifer Dreiling, Marius P. Isken, Walter D. Mooney, Martin C. Chapman, and Richard W. Godbee. October 2014.

PEER 2014/14 *Scaling Relations between Seismic Moment and Rupture Area of Earthquakes in Stable Continental Regions*. Paul Somerville. August 2014.

PEER 2014/13 *PEER Preliminary Notes and Observations on the August 24, 2014, South Napa Earthquake*. Grace S. Kang and Stephen A. Mahin, Editors. September 2014.

PEER 2014/12 *Reference-Rock Site Conditions for Central and Eastern North America: Part II – Attenuation (Kappa) Definition*. Kenneth W. Campbell, Youssef M.A. Hashash, Byungmin Kim, Albert R. Kottke, Ellen M. Rathje, Walter J. Silva, and Jonathan P. Stewart. August 2014.

PEER 2014/11 *Reference-Rock Site Conditions for Central and Eastern North America: Part I - Velocity Definition*. Youssef M.A. Hashash, Albert R. Kottke, Jonathan P. Stewart, Kenneth W. Campbell, Byungmin Kim, Ellen M. Rathje, Walter J. Silva, Sissy Nikolaou, and Cheryl Moss. August 2014.

PEER 2014/10 *Evaluation of Collapse and Non-Collapse of Parallel Bridges Affected by Liquefaction and Lateral Spreading*. Benjamin Turner, Scott J. Brandenberg, and Jonathan P. Stewart. August 2014.

PEER 2014/09 *PEER Arizona Strong-Motion Database and GMPEs Evaluation*. Tadahiro Kishida, Robert E. Kayen, Olga-Joan Ktenidou, Walter J. Silva, Robert B. Darragh, and Jennie Watson-Lamprey. June 2014.

PEER 2014/08 *Unbonded Pretensioned Bridge Columns with Rocking Detail*. Jeffrey A. Schaefer, Bryan Kennedy, Marc O. Eberhard, and John F. Stanton. June 2014.

PEER 2014/07 *Northridge 20 Symposium Summary Report: Impacts, Outcomes, and Next Steps*. May 2014.

PEER 2014/06 *Report of the Tenth Planning Meeting of NEES/E-Defense Collaborative Research on Earthquake Engineering*. December 2013.

PEER 2014/05 *Seismic Velocity Site Characterization of Thirty-One Chilean Seismometer Stations by Spectral Analysis of Surface Wave Dispersion*. Robert Kayen, Brad D. Carkin, Skye Corbet, Camilo Pinilla, Allan Ng, Edward Gorbis, and Christine Truong. April 2014.

PEER 2014/04 Effect of Vertical Acceleration on Shear Strength of Reinforced Concrete Columns. Hyerin Lee and Khalid M. Mosalam. April 2014.

PEER 2014/03 *Retest of Thirty-Year-Old Neoprene Isolation Bearings.* James M. Kelly and Niel C. Van Engelen. March 2014.

PEER 2014/02 *Theoretical Development of Hybrid Simulation Applied to Plate Structures.* Ahmed A. Bakhaty, Khalid M. Mosalam, and Sanjay Govindjee. January 2014.

PEER 2014/01 *Performance-Based Seismic Assessment of Skewed Bridges.* Peyman Kaviani, Farzin Zareian, and Ertugrul Taciroglu. January 2014.

PEER 2013/26 *Urban Earthquake Engineerin*g. Proceedings of the U.S.-Iran Seismic Workshop. December 2013.

PEER 2013/25 *Earthquake Engineering for Resilient Communities: 2013 PEER Internship Program Research Report Collection.* Heidi Tremayne (Editor), Stephen A. Mahin (Editor), Jorge Archbold Monterossa, Matt Brosman, Shelly Dean, Katherine deLaveaga, Curtis Fong, Donovan Holder, Rakeeb Khan, Elizabeth Jachens, David Lam, Daniela Martinez Lopez, Mara Minner, Geffen Oren, Julia Pavicic, Melissa Quinonez, Lorena Rodriguez, Sean Salazar, Kelli Slaven, Vivian Steyert, Jenny Taing, and Salvador Tena. December 2013.

PEER 2013/24 *NGA-West2 Ground Motion Prediction Equations for Vertical Ground Motions*. September 2013.

PEER 2013/23 *Coordinated Planning and Preparedness for Fire Following Major Earthquakes*. Charles Scawthorn. November 2013.

PEER 2013/22 *GEM-PEER Task 3 Project: Selection of a Global Set of Ground Motion Prediction Equations.* Jonathan P. Stewart, John Douglas, Mohammad B. Javanbarg, Carola Di Alessandro, Yousef Bozorgnia, Norman A. Abrahamson, David M. Boore, Kenneth W. Campbell, Elise Delavaud, Mustafa Erdik, and Peter J. Stafford. December 2013.

PEER 2013/21 *Seismic Design and Performance of Bridges with Columns on Rocking Foundations*. Grigorios Antonellis and Marios Panagiotou. September 2013.

PEER 2013/20 *Experimental and Analytical Studies on the Seismic Behavior of Conventional and Hybrid Braced Frames*. Jiun-Wei Lai and Stephen A. Mahin. September 2013.

PEER 2013/19 *Toward Resilient Communities: A Performance-Based Engineering Framework for Design and Evaluation of the Built Environment.* Michael William Mieler, Bozidar Stojadinovic, Robert J. Budnitz, Stephen A. Mahin, and Mary C. Comerio. September 2013.

PEER 2013/18 *Identification of Site Parameters that Improve Predictions of Site Amplification*. Ellen M. Rathje and Sara Navidi. July 2013.

PEER 2013/17 *Response Spectrum Analysis of Concrete Gravity Dams Including Dam-Water-Foundation Interaction*. Arnkjell Løkke and Anil K. Chopra. July 2013.

PEER 2013/16 *Effect of Hoop Reinforcement Spacing on the Cyclic Response of Large Reinforced Concrete Special Moment Frame Beams.* Marios Panagiotou, Tea Visnjic, Grigorios Antonellis, Panagiotis Galanis, and Jack P. Moehle. June 2013.

PEER 2013/15 *A Probabilistic Framework to Include the Effects of Near-Fault Directivity in Seismic Hazard Assessment*. Shrey Kumar Shahi, Jack W. Baker. October 2013.

PEER 2013/14 *Hanging-Wall Scaling using Finite-Fault Simulations.* Jennifer L. Donahue and Norman A. Abrahamson. September 2013.

PEER 2013/13 *Semi-Empirical Nonlinear Site Amplification and its Application in NEHRP Site Factors*. Jonathan P. Stewart and Emel Seyhan. November 2013.

PEER 2013/12 *Nonlinear Horizontal Site Response for the NGA-West2 Project.* Ronnie Kamai, Norman A. Abramson, Walter J. Silva. May 2013.

PEER 2013/11 *Epistemic Uncertainty for NGA-West2 Models.* Linda Al Atik and Robert R. Youngs. May 2013.

PEER 2013/10 *NGA-West 2 Models for Ground-Motion Directionality.* Shrey K. Shahi and Jack W. Baker. May 2013.

PEER 2013/09 *Final Report of the NGA-West2 Directivity Working Group.* Paul Spudich, Jeffrey R. Bayless, Jack W. Baker, Brian S.J. Chiou, Badie Rowshandel, Shrey Shahi, and Paul Somerville. May 2013.

PEER 2013/08 *NGA-West2 Model for Estimating Average Horizontal Values of Pseudo-Absolute Spectral Accelerations Generated by Crustal Earthquakes*. I. M. Idriss. May 2013.

PEER 2013/07 *Update of the Chiou and Youngs NGA Ground Motion Model for Average Horizontal Component of Peak Ground Motion and Response Spectra*. Brian Chiou and Robert Youngs. May 2013.

PEER 2013/06 *NGA-West2 Campbell-Bozorgnia Ground Motion Model for the Horizontal Components of PGA, PGV, and 5%-Damped Elastic Pseudo-Acceleration Response Spectra for Periods Ranging from 0.01 to 10 sec.* Kenneth W. Campbell and Yousef Bozorgnia. May 2013.

PEER 2013/05 *NGA-West 2 Equations for Predicting Response Spectral Accelerations for Shallow Crustal Earthquakes*. David M. Boore, Jonathan P. Stewart, Emel Seyhan, and Gail M. Atkinson. May 2013.

PEER 2013/04 *Update of the AS08 Ground-Motion Prediction Equations Based on the NGA-West2 Data Set*. Norman Abrahamson, Walter Silva, and Ronnie Kamai. May 2013.

PEER 2013/03 *PEER NGA-West2 Database.* Timothy D. Ancheta, Robert B. Darragh, Jonathan P. Stewart, Emel Seyhan, Walter J. Silva, Brian S.J. Chiou, Katie E. Wooddell, Robert W. Graves, Albert R. Kottke, David M. Boore, Tadahiro Kishida, and Jennifer L. Donahue. May 2013.

PEER 2013/02 *Hybrid Simulation of the Seismic Response of Squat Reinforced Concrete Shear Walls*. Catherine A. Whyte and Bozidar Stojadinovic. May 2013.

PEER 2013/01 *Housing Recovery in Chile: A Qualitative Mid-program Review*. Mary C. Comerio. February 2013.

PEER 2012/08 *Guidelines for Estimation of Shear Wave Velocity.* Bernard R. Wair, Jason T. DeJong, and Thomas Shantz. December 2012.

PEER 2012/07 *Earthquake Engineering for Resilient Communities: 2012 PEER Internship Program Research Report Collection.* Heidi Tremayne (Editor), Stephen A. Mahin (Editor), Collin Anderson, Dustin Cook, Michael Erceg, Carlos Esparza, Jose Jimenez, Dorian Krausz, Andrew Lo, Stephanie Lopez, Nicole McCurdy, Paul Shipman, Alexander Strum, Eduardo Vega. December 2012.

PEER 2012/06 *Fragilities for Precarious Rocks at Yucca Mountain.* Matthew D. Purvance, Rasool Anooshehpoor, and James N. Brune. December 2012.

PEER 2012/05 *Development of Simplified Analysis Procedure for Piles in Laterally Spreading Layered Soils.* Christopher R. McGann, Pedro Arduino, and Peter Mackenzie–Helnwein. December 2012.

PEER 2012/04 *Unbonded Pre-Tensioned Columns for Bridges in Seismic Regions.* Phillip M. Davis, Todd M. Janes, Marc O. Eberhard, and John F. Stanton. December 2012.

PEER 2012/03 *Experimental and Analytical Studies on Reinforced Concrete Buildings with Seismically Vulnerable Beam-Column Joints*. Sangjoon Park and Khalid M. Mosalam. October 2012.

PEER 2012/02 *Seismic Performance of Reinforced Concrete Bridges Allowed to Uplift during Multi-Directional Excitation*. Andres Oscar Espinoza and Stephen A. Mahin. July 2012.

PEER 2012/01 *Spectral Damping Scaling Factors for Shallow Crustal Earthquakes in Active Tectonic Regions.* Sanaz Rezaeian, Yousef Bozorgnia, I. M. Idriss, Kenneth Campbell, Norman Abrahamson, and Walter Silva. July 2012.

PEER 2011/10 *Earthquake Engineering for Resilient Communities: 2011 PEER Internship Program Research Report Collection*. Heidi Faison and Stephen A. Mahin, Editors. December 2011.

PEER 2011/09 *Calibration of Semi-Stochastic Procedure for Simulating High-Frequency Ground Motions*. Jonathan P. Stewart, Emel Seyhan, and Robert W. Graves. December 2011.

PEER 2011/08 *Water Supply in regard to Fire Following Earthquake*. Charles Scawthorn. November 2011.

PEER 2011/07 *Seismic Risk Management in Urban Areas*. Proceedings of a U.S.-Iran-Turkey Seismic Workshop. September 2011.

PEER 2011/06 *The Use of Base Isolation Systems to Achieve Complex Seismic Performance Objectives*. Troy A. Morgan and Stephen A. Mahin. July 2011.

PEER 2011/05 *Case Studies of the Seismic Performance of Tall Buildings Designed by Alternative Means.* Task 12 Report for the Tall Buildings Initiative. Jack Moehle, Yousef Bozorgnia, Nirmal Jayaram, Pierson Jones, Mohsen Rahnama, Nilesh Shome, Zeynep Tuna, John Wallace, Tony Yang, and Farzin Zareian. July 2011.

PEER 2011/04 *Recommended Design Practice for Pile Foundations in Laterally Spreading Ground.* Scott A. Ashford, Ross W. Boulanger, and Scott J. Brandenberg. June 2011.

PEER 2011/03 *New Ground Motion Selection Procedures and Selected Motions for the PEER Transportation Research Program*. Jack W. Baker, Ting Lin, Shrey K. Shahi, and Nirmal Jayaram. March 2011.

PEER 2011/02 *A Bayesian Network Methodology for Infrastructure Seismic Risk Assessment and Decision Support*. Michelle T. Bensi, Armen Der Kiureghian, and Daniel Straub. March 2011.

PEER 2011/01 *Demand Fragility Surfaces for Bridges in Liquefied and Laterally Spreading Ground*. Scott J. Brandenberg, Jian Zhang, Pirooz Kashighandi, Yili Huo, and Minxing Zhao. March 2011.

PEER 2010/05 *Guidelines for Performance-Based Seismic Design of Tall Buildings.* Developed by the Tall Buildings Initiative. November 2010.

PEER 2010/04 *Application Guide for the Design of Flexible and Rigid Bus Connections between Substation Equipment Subjected to Earthquakes.* Jean-Bernard Dastous and Armen Der Kiureghian. September 2010.

PEER 2010/03 *Shear Wave Velocity as a Statistical Function of Standard Penetration Test Resistance and Vertical Effective Stress at Caltrans Bridge Sites.* Scott J. Brandenberg, Naresh Bellana, and Thomas Shantz. June 2010.

PEER 2010/02 *Stochastic Modeling and Simulation of Ground Motions for Performance-Based Earthquake Engineering.* Sanaz Rezaeian and Armen Der Kiureghian. June 2010.

PEER 2010/01 *Structural Response and Cost Characterization of Bridge Construction Using Seismic Performance Enhancement Strategies.* Ady Aviram, Božidar Stojadinović, Gustavo J. Parra-Montesinos, and Kevin R. Mackie. March 2010.

PEER 2009/03 *The Integration of Experimental and Simulation Data in the Study of Reinforced Concrete Bridge Systems Including Soil-Foundation-Structure Interaction.* Matthew Dryden and Gregory L. Fenves. November 2009.

PEER 2009/02 *Improving Earthquake Mitigation through Innovations and Applications in Seismic Science, Engineering, Communication, and Response*. Proceedings of a U.S.-Iran Seismic Workshop. October 2009.

PEER 2009/01 *Evaluation of Ground Motion Selection and Modification Methods: Predicting Median Interstory Drift Response of Buildings*. Curt B. Haselton, Editor. June 2009.

PEER 2008/10 *Technical Manual for Strata.* Albert R. Kottke and Ellen M. Rathje. February 2009.

PEER 2008/09 *NGA Model for Average Horizontal Component of Peak Ground Motion and Response Spectra.* Brian S.-J. Chiou and Robert R. Youngs. November 2008.

PEER 2008/08 *Toward Earthquake-Resistant Design of Concentrically Braced Steel Structures*. Patxi Uriz and Stephen A. Mahin. November 2008.

PEER 2008/07 *Using OpenSees for Performance-Based Evaluation of Bridges on Liquefiable Soils*. Stephen L. Kramer, Pedro Arduino, and HyungSuk Shin. November 2008.

PEER 2008/06 *Shaking Table Tests and Numerical Investigation of Self-Centering Reinforced Concrete Bridge Columns*. Hyung IL Jeong, Junichi Sakai, and Stephen A. Mahin. September 2008.

PEER 2008/05 *Performance-Based Earthquake Engineering Design Evaluation Procedure for Bridge Foundations Undergoing Liquefaction-Induced Lateral Ground Displacement*. Christian A. Ledezma and Jonathan D. Bray. August 2008.

PEER 2008/04 *Benchmarking of Nonlinear Geotechnical Ground Response Analysis Procedures.* Jonathan P. Stewart, Annie On-Lei Kwok, Youssef M. A. Hashash, Neven Matasovic, Robert Pyke, Zhiliang Wang, and Zhaohui Yang. August 2008.

PEER 2008/03 *Guidelines for Nonlinear Analysis of Bridge Structures in California.* Ady Aviram, Kevin R. Mackie, and Božidar Stojadinović. August 2008.

PEER 2008/02 *Treatment of Uncertainties in Seismic-Risk Analysis of Transportation Systems*. Evangelos Stergiou and Anne S. Kiremidjian. July 2008.

PEER 2008/01 *Seismic Performance Objectives for Tall Buildings.* William T. Holmes, Charles Kircher, William Petak, and Nabih Youssef. August 2008.

PEER 2007/12 *An Assessment to Benchmark the Seismic Performance of a Code-Conforming Reinforced Concrete Moment-Frame Building.* Curt Haselton, Christine A. Goulet, Judith Mitrani-Reiser, James L. Beck, Gregory G. Deierlein, Keith A. Porter, Jonathan P. Stewart, and Ertugrul Taciroglu. August 2008.

PEER 2007/11 *Bar Buckling in Reinforced Concrete Bridge Columns.* Wayne A. Brown, Dawn E. Lehman, and John F. Stanton. February 2008.

PEER 2007/10 *Computational Modeling of Progressive Collapse in Reinforced Concrete Frame Structures*. Mohamed M. Talaat and Khalid M. Mosalam. May 2008.

PEER 2007/09 *Integrated Probabilistic Performance-Based Evaluation of Benchmark Reinforced Concrete Bridges*. Kevin R. Mackie, John-Michael Wong, and Božidar Stojadinović. January 2008.

PEER 2007/08 *Assessing Seismic Collapse Safety of Modern Reinforced Concrete Moment-Frame Buildings*. Curt B. Haselton and Gregory G. Deierlein. February 2008.

PEER 2007/07 *Performance Modeling Strategies for Modern Reinforced Concrete Bridge Columns*. Michael P. Berry and Marc O. Eberhard. April 2008.

PEER 2007/06 *Development of Improved Procedures for Seismic Design of Buried and Partially Buried Structures*. Linda Al Atik and Nicholas Sitar. June 2007.

PEER 2007/05 *Uncertainty and Correlation in Seismic Risk Assessment of Transportation Systems*. Renee G. Lee and Anne S. Kiremidjian. July 2007.

PEER 2007/04 *Numerical Models for Analysis and Performance-Based Design of Shallow Foundations Subjected to Seismic Loading.* Sivapalan Gajan, Tara C. Hutchinson, Bruce L. Kutter, Prishati Raychowdhury, José A. Ugalde, and Jonathan P. Stewart. May 2008.

PEER 2007/03 *Beam-Column Element Model Calibrated for Predicting Flexural Response Leading to Global Collapse of RC Frame Buildings*. Curt B. Haselton, Abbie B. Liel, Sarah Taylor Lange, and Gregory G. Deierlein. May 2008.

PEER 2007/02 *Campbell-Bozorgnia NGA Ground Motion Relations for the Geometric Mean Horizontal Component of Peak and Spectral Ground Motion Parameters*. Kenneth W. Campbell and Yousef Bozorgnia. May 2007.

PEER 2007/01 *Boore-Atkinson NGA Ground Motion Relations for the Geometric Mean Horizontal Component of Peak and Spectral Ground Motion Parameters*. David M. Boore and Gail M. Atkinson. May 2007.

PEER 2006/12 Societal Implications of Performance-Based Earthquake Engineering. Peter J. May. May 2007.

PEER 2006/11 *Probabilistic Seismic Demand Analysis Using Advanced Ground Motion Intensity Measures, Attenuation Relationships, and Near-Fault Effects*. Polsak Tothong and C. Allin Cornell. March 2007.

PEER 2006/10 *Application of the PEER PBEE Methodology to the I-880 Viaduct*. Sashi Kunnath. February 2007.

PEER 2006/09 *Quantifying Economic Losses from Travel Forgone Following a Large Metropolitan Earthquake*. James Moore, Sungbin Cho, Yue Yue Fan, and Stuart Werner. November 2006.

PEER 2006/08 *Vector-Valued Ground Motion Intensity Measures for Probabilistic Seismic Demand Analysis*. Jack W. Baker and C. Allin Cornell. October 2006.

PEER 2006/07 *Analytical Modeling of Reinforced Concrete Walls for Predicting Flexural and Coupled–Shear-Flexural Responses*. Kutay Orakcal, Leonardo M. Massone, and John W. Wallace. October 2006.

PEER 2006/06 *Nonlinear Analysis of a Soil-Drilled Pier System under Static and Dynamic Axial Loading*. Gang Wang and Nicholas Sitar. November 2006.

PEER 2006/05 *Advanced Seismic Assessment Guidelines.* Paolo Bazzurro, C. Allin Cornell, Charles Menun, Maziar Motahari, and Nicolas Luco. September 2006.

PEER 2006/04 *Probabilistic Seismic Evaluation of Reinforced Concrete Structural Components and Systems*. Tae Hyung Lee and Khalid M. Mosalam. August 2006.

PEER 2006/03 *Performance of Lifelines Subjected to Lateral Spreading*. Scott A. Ashford and Teerawut Juirnarongrit. July 2006.

PEER 2006/02 *Pacific Earthquake Engineering Research Center Highway Demonstration Project.* Anne Kiremidjian, James Moore, Yue Yue Fan, Nesrin Basoz, Ozgur Yazali, and Meredith Williams. April 2006.

PEER 2006/01 *Bracing Berkeley. A Guide to Seismic Safety on the UC Berkeley Campus.* Mary C. Comerio, Stephen Tobriner, and Ariane Fehrenkamp. January 2006.

PEER 2005/17 *Earthquake Simulation Tests on Reducing Residual Displacements of Reinforced Concrete Bridges.* Junichi Sakai, Stephen A Mahin, and Andres Espinoza. December 2005.

PEER 2005/16 *Seismic Response and Reliability of Electrical Substation Equipment and Systems.* Junho Song, Armen Der Kiureghian, and Jerome L. Sackman. April 2006.

PEER 2005/15 *CPT-Based Probabilistic Assessment of Seismic Soil Liquefaction Initiation.* R. E. S. Moss, R. B. Seed, R. E. Kayen, J. P. Stewart, and A. Der Kiureghian. April 2006.

PEER 2005/14 *Workshop on Modeling of Nonlinear Cyclic Load-Deformation Behavior of Shallow Foundations*. Bruce L. Kutter, Geoffrey Martin, Tara Hutchinson, Chad Harden, Sivapalan Gajan, and Justin Phalen. March 2006.

PEER 2005/13 *Stochastic Characterization and Decision Bases under Time-Dependent Aftershock Risk in Performance-Based Earthquake Engineering*. Gee Liek Yeo and C. Allin Cornell. July 2005.

PEER 2005/12 *PEER Testbed Study on a Laboratory Building: Exercising Seismic Performance Assessment.* Mary C. Comerio, Editor. November 2005.

PEER 2005/11 *Van Nuys Hotel Building Testbed Report: Exercising Seismic Performance Assessment.* Helmut Krawinkler, Editor. October 2005.

PEER 2005/10 *First NEES/E-Defense Workshop on Collapse Simulation of Reinforced Concrete Building Structures.* September 2005.

PEER 2005/09 *Test Applications of Advanced Seismic Assessment Guidelines.* Joe Maffei, Karl Telleen, Danya Mohr, William Holmes, and Yuki Nakayama. August 2006.

PEER 2005/08 *Damage Accumulation in Lightly Confined Reinforced Concrete Bridge Columns.* R. Tyler Ranf, Jared M. Nelson, Zach Price, Marc O. Eberhard, and John F. Stanton. April 2006.

PEER 2005/07 *Experimental and Analytical Studies on the Seismic Response of Freestanding and Anchored Laboratory Equipment.* Dimitrios Konstantinidis and Nicos Makris. January 2005.

PEER 2005/06 *Global Collapse of Frame Structures under Seismic Excitations*. Luis F. Ibarra and Helmut Krawinkler. September 2005.

PEER 2005//05 *Performance Characterization of Bench- and Shelf-Mounted Equipment.* Samit Ray Chaudhuri and Tara C. Hutchinson. May 2006.

PEER 2005/04 *Numerical Modeling of the Nonlinear Cyclic Response of Shallow Foundations.* Chad Harden, Tara Hutchinson, Geoffrey R. Martin, and Bruce L. Kutter. August 2005.

PEER 2005/03 *A Taxonomy of Building Components for Performance-Based Earthquake Engineering.* Keith A. Porter. September 2005.

PEER 2005/02 *Fragility Basis for California Highway Overpass Bridge Seismic Decision Making*. Kevin R. Mackie and Božidar Stojadinović. June 2005.

PEER 2005/01 *Empirical Characterization of Site Conditions on Strong Ground Motion.* Jonathan P. Stewart, Yoojoong Choi, and Robert W. Graves. June 2005.

PEER 2004/09 *Electrical Substation Equipment Interaction: Experimental Rigid Conductor Studies.* Christopher Stearns and André Filiatrault. February 2005.

PEER 2004/08 *Seismic Qualification and Fragility Testing of Line Break 550-kV Disconnect Switches.* Shakhzod M. Takhirov, Gregory L. Fenves, and Eric Fujisaki. January 2005.

PEER 2004/07 *Ground Motions for Earthquake Simulator Qualification of Electrical Substation Equipment.* Shakhzod M. Takhirov, Gregory L. Fenves, Eric Fujisaki, and Don Clyde. January 2005.

PEER 2004/06 *Performance-Based Regulation and Regulatory Regimes.* Peter J. May and Chris Koski. September 2004.

PEER 2004/05 *Performance-Based Seismic Design Concepts and Implementation: Proceedings of an International Workshop.* Peter Fajfar and Helmut Krawinkler, Editors. September 2004.

PEER 2004/04 *Seismic Performance of an Instrumented Tilt-up Wall Building.* James C. Anderson and Vitelmo V. Bertero. July 2004.

PEER 2004/03 *Evaluation and Application of Concrete Tilt-up Assessment Methodologies.* Timothy Graf and James O. Malley. October 2004.

PEER 2004/02 *Analytical Investigations of New Methods for Reducing Residual Displacements of Reinforced Concrete Bridge Columns.* Junichi Sakai and Stephen A. Mahin. August 2004.

PEER 2004/01 *Seismic Performance of Masonry Buildings and Design Implications.* Kerri Anne Taeko Tokoro, James C. Anderson, and Vitelmo V. Bertero. February 2004.

PEER 2003/18 *Performance Models for Flexural Damage in Reinforced Concrete Columns.* Michael Berry and Marc Eberhard. August 2003.

PEER 2003/17 *Predicting Earthquake Damage in Older Reinforced Concrete Beam-Column Joints.* Catherine Pagni and Laura Lowes. October 2004.

PEER 2003/16 *Seismic Demands for Performance-Based Design of Bridges.* Kevin Mackie and Božidar Stojadinović. August 2003.

PEER 2003/15 *Seismic Demands for Nondeteriorating Frame Structures and Their Dependence on Ground Motions.* Ricardo Antonio Medina and Helmut Krawinkler. May 2004.

PEER 2003/14 *Finite Element Reliability and Sensitivity Methods for Performance-Based Earthquake Engineering*. Terje Haukaas and Armen Der Kiureghian. April 2004.

PEER 2003/13 *Effects of Connection Hysteretic Degradation on the Seismic Behavior of Steel Moment-Resisting Frames.* Janise E. Rodgers and Stephen A. Mahin. March 2004.

PEER 2003/12 *Implementation Manual for the Seismic Protection of Laboratory Contents: Format and Case Studies*. William T. Holmes and Mary C. Comerio. October 2003.

PEER 2003/11 *Fifth U.S.-Japan Workshop on Performance-Based Earthquake Engineering Methodology for Reinforced Concrete Building Structures*. February 2004.

PEER 2003/10 *A Beam-Column Joint Model for Simulating the Earthquake Response of Reinforced Concrete Frames.* Laura N. Lowes, Nilanjan Mitra, and Arash Altoontash. February 2004.

PEER 2003/09 *Sequencing Repairs after an Earthquake: An Economic Approach.* Marco Casari and Simon J. Wilkie. April 2004.

PEER 2003/08 *A Technical Framework for Probability-Based Demand and Capacity Factor Design (DCFD) Seismic Formats*. Fatemeh Jalayer and C. Allin Cornell. November 2003.

PEER 2003/07 *Uncertainty Specification and Propagation for Loss Estimation Using FOSM Methods.* Jack W. Baker and C. Allin Cornell. September 2003.

PEER 2003/06 *Performance of Circular Reinforced Concrete Bridge Columns under Bidirectional Earthquake Loading*. Mahmoud M. Hachem, Stephen A. Mahin, and Jack P. Moehle. February 2003.

PEER 2003/05 *Response Assessment for Building-Specific Loss Estimation.* Eduardo Miranda and Shahram Taghavi. September 2003.

PEER 2003/04 *Experimental Assessment of Columns with Short Lap Splices Subjected to Cyclic Loads*. Murat Melek, John W. Wallace, and Joel Conte. April 2003.

PEER 2003/03 *Probabilistic Response Assessment for Building-Specific Loss Estimation*. Eduardo Miranda and Hesameddin Aslani. September 2003.

PEER 2003/02 *Software Framework for Collaborative Development of Nonlinear Dynamic Analysis Program*. Jun Peng and Kincho H. Law. September 2003.

PEER 2003/01 *Shake Table Tests and Analytical Studies on the Gravity Load Collapse of Reinforced Concrete Frames.* Kenneth John Elwood and Jack P. Moehle. November 2003.

PEER 2002/24 *Performance of Beam to Column Bridge Joints Subjected to a Large Velocity Pulse.* Natalie Gibson, André Filiatrault, and Scott A. Ashford. April 2002.

PEER 2002/23 *Effects of Large Velocity Pulses on Reinforced Concrete Bridge Columns.* Greg L. Orozco and Scott A. Ashford. April 2002.

PEER 2002/22 *Characterization of Large Velocity Pulses for Laboratory Testing.* Kenneth E. Cox and Scott A. Ashford. April 2002.

PEER 2002/21 *Fourth U.S.-Japan Workshop on Performance-Based Earthquake Engineering Methodology for Reinforced Concrete Building Structures*. December 2002.

PEER 2002/20 *Barriers to Adoption and Implementation of PBEE Innovations.* Peter J. May. August 2002.

PEER 2002/19 *Economic-Engineered Integrated Models for Earthquakes: Socioeconomic Impacts.* Peter Gordon, James E. Moore II, and Harry W. Richardson. July 2002.

PEER 2002/18 *Assessment of Reinforced Concrete Building Exterior Joints with Substandard Details.* Chris P. Pantelides, Jon Hansen, Justin Nadauld, and Lawrence D. Reaveley. May 2002.

PEER 2002/17 *Structural Characterization and Seismic Response Analysis of a Highway Overcrossing Equipped with Elastomeric Bearings and Fluid Dampers: A Case Study*. Nicos Makris and Jian Zhang. November 2002.

PEER 2002/16 *Estimation of Uncertainty in Geotechnical Properties for Performance-Based Earthquake Engineering*. Allen L. Jones, Steven L. Kramer, and Pedro Arduino. December 2002.

PEER 2002/15 *Seismic Behavior of Bridge Columns Subjected to Various Loading Patterns*. Asadollah Esmaeily-Gh. and Yan Xiao. December 2002.

PEER 2002/14 *Inelastic Seismic Response of Extended Pile Shaft Supported Bridge Structures.* T.C. Hutchinson, R.W. Boulanger, Y.H. Chai, and I.M. Idriss. December 2002.

PEER 2002/13 *Probabilistic Models and Fragility Estimates for Bridge Components and Systems.* Paolo Gardoni, Armen Der Kiureghian, and Khalid M. Mosalam. June 2002.

PEER 2002/12 *Effects of Fault Dip and Slip Rake on Near-Source Ground Motions: Why Chi-Chi Was a Relatively Mild M7.6 Earthquake*. Brad T. Aagaard, John F. Hall, and Thomas H. Heaton. December 2002.

PEER 2002/11 *Analytical and Experimental Study of Fiber-Reinforced Strip Isolators*. James M. Kelly and Shakhzod M. Takhirov. September 2002.

PEER 2002/10 *Centrifuge Modeling of Settlement and Lateral Spreading with Comparisons to Numerical Analyses***.** Sivapalan Gajan and Bruce L. Kutter. January 2003.

PEER 2002/09 *Documentation and Analysis of Field Case Histories of Seismic Compression during the 1994 Northridge, California, Earthquake*. Jonathan P. Stewart, Patrick M. Smith, Daniel H. Whang, and Jonathan D. Bray. October 2002.

PEER 2002/08 *Component Testing, Stability Analysis and Characterization of Buckling-Restrained Unbonded Braces™*. Cameron Black, Nicos Makris, and Ian Aiken. September 2002.

PEER 2002/07 *Seismic Performance of Pile-Wharf Connections.* Charles W. Roeder, Robert Graff, Jennifer Soderstrom, and Jun Han Yoo. December 2001.

PEER 2002/06 *The Use of Benefit-Cost Analysis for Evaluation of Performance-Based Earthquake Engineering Decisions*. Richard O. Zerbe and Anthony Falit-Baiamonte. September 2001.

PEER 2002/05 *Guidelines, Specifications, and Seismic Performance Characterization of Nonstructural Building Components and Equipment*. André Filiatrault, Constantin Christopoulos, and Christopher Stearns. September 2001.

PEER 2002/04 *Consortium of Organizations for Strong-Motion Observation Systems and the Pacific Earthquake Engineering Research Center Lifelines Program: Invited Workshop on Archiving and Web Dissemination of Geotechnical Data, 4–5 October 2001*. September 2002.

PEER 2002/03 *Investigation of Sensitivity of Building Loss Estimates to Major Uncertain Variables for the Van Nuys Testbed*. Keith A. Porter, James L. Beck, and Rustem V. Shaikhutdinov. August 2002.

PEER 2002/02 *The Third U.S.-Japan Workshop on Performance-Based Earthquake Engineering Methodology for Reinforced Concrete Building Structures*. July 2002.

PEER 2002/01 *Nonstructural Loss Estimation: The UC Berkeley Case Study.* Mary C. Comerio and John C. Stallmeyer. December 2001.

PEER 2001/16 *Statistics of SDF-System Estimate of Roof Displacement for Pushover Analysis of Buildings.* Anil K. Chopra, Rakesh K. Goel, and Chatpan Chintanapakdee. December 2001.

PEER 2001/15 *Damage to Bridges during the 2001 Nisqually Earthquake.* R. Tyler Ranf, Marc O. Eberhard, and Michael P. Berry. November 2001.

PEER 2001/14 *Rocking Response of Equipment Anchored to a Base Foundation.* Nicos Makris and Cameron J. Black. September 2001.

PEER 2001/13 *Modeling Soil Liquefaction Hazards for Performance-Based Earthquake Engineering*. Steven L. Kramer and Ahmed-W. Elgamal. February 2001.

PEER 2001/12 *Development of Geotechnical Capabilities in OpenSees*. Boris Jeremić. September 2001.

PEER 2001/11 *Analytical and Experimental Study of Fiber-Reinforced Elastomeric Isolators*. James M. Kelly and Shakhzod M. Takhirov. September 2001.

PEER 2001/10 *Amplification Factors for Spectral Acceleration in Active Regions.* Jonathan P. Stewart, Andrew H. Liu, Yoojoong Choi, and Mehmet B. Baturay. December 2001.

PEER 2001/09 *Ground Motion Evaluation Procedures for Performance-Based Design.* Jonathan P. Stewart, Shyh-Jeng Chiou, Jonathan D. Bray, Robert W. Graves, Paul G. Somerville, and Norman A. Abrahamson. September 2001.

PEER 2001/08 *Experimental and Computational Evaluation of Reinforced Concrete Bridge Beam-Column Connections for Seismic Performance*. Clay J. Naito, Jack P. Moehle, and Khalid M. Mosalam. November 2001.

PEER 2001/07 *The Rocking Spectrum and the Shortcomings of Design Guidelines.* Nicos Makris and Dimitrios Konstantinidis. August 2001.

PEER 2001/06 *Development of an Electrical Substation Equipment Performance Database for Evaluation of Equipment Fragilities*. Thalia Agnanos. April 1999.

PEER 2001/05 *Stiffness Analysis of Fiber-Reinforced Elastomeric Isolators.* Hsiang-Chuan Tsai and James M. Kelly. May 2001.

PEER 2001/04 *Organizational and Societal Considerations for Performance-Based Earthquake Engineering*. Peter J. May. April 2001.

PEER 2001/03 *A Modal Pushover Analysis Procedure to Estimate Seismic Demands for Buildings: Theory and Preliminary Evaluation*. Anil K. Chopra and Rakesh K. Goel. January 2001.

PEER 2001/02 *Seismic Response Analysis of Highway Overcrossings Including Soil-Structure Interaction*. Jian Zhang and Nicos Makris. March 2001.

PEER 2001/01 *Experimental Study of Large Seismic Steel Beam-to-Column Connections.* Egor P. Popov and Shakhzod M. Takhirov. November 2000.

PEER 2000/10 *The Second U.S.-Japan Workshop on Performance-Based Earthquake Engineering Methodology for Reinforced Concrete Building Structures*. March 2000.

PEER 2000/09 *Structural Engineering Reconnaissance of the August 17, 1999 Earthquake: Kocaeli (Izmit), Turkey.* Halil Sezen, Kenneth J. Elwood, Andrew S. Whittaker, Khalid Mosalam, John J. Wallace, and John F. Stanton. December 2000.

PEER 2000/08 *Behavior of Reinforced Concrete Bridge Columns Having Varying Aspect Ratios and Varying Lengths of Confinement*. Anthony J. Calderone, Dawn E. Lehman, and Jack P. Moehle. January 2001.

PEER 2000/07 *Cover-Plate and Flange-Plate Reinforced Steel Moment-Resisting Connections*. Taejin Kim, Andrew S. Whittaker, Amir S. Gilani, Vitelmo V. Bertero, and Shakhzod M. Takhirov. September 2000.

PEER 2000/06 *Seismic Evaluation and Analysis of 230-kV Disconnect Switches*. Amir S. J. Gilani, Andrew S. Whittaker, Gregory L. Fenves, Chun-Hao Chen, Henry Ho, and Eric Fujisaki. July 2000.

PEER 2000/05 *Performance-Based Evaluation of Exterior Reinforced Concrete Building Joints for Seismic Excitation*. Chandra Clyde, Chris P. Pantelides, and Lawrence D. Reaveley. July 2000.

PEER 2000/04 *An Evaluation of Seismic Energy Demand: An Attenuation Approach*. Chung-Che Chou and Chia-Ming Uang. July 1999.

PEER 2000/03 *Framing Earthquake Retrofitting Decisions: The Case of Hillside Homes in Los Angeles*. Detlof von Winterfeldt, Nels Roselund, and Alicia Kitsuse. March 2000.

PEER 2000/02 *U.S.-Japan Workshop on the Effects of Near-Field Earthquake Shaking*. Andrew Whittaker, Editor. July 2000.

PEER 2000/01 *Further Studies on Seismic Interaction in Interconnected Electrical Substation Equipment*. Armen Der Kiureghian, Kee-Jeung Hong, and Jerome L. Sackman. November 1999.

PEER 1999/14 *Seismic Evaluation and Retrofit of 230-kV Porcelain Transformer Bushings*. Amir S. Gilani, Andrew S. Whittaker, Gregory L. Fenves, and Eric Fujisaki. December 1999.

PEER 1999/13 *Building Vulnerability Studies: Modeling and Evaluation of Tilt-up and Steel Reinforced Concrete Buildings*. John W. Wallace, Jonathan P. Stewart, and Andrew S. Whittaker, Editors. December 1999.

PEER 1999/12 *Rehabilitation of Nonductile RC Frame Building Using Encasement Plates and Energy-Dissipating Devices*. Mehrdad Sasani, Vitelmo V. Bertero, James C. Anderson. December 1999.

PEER 1999/11 *Performance Evaluation Database for Concrete Bridge Components and Systems under Simulated Seismic Loads*. Yael D. Hose and Frieder Seible. November 1999.

PEER 1999/10 *U.S.-Japan Workshop on Performance-Based Earthquake Engineering Methodology for Reinforced Concrete Building Structures*. December 1999.

PEER 1999/09 *Performance Improvement of Long Period Building Structures Subjected to Severe Pulse-Type Ground Motions*. James C. Anderson, Vitelmo V. Bertero, and Raul Bertero. October 1999.

PEER 1999/08 *Envelopes for Seismic Response Vectors*. Charles Menun and Armen Der Kiureghian. July 1999.

PEER 1999/07 *Documentation of Strengths and Weaknesses of Current Computer Analysis Methods for Seismic Performance of Reinforced Concrete Members*. William F. Cofer. November 1999.

PEER 1999/06 *Rocking Response and Overturning of Anchored Equipment under Seismic Excitations*. Nicos Makris and Jian Zhang. November 1999.

PEER 1999/05 *Seismic Evaluation of 550 kV Porcelain Transformer Bushings*. Amir S. Gilani, Andrew S. Whittaker, Gregory L. Fenves, and Eric Fujisaki. October 1999.

PEER 1999/04 *Adoption and Enforcement of Earthquake Risk-Reduction Measures*. Peter J. May, Raymond J. Burby, T. Jens Feeley, and Robert Wood. August 1999.

PEER 1999/03 *Task 3 Characterization of Site Response General Site Categories*. Adrian Rodriguez-Marek, Jonathan D. Bray and Norman Abrahamson. February 1999.

PEER 1999/02 *Capacity-Demand-Diagram Methods for Estimating Seismic Deformation of Inelastic Structures: SDF Systems*. Anil K. Chopra and Rakesh Goel. April 1999.

PEER 1999/01 *Interaction in Interconnected Electrical Substation Equipment Subjected to Earthquake Ground Motions*. Armen Der Kiureghian, Jerome L. Sackman, and Kee-Jeung Hong. February 1999.

PEER 1998/08 *Behavior and Failure Analysis of a Multiple-Frame Highway Bridge in the 1994 Northridge Earthquake*. Gregory L. Fenves and Michael Ellery. December 1998.

PEER 1998/07 *Empirical Evaluation of Inertial Soil-Structure Interaction Effects*. Jonathan P. Stewart, Raymond B. Seed, and Gregory L. Fenves. November 1998.

PEER 1998/06 *Effect of Damping Mechanisms on the Response of Seismic Isolated Structures*. Nicos Makris and Shih-Po Chang. November 1998.

PEER 1998/05 *Rocking Response and Overturning of Equipment under Horizontal Pulse-Type Motions*. Nicos Makris and Yiannis Roussos. October 1998.

PEER 1998/04 *Pacific Earthquake Engineering Research Invitational Workshop Proceedings, May 14–15, 1998: Defining the Links between Planning, Policy Analysis, Economics and Earthquake Engineering*. Mary Comerio and Peter Gordon. September 1998.

PEER 1998/03 *Repair/Upgrade Procedures for Welded Beam to Column Connections*. James C. Anderson and Xiaojing Duan. May 1998.

PEER 1998/02 *Seismic Evaluation of 196 kV Porcelain Transformer Bushings.* Amir S. Gilani, Juan W. Chavez, Gregory L. Fenves, and Andrew S. Whittaker. May 1998.

PEER 1998/01 *Seismic Performance of Well-Confined Concrete Bridge Columns.* Dawn E. Lehman and Jack P. Moehle. December 2000.

PEER REPORTS: ONE HUNDRED SERIES

The following PEER reports are available by Internet only at http://peer.berkeley.edu/publications/peer_reports_complete.html.

PEER 2012/103 *Performance-Based Seismic Demand Assessment of Concentrically Braced Steel Frame Buildings.* Chui-Hsin Chen and Stephen A. Mahin. December 2012.

PEER 2012/102 *Procedure to Restart an Interrupted Hybrid Simulation: Addendum to PEER Report 2010/103.* Vesna Terzic and Bozidar Stojadinovic. October 2012.

PEER 2012/101 *Mechanics of Fiber Reinforced Bearings.* James M. Kelly and Andrea Calabrese. February 2012.

PEER 2011/107 *Nonlinear Site Response and Seismic Compression at Vertical Array Strongly Shaken by 2007 Niigata-ken Chuetsu-oki Earthquake.* Eric Yee, Jonathan P. Stewart, and Kohji Tokimatsu. December 2011.

PEER 2011/106 *Self Compacting Hybrid Fiber Reinforced Concrete Composites for Bridge Columns.* Pardeep Kumar, Gabriel Jen, William Trono, Marios Panagiotou, and Claudia Ostertag. September 2011.

PEER 2011/105 *Stochastic Dynamic Analysis of Bridges Subjected to Spacially Varying Ground Motions.* Katerina Konakli and Armen Der Kiureghian. August 2011.

PEER 2011/104 *Design and Instrumentation of the 2010 E-Defense Four-Story Reinforced Concrete and Post-Tensioned Concrete Buildings.* Takuya Nagae, Kenichi Tahara, Taizo Matsumori, Hitoshi Shiohara, Toshimi Kabeyasawa, Susumu Kono, Minehiro Nishiyama (Japanese Research Team) and John Wallace, Wassim Ghannoum, Jack Moehle, Richard Sause, Wesley Keller, Zeynep Tuna (U.S. Research Team). June 2011.

PEER 2011/103 *In-Situ Monitoring of the Force Output of Fluid Dampers: Experimental Investigation.* Dimitrios Konstantinidis, James M. Kelly, and Nicos Makris. April 2011.

PEER 2011/102 *Ground-Motion Prediction Equations 1964–2010.* John Douglas. April 2011.

PEER 2011/101 *Report of the Eighth Planning Meeting of NEES/E-Defense Collaborative Research on Earthquake Engineering.* Convened by the Hyogo Earthquake Engineering Research Center (NIED), NEES Consortium, Inc. February 2011.

PEER 2010/111 *Modeling and Acceptance Criteria for Seismic Design and Analysis of Tall Buildings.* Task 7 Report for the Tall Buildings Initiative - Published jointly by the Applied Technology Council. October 2010.

PEER 2010/110 *Seismic Performance Assessment and Probabilistic Repair Cost Analysis of Precast Concrete Cladding Systems for Multistory Buildlings.* Jeffrey P. Hunt and Božidar Stojadinovic. November 2010.

PEER 2010/109 *Report of the Seventh Joint Planning Meeting of NEES/E-Defense Collaboration on Earthquake Engineering. Held at the E-Defense, Miki, and Shin-Kobe, Japan, September 18–19, 2009.* August 2010.

PEER 2010/108 *Probabilistic Tsunami Hazard in California.* Hong Kie Thio, Paul Somerville, and Jascha Polet, preparers. October 2010.

PEER 2010/107 *Performance and Reliability of Exposed Column Base Plate Connections for Steel Moment-Resisting Frames.* Ady Aviram, Božidar Stojadinovic, and Armen Der Kiureghian. August 2010.

PEER 2010/106 *Verification of Probabilistic Seismic Hazard Analysis Computer Programs.* Patricia Thomas, Ivan Wong, and Norman Abrahamson. May 2010.

PEER 2010/105 *Structural Engineering Reconnaissance of the April 6, 2009, Abruzzo, Italy, Earthquake, and Lessons Learned.* M. Selim Günay and Khalid M. Mosalam. April 2010.

PEER 2010/104 *Simulating the Inelastic Seismic Behavior of Steel Braced Frames, Including the Effects of Low-Cycle Fatigue.* Yuli Huang and Stephen A. Mahin. April 2010.

PEER 2010/103 *Post-Earthquake Traffic Capacity of Modern Bridges in California.* Vesna Terzic and Božidar Stojadinović. March 2010.

PEER 2010/102 *Analysis of Cumulative Absolute Velocity (CAV) and JMA Instrumental Seismic Intensity (I_{JMA}) Using the PEER–NGA Strong Motion Database.* Kenneth W. Campbell and Yousef Bozorgnia. February 2010.

PEER 2010/101 *Rocking Response of Bridges on Shallow Foundations.* Jose A. Ugalde, Bruce L. Kutter, and Boris Jeremic. April 2010.

PEER 2009/109 *Simulation and Performance-Based Earthquake Engineering Assessment of Self-Centering Post-Tensioned Concrete Bridge Systems.* Won K. Lee and Sarah L. Billington. December 2009.

PEER 2009/108 *PEER Lifelines Geotechnical Virtual Data Center.* J. Carl Stepp, Daniel J. Ponti, Loren L. Turner, Jennifer N. Swift, Sean Devlin, Yang Zhu, Jean Benoit, and John Bobbitt. September 2009.

PEER 2009/107 *Experimental and Computational Evaluation of Current and Innovative In-Span Hinge Details in Reinforced Concrete Box-Girder Bridges: Part 2: Post-Test Analysis and Design Recommendations.* Matias A. Hube and Khalid M. Mosalam. December 2009.

PEER 2009/106 *Shear Strength Models of Exterior Beam-Column Joints without Transverse Reinforcement.* Sangjoon Park and Khalid M. Mosalam. November 2009.

PEER 2009/105 *Reduced Uncertainty of Ground Motion Prediction Equations through Bayesian Variance Analysis.* Robb Eric S. Moss. November 2009.

PEER 2009/104 *Advanced Implementation of Hybrid Simulation.* Andreas H. Schellenberg, Stephen A. Mahin, Gregory L. Fenves. November 2009.

PEER 2009/103 *Performance Evaluation of Innovative Steel Braced Frames.* T. Y. Yang, Jack P. Moehle, and Božidar Stojadinovic. August 2009.

PEER 2009/102 *Reinvestigation of Liquefaction and Nonliquefaction Case Histories from the 1976 Tangshan Earthquake.* Robb Eric Moss, Robert E. Kayen, Liyuan Tong, Songyu Liu, Guojun Cai, and Jiaer Wu. August 2009.

PEER 2009/101 *Report of the First Joint Planning Meeting for the Second Phase of NEES/E-Defense Collaborative Research on Earthquake Engineering.* Stephen A. Mahin et al. July 2009.

PEER 2008/104 *Experimental and Analytical Study of the Seismic Performance of Retaining Structures.* Linda Al Atik and Nicholas Sitar. January 2009.

PEER 2008/103 *Experimental and Computational Evaluation of Current and Innovative In-Span Hinge Details in Reinforced Concrete Box-Girder Bridges. Part 1: Experimental Findings and Pre-Test Analysis.* Matias A. Hube and Khalid M. Mosalam. January 2009.

PEER 2008/102 *Modeling of Unreinforced Masonry Infill Walls Considering In-Plane and Out-of-Plane Interaction.* Stephen Kadysiewski and Khalid M. Mosalam. January 2009.

PEER 2008/101 *Seismic Performance Objectives for Tall Buildings.* William T. Holmes, Charles Kircher, William Petak, and Nabih Youssef. August 2008.

PEER 2007/101 *Generalized Hybrid Simulation Framework for Structural Systems Subjected to Seismic Loading*. Tarek Elkhoraibi and Khalid M. Mosalam. July 2007.

PEER 2007/100 *Seismic Evaluation of Reinforced Concrete Buildings Including Effects of Masonry Infill Walls*. Alidad Hashemi and Khalid M. Mosalam. July 2007.

The Pacifi c Earthquake Engineering Research Center (PEER) is a multi-institutional research and education center with headquarters at the University of California, Berkeley. Investigators from over 20 universities, several consulting companies, and researchers at various state and federal government agencies contribute to research programs focused on performance-based earthquake engineering.

These research programs aim to identify and reduce the risks from major earthquakes to life safety and to the economy by including research in a wide variety of disciplines including structural and geotechnical engineering, geology/seismology, lifelines, transportation, architecture, economics, risk management, and public policy.

PEER is supported by federal, state, local, and regional agencies, together with industry partners.

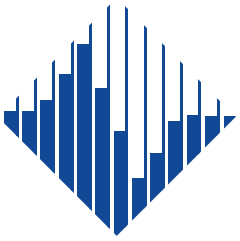

PEER Core Institutions

University of California, Berkeley (Lead Institution)
California Institute of Technology
Oregon State University
Stanford University
University of California, Davis
University of California, Irvine
University of California, Los Angeles
University of California, San Diego
University of Nevada, Reno
University of Southern California
University of Washington

PEER reports can be ordered at https://peer.berkeley.edu/peer-reports or by contacting

Pacific Earthquake Engineering Research Center
University of California, Berkeley
325 Davis Hall, Mail Code 1792
Berkeley, CA 94720-1792
Tel: 510-642-3437
Email: peer_center@berkeley.edu

ISSN 2770-8314
https://doi.org/10.55461/GPHH9609